

Old Dominion University

ODU Digital Commons

Mechanical & Aerospace Engineering Theses & Dissertations

Mechanical & Aerospace Engineering

Winter 2015

Uncertainty Estimates and Prediction Interval Development for Internal Strain Gage Balance Calibration Systems

Kenneth G. Toro
Old Dominion University

Follow this and additional works at: https://digitalcommons.odu.edu/mae_etds



Part of the [Aerospace Engineering Commons](#)

Recommended Citation

Toro, Kenneth G.. "Uncertainty Estimates and Prediction Interval Development for Internal Strain Gage Balance Calibration Systems" (2015). Doctor of Philosophy (PhD), Dissertation, Mechanical & Aerospace Engineering, Old Dominion University, DOI: 10.25777/f0d8-sy14
https://digitalcommons.odu.edu/mae_etds/163

This Dissertation is brought to you for free and open access by the Mechanical & Aerospace Engineering at ODU Digital Commons. It has been accepted for inclusion in Mechanical & Aerospace Engineering Theses & Dissertations by an authorized administrator of ODU Digital Commons. For more information, please contact digitalcommons@odu.edu.

UNCERTAINTY ESTIMATES AND PREDICTION
INTERVAL DEVELOPMENT FOR INTERNAL STRAIN
GAGE BALANCE CALIBRATION SYSTEMS

by

Kenneth G. Toro

B.S. May 2010, Embry-Riddle Aeronautical University

M.S. August 2013, Old Dominion University


A Dissertation Submitted to the Faculty of
Old Dominion University in Partial Fulfillment of the
Requirements for the Degree of

DOCTOR OF PHILOSOPHY

AEROSPACE ENGINEERING

OLD DOMINION UNIVERSITY

December 2015

Approved by: 


Drew Landman (Director)

Colin Britcher (Member)

~~Sean~~ Commo (Member)

Gene Hou (Member)

ABSTRACT

UNCERTAINTY ESTIMATES AND PREDICTION INTERVAL DEVELOPMENT FOR INTERNAL STRAIN GAGE BALANCE CALIBRATION SYSTEMS

Kenneth G. Toro
Old Dominion University, 2015
Director: Dr. Drew Landman

Currently, there is a lack of the use of mathematically rigorous methods to evaluate the performance of multivariate force measurement systems. The specific problem addressed in the research stems from the practical issues faced by test engineers when wind tunnel models with internal strain gage balances are readied for test. Check loads are applied and the question that needs to be answered is whether or not the balance is reading within acceptable limits. These systems tend to be difficult to characterize uncertainty, primarily due to their multivariate nature, but also due to the desire for an estimate on the explanatory variable of the system, instead of the response. This estimation of the explanatory variable is inherent to the calibration problem. For systems that are modeled using non-linear terms, no closed form solution will exist for the explanatory variable. This research details the development of a prediction interval which includes the measurement error in the calibration and check systems. The 20,000 lb. manual stand for calibrating balances used in the National Transonic Facility (NTF) is employed by NASA Langley Research Center and the case study for the work. The uncertainty estimates were developed using the propagation of error method on derived physics equations for the system. The uncertainty estimates were integrated into the developed prediction interval, which demonstrated a capture rate of 96% for a trial set of check loads using a 95% level of condence. Comparisons are made to prediction interval capture rates for the Single Vector System using a common set of check loads on an NTF balance.

ACKNOWLEDGMENTS

I would primarily like to thank my patient and supportive advisor and friend, Dr. Drew Landman of Old Dominion University, for his support and knowledge. I began working with him in 2011 when I began my studies as a master's student. He has led and advised me throughout the entire process of completing my research for both my master's and this current research.

Secondarily, I would like to thank all the members of the National Force Measurement Technology Capability (NFMTC) for their pooled knowledge of internal strain gage balances and funding of this study. This group includes Dr. Peter Parker of NASA Langley Research Center (LaRC) who contributed his wealth of knowledge and understanding of force measurement systems. His knowledge, experience and guidance were crucial in the completion of this research. Also included in the NFMTC is Dr. Sean Commo of NASA LaRC who supported the research and providing his knowledge of statistics and uncertainty analysis.

I would like also recognize (Jerald) Gregory Jones of Modern Machine and Tool Co., Inc. for his vast knowledge of balance calibration from all his years of experience. Without his hands-on experience with the manual calibration systems implemented at NASA LaRC this research would have not gone as smoothly.

NOMENCLATURE

| | |
|--------------|---|
| β | Regression Coefficient |
| \mathbf{F} | Force Vector |
| \mathbf{M} | Moment Vector |
| \mathbf{r} | Position Vector |
| ϵ | Random Error |
| ϕ | Roll Angle |
| ψ | Yaw Angle |
| θ | Pitch Angle |
| C_D | Drag Coefficient |
| C_i | Cosine of i |
| D | Drag |
| P | Applied Load |
| q | Dynamic Pressure |
| rF_i | The i^{th} Response Component |
| S | Wing Planform Area |
| S_i | Sine of i |
| s_i | Uncertainty Estimate of i |
| ABCS | Automatic Balance Calibration System |
| AGARD | Advisory Group for Aerospace Research and Development |
| AIAA | American Institute of Aeronautics and Astronautics |
| AMS | Angle Measurement System |

BBD Box-Behnken Design

BMC Balance Moment Center

CCD Central Composite Design

CFD Computational Fluid Dynamics

CMM Coordinate Measurement Machine

CRM Common Research Model

ETW European Transonic Wind-Tunnel

EU Engineering Units

FAVOR Facility Analysis Verification and Operational Reliability

GLS Generalized Least Squares

IBTWG Internal Balance Technology Working Group

ILS In-Situ Load System

JAXA Japanese Aerospace Exploration Agency

LaRC Langley Research Center

MCS Monte Carlo Simulation

MSE Mean Square Error

NASA National Aeronautics and Space Administration

NIST National Institute of Standard and Technology

NTF National Transonic Facility

OFAT One-Factor-at-a-Time

QA Quality Assurance

RSM Response Surface Methods

RSS Root-Sum Square

SVS Single-Vector System

VIF Variance Inflation Factor

WTMS Wind-Tunnel Model System

TABLE OF CONTENTS

| | Page |
|---|------|
| LIST OF TABLES | x |
| LIST OF FIGURES | xii |
| Chapter | |
| 1. INTRODUCTION | 1 |
| 1.1 BACKGROUND | 4 |
| 2. LITERATURE STUDY | 17 |
| 2.1 ESTIMATION OF THE UNCERTAINTY IN INTERNAL BAL- ANCE CALIBRATION THROUGH COMPREHENSIVE ERROR PROPAGATION | 17 |
| 2.2 CALIBRATION UNCERTAINTY ESTIMATION OF A STRAIN- GAGE EXTERNAL BALANCE | 27 |
| 2.3 DETERMINATION OF MEASUREMENT UNCERTAINTIES OF MULTI-COMPONENT WIND TUNNEL BALANCES | 36 |
| 3. PREDICTION INTERVAL DEVELOPMENT | 48 |
| 3.1 FORWARD PREDICTION INTERVAL | 50 |
| 3.2 REVERSAL OF THE PREDICTION INTERVAL | 54 |
| 4. MANUAL STAND UNCERTAINTY | 58 |
| 4.1 INDIVIDUAL UNCERTAINTY SOURCES | 59 |
| 4.2 OVERALL SYSTEM UNCERTAINTY | 85 |
| 4.3 UNCERTAINTY ESTIMATE VALIDATION | 90 |
| 5. UNCERTAINTY AND PREDICTION INTERVAL INTEGRATION | 93 |
| 6. CONCLUSIONS | 104 |
| APPENDICES | |
| A. PREDICTION INTERVAL MATLAB CODE | 111 |
| A.1 PREDICTION INTERVAL FRONT END | 111 |
| A.2 PREDICTION INTERVAL BACK END | 112 |
| B. MANUAL STAND UNCERTAINTY MATLAB CODE - PROPAGATION OF ERROR | 122 |
| B.1 INTERFACE SCRIPT | 122 |
| B.2 UNCERTAINTY ESTIMATOR | 123 |

| | |
|---|---------|
| C. MANUAL STAND UNCERTAINTY MATLAB CODE - MONTE CARLO SIMULATION | 134 |
| C.1 INTERFACE SCRIPT | 134 |
| C.2 SYSTEM MODEL..... | 135 |
| VITA..... | 146 |

LIST OF TABLES

| Table | Page |
|--|------|
| 1. Transonic Wind-Tunnel Model Parameters | 2 |
| 2. Calibration Variance Inflation Factors | 19 |
| 3. Boeing St. Louis Calibration System Uncertainty Estimates | 21 |
| 4. Comparison of Jitter and Regression Uncertainties for Forces | 24 |
| 5. Comparison of Jitter and Regression Uncertainties for Moments | 25 |
| 6. Sample Load Table | 29 |
| 7. Sample Load Schedule | 29 |
| 8. Friction Estimates | 32 |
| 9. Regression Estimates for Y_1 | 34 |
| 10. Estimated Applied Forces and Uncertainties, kg (Force) or kg m (Moments) | 34 |
| 11. Regression Goodness of Fit Results | 35 |
| 12. Load Component Notations | 36 |
| 13. Position Uncertainty Sources | 66 |
| 14. Load Position Uncertainty Estimates | 68 |
| 15. Angle Uncertainty Sources | 69 |
| 16. Body Angle Uncertainty Estimates | 69 |
| 17. Angle Uncertainty Sources | 72 |
| 18. Balances Sensitivities and Uncertainty Estimates | 73 |
| 19. NTF-113C Moment Arm Properties | 82 |
| 20. Arm Load Position Uncertainty Estimates | 83 |
| 21. Data Acquisition Uncertainty Estimates | 85 |
| 22. Manual Stand Load Combinations | 87 |

23. NTF-113C Design Loads 88

24. NTF-113C Calibration Properties 88

25. Load Combinations and Uncertainty Results 89

26. Average Uncertainty Estimates 90

27. MCS Standard Deviation Results 92

28. Average Difference Between Error Propagation and MCS Results 92

29. ILS Demonstration Applied Loads 94

30. Calibration and Check System Uncertainties 95

31. Prediction Interval Capture Rates 101

32. Manual Stand Prediction Interval Half Widths, Percent F.S. 101

33. SVS Prediction Interval Capture Rates 102

34. SVS Prediction Interval Half Widths, Percent F.S. 103

LIST OF FIGURES

| Figure | Page |
|---|------|
| 1. FAVOR WTMS in the NASA GRC 8x6 ft Supersonic Wind Tunnel (Credit: NASA) | 3 |
| 2. Internal Strain-Gage Balance, NASA NTF Family (Credit: NASA) | 5 |
| 3. Balance Coordinate System | 6 |
| 4. Typical Manual Stand Calibration (Credit: NASA) | 7 |
| 5. Single-Vector Concept Diagram | 10 |
| 6. Single-Vector System Mechanical Assembly (Credit: NASA) | 10 |
| 7. In-Situ Load System Assembly (Credit: NASA) | 11 |
| 8. Triumph ABCS (Credit: Triumph) | 14 |
| 9. Japan Aerospace Exploration Agency (JAXA) ABCS (Credit: JAXA) ... | 14 |
| 10. Load Chain Detail (Credit: Triumph) | 15 |
| 11. Boeing St. Louis Calibration Setup | 18 |
| 12. Ratio of Including and Excluding Correlation | 26 |
| 13. TA-2 Balance Calibration Setup | 27 |
| 14. Calibration Resolution for X_6 | 33 |
| 15. 748 Histogram of Residuals in F_z | 44 |
| 16. UT61B Histogram of Residuals in F_z | 44 |
| 17. 748 Predicted Error in F_z | 45 |
| 18. UT61B Predicted Error in F_z | 45 |
| 19. 748 Proof Load Residuals in F_z | 46 |
| 20. UT61B Proof Load Residuals in F_z | 47 |
| 21. Example of Statistical Intervals | 49 |

| | | |
|-----|---|-----|
| 22. | NASA LaRC 20K Manual Stand (Credit: NASA) | 59 |
| 23. | Balance Coordinate System, with Rotations | 60 |
| 24. | Misaligned Fixture with Applied Load | 62 |
| 25. | F_y Cable Load Example | 70 |
| 26. | Typical Bell Crank Arrangement | 71 |
| 27. | Catenary Shape Example | 75 |
| 28. | M_x and M_y Arm Load Example | 81 |
| 29. | Triangle Analog for Deflected Beam | 82 |
| 30. | F_x Histogram | 91 |
| 31. | ILS Check Load Demonstration at NASA LaRC NTF | 94 |
| 32. | F_x Residuals vs. Run | 96 |
| 33. | F_y Residuals vs. Run | 97 |
| 34. | F_z Residuals vs. Run | 97 |
| 35. | M_x Residuals vs. Run | 98 |
| 36. | M_y Residuals vs. Run | 99 |
| 37. | M_z Residuals vs. Run | 100 |

CHAPTER 1

INTRODUCTION

The desired research objectives of aircraft wind-tunnel testing dictates the data accuracy that is required. In many research cases the uncertainties of the instruments are not rigorously taken into account in wind-tunnel test results. It is good practice to implement statistically-based intervals and uncertainties on experimental measurements to increase the understanding of the data. Currently there is a lack of a standard prediction interval used for strain-gage force balances, which are the primary force measurement instrument for wind-tunnel testing. A thorough understanding of the uncertainty and prediction intervals can benefit a researcher in several ways including verifying the instrument's accuracy requirements, performing system level checkouts, and increasing the validity of their data.

Aircraft wind-tunnel testing can be broken down into several key areas: performance, small configuration changes, and computational fluid dynamics (CFD) validation. An aircraft's drag coefficient (C_D) is considered to be one of the crucial performance parameters, especially with current interests in reduction of fuel consumption. According to the Advisory Group for Aerospace Research and Development (AGARD), for force measurement systems it is stated that for both a small configuration change and CFD validation a minimum detectable increment of 0.0001 (1 count) C_D should be required [1]. Performance testing requires a less stringent C_D accuracy of 0.0005. To understand these drag requirements in force units the following expression is used [2]:

$$\Delta D = qS\Delta C_D \quad (1)$$

where ΔD is the drag force accuracy requirement, q is the tunnel dynamic pressure, S is the model planform area, and ΔC_D is the desired drag coefficient accuracy. From this equation, it can be seen that the force measurement and drag coefficient accuracies are proportional to each other, scaled by the tunnel conditions and model planform area. Due to this relationship the uncertainty in both the tunnel conditions and model area will affect the force measurement requirement. For the purpose of

TABLE 1: Transonic Wind-Tunnel Model Parameters

| | NASA CRM | FAST-MAC |
|----------------------------|--------------|--------------|
| Balance | NTF-118 | NTF-117 |
| S (ft ²) | 3.01 | 6.06 |
| q (lbs/ft ²) | 1314 to 1990 | 1595 to 1996 |
| ΔD (lbs) | 0.396 | 0.967 |

this example it is assumed that the force measurement system is the only uncertainty in C_D .

From Equation 1, the drag force accuracy requirements can be solved, if the other parameters are known. From recent wind-tunnel testing, the model dimensions and tunnel conditions can be used to estimate the test requirements and compare against actual measurement accuracies. Table 1 lists the wind-tunnel model parameters from the Fundamental Aerodynamics Subsonic/Transonic-Modular Active Control (FAST-MAC) and Common Research Model (CRM) tests, which were both conducted at the NASA Langley Research Center (LaRC) National Transonic Facility (NTF) [3–5].

The ΔD values in Table 1 use the model planform area and the lowest dynamic pressure of the tunnel condition to give the minimal measurement accuracy requirements. These values can be compared to the quoted two-standard deviation balance accuracies for axial force which are 0.91 and 5.99 lbs for the NTF-118 and NTF-117 force balances, respectively. From this it is seen that neither balance can make a reliable 1 drag count measurement for the given model and tunnel parameters. Due to this realization that 1 drag count is not feasible, the FAST-MAC testing increased the requirement to 5 counts, which is only achievable for high dynamic pressures [6].

Wind-tunnel model systems (WTMS) are becoming ever more complex with increased instrumentation and high pressure lines, which bridge the metric (sensing) and non-metric (fixed) ends of a balance, such as the FAST-MAC model. Fouling, especially hard fouling that results from inadvertent contact, will impact the predictive capability of the balance. Understanding the instrument’s uncertainty can be used to help validate the performance of the calibration model used for the instrument with the increased balance bridging via check loads and prediction intervals to ensure that research goals can be met.

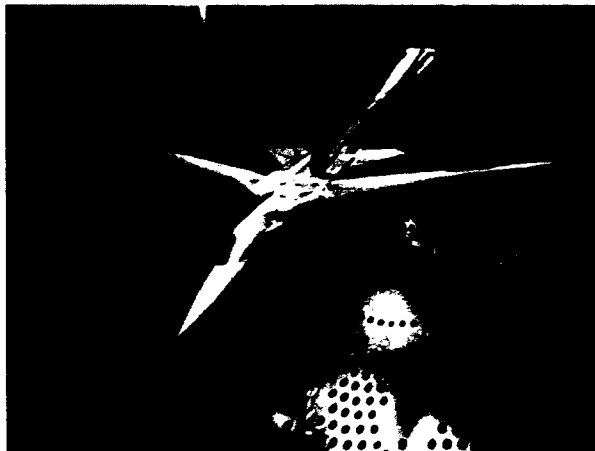


FIG. 1: FAVOR WTMS in the NASA GRC 8x6 ft Supersonic Wind Tunnel (Credit: NASA)

A recent study of several transonic wind tunnels in the United States, Facility Analysis Verification and Operational Reliability (FAVOR) project, attempted to gain insight into differences that may exist between selected facilities [7]. The objectives of the study included understanding and comparing facility processes, test methods, techniques, procedures, data-reduction methods, flow quality, and acquired aerodynamic data. In order to accomplish these objectives a wind-tunnel model was assembled with a force balance and support sting, which form the WTMS. This WTMS remained as a single piece until all testing was completed to help reduce variability due to assembling the WTMS, as shown in Figure 1. The results from this study were inconclusive in determining the root cause of differences that were observed between facilities. Consistent check loads and use of a prediction interval may have been helpful to either validate the WTMS and/or help determine cross-facility differences.

Strain-gage force balances are considered to be the most reliable method of force measurement for wind-tunnel models. Force balances have been incrementally innovated over several decades to the current state, which provides exceptional accuracy and precision [8–10]. However, there are no current accepted standard methods for quantifying and stating inherent uncertainties in force balance measurements. Force balances do not fall under the jurisdiction of the National Institute of Standard and Technology (NIST), who create standards and uncertainty qualifications for most

measurement systems. The responsibility of quantifying the uncertainty is left to the users and manufacturers, which tend to create myriad solutions.

The Internal Balance Technology Working Group (IBTWG) was formed under the Ground Testing Technical Committee of the American Institute of Aeronautics and Astronautics (AIAA) and was tasked with facilitating dialogue between the technology users. A recommended practices document for the calibration and use of strain-gage balances was released by the IBTWG in an effort to help standardize how balances are calibrated and how data are handled and processed [11]. Within this document little to no information is provided on how balance accuracy should be quoted. Additionally, the document lacks discussion of a rigorous check-load process for ensuring the performance of force balances for research goals.

Currently, NASA LaRC uses two standard deviations, 2σ , of the back-computed residuals for the calibration loads for quoting the balance accuracies [12]. This method of quoting uncertainty assumes that the variance is constant throughout the calibration range and only includes the modeling error. From response surface methods (RSM), the variance of a model is found to be not constant through out the calibration range, due to modeling error [13]. Several papers and the IBTWG-II have shown interest in the need for a standardized rigorous quoted accuracy for strain-gage balances [14–16].

1.1 BACKGROUND

1.1.1 STRAIN GAGE BALANCES

Direct measurement of aerodynamic forces acting on a wind-tunnel model remains a critical ground test technology [17]. Multi-dimensional strain-gage balances still remain the paradigm for ground test force measurement, due to their high accuracy and good repeatability. Strain-gage balances are a series of complex structural springs or flexures that are optimized to isolate individual load components to certain flexures, where an example is shown in Figure 2. Foil strain gages are attached to the flexures in order to provide a voltage response to the local deformations when arranged in Wheatstone bridges, i.e. a function of the applied loads.

Prior to use, the electrical response of a balance to applied loads is characterized by estimating a mathematical model that relates the balance outputs to known loads. Due to the structural complexity of internal force balances, the typical mathematical

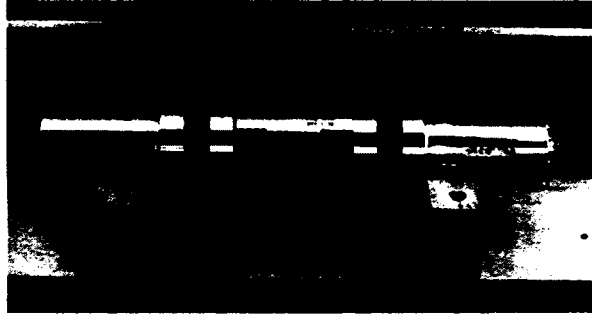


FIG. 2: Internal Strain-Gage Balance, NASA NTF Family (Credit: NASA)

model required for the response is of higher order, typically second or third order. Strain-gage balances are primarily linear in response, but second order or higher terms are generally used to increase the accuracy of the balance. These higher order terms can originate from manufacturing and instrumentation inaccuracies. From over 30 years of balance calibration experience, a quadratic Taylor series mathematical model was determined to best represent the output of single-piece internal strain-gage balances. The current standard model implemented at NASA LaRC for force balances is shown in Equation 2 [18]:

$$rF_k = \beta_{0_k} + \sum_{i=1}^6 \beta_{i_k} F_i + \sum_{i=1}^6 \sum_{j=i}^6 \beta_{ij_k} F_i F_j + \epsilon \quad (2)$$

where rF_k is the k^{th} bridge response voltage, F_i are the applied forces and moments, β_i are the estimated calibration coefficients, and ϵ is the random error which has a zero mean and a variance of σ^2 . From this equation, it can be seen that during wind-tunnel testing the estimation of F_i , the applied forces and moments, is desired. With this formulation F_i cannot be solved directly through a closed form solution but maybe solved numerically by using an optimization/iterating routine such as Newton Raphson [18].

The forces and moments that are applied to the balance are assumed to act about a chosen virtual center. Typically, the virtual center, or balance moment center (BMC), is positioned in between the forward- and aft-cage sections. The balance coordinate system adheres to the right-hand rule convention as is shown in Figure 3. However, most wind tunnels prefer to implement an aerodynamic coordinate system where F_x and F_z have opposite signs from what is illustrated in the figure. This

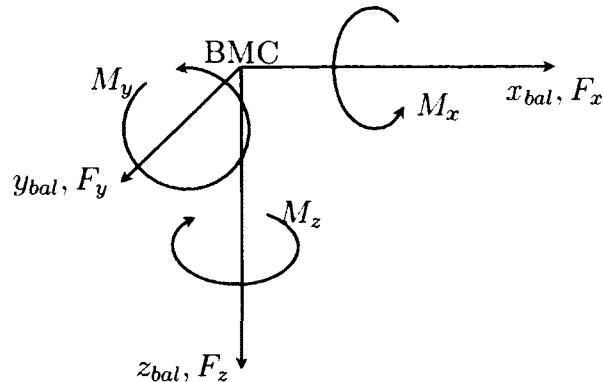


FIG. 3: Balance Coordinate System

was done historically, since normal force, F_z , and axial force, F_x , aerodynamically act in the negative directions of their associated axis, namely lift and drag. For the purpose of this paper the balance coordinate system shown in Figure 3 will be used exclusively, since physics equations are based upon this system.

1.1.2 LOAD APPLICATION SYSTEMS

For the balance characterization experiment, known loads are applied by either calibrated dead weights or by actuators through high accuracy load cells. Any system used to apply known loads will have uncertainties, thus an accepted practice is to use a system that is at least 4 times more accurate than the desired accuracy of the instrument being calibrated. Currently there are three methods for applying loads to a balance: a manual stand, single vector systems, or an automatic balance calibration system. Each of these system types will be explained in detail in the following sections.

1.1.3 MANUAL STAND

Traditionally, balances were calibrated on what is recognized as a manual stand, where loads were applied “manually” with dead weights. Manual stands employ a grooved calibration body that is attached to the balance where hangers can apply loads. Dead weight loads are applied through a series of knife-edges which allow a load to be placed at a specific point with no transfer of moments. To ensure that applied forces act in their primary direction, the balance has to remain nominally

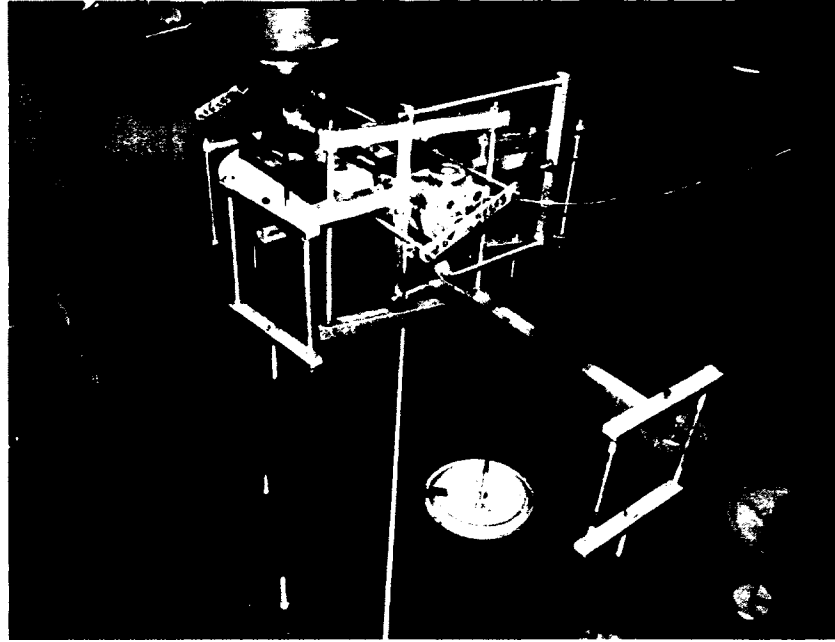


FIG. 4: Typical Manual Stand Calibration (Credit: NASA)

level. Cables and pulleys or bell cranks are required to apply loads to the balance for the axis components that are not aligned with the gravity vector, i.e. forces in the x - and y -component when the z -axis is aligned with gravity. An example of a balance calibration performed on a manual stand is shown in Figure 4.

Moments are applied to the balance by placing loads away from BMC. This can be accomplished by either placement of the knife-edge offset from BMC along the calibration body or the addition of moment arms to the calibration body. From this description of the manual stand, it can be realized that in order to apply multi-component loads, the hardware arrangement can be complex. Ensuring that all the applied forces are orthogonal can become laborious, since adjusting one load path may affect another. Due to this complexity of a 5- or 6-component load point, up to a full working day (8 hours) can be spent building up, adjusting the hardware and ultimately acquiring data. Due to this drawback, very few 5- or 6-component load points are used in a manual calibration load schedule.

Due to the restriction on multi-component loads, a one-factor-at-a-time (OFAT) load schedule was adopted and implemented for calibrations performed on a manual stand. An OFAT experiment varies one factor (load) while the others are held constant instead of simultaneously changing every factor. OFAT experimental designs

can lead to high numbers of points in order to extract the information required to estimate a calibration model. The OFAT balance calibration design that is employed by NASA LaRC contains up to 729-points in the load schedule [19, 20]. Typically, calibration times can be up to four weeks using this type of experiment, due to the long setup durations. Long experiment duration not only consumes resources, but can also lead to variability in the data obtained, since day-to-day differences can exist in the experimental environment, such as calibrator or laboratory temperature and humidity.

A manual stand is not relegated to only load schedules based on an OFAT design, however specifying large numbers of multi-component loads is inefficient on these systems. A recent study demonstrated the practicality of a Box-Behnken Design (BBD) using a manual stand [20]. A BBD is a fundamental response surface methodology (RSM) design, which implements statistical principles to gather more information about a system with fewer points than an OFAT method. A BBD can be modified so that it only requires a series of 2 or 3-component loads for a 6-component system, which can be done with moderate efficiency on a manual stand.

Despite the limitations of manual calibration, it is seen as one of the most precise methods to apply known loads to a balance. The precision and results of the calibration are affected by the operator that performed the experimentation due to the precision of manually setting up the equipment required to apply a load. This precision is due to the fact that there is high transparency of the system, since it is easy to see how the load is being applied to the balance.

The main disadvantage of a manual stand is the infrastructure that is required. Calibration hardware is unique for a given balance or range of balances, which requires a large inventory of hangers, moment arms and weights. The systems also have a large footprint, requiring up to a volume of a 20-foot sided cube or more for large (3,000 to 20,000 pounds) capacity balances. For large loads, weight baskets are required to locate the dead weights and to apply the load to the balance.

1.1.4 SINGLE VECTOR BASED

NASA LaRC has developed the single-vector concept, which can apply a multi-component load, up to six-components, while using a single load pan [21, 22]. This greatly reduces the hardware complexity required to generate a multi-component load, and ultimately can reduce the size of a load schedule.

Unlike the manual stand, which was discussed in the previous section, the single-vector concept is based on orienting the balance through a range of angles. The balance coordinate system is rotated from a gravity reference, where the gravity vector may have no zero components. In contrast, the manual stand requires that one component of the normalized-gravity vector be unity while the other two components are zero, which signifies that the balance is level in one dimension. Using the single-vector concept, this directly results in up to a three-component force vector since the applied force is in the gravity direction:

$$\mathbf{F} = m\mathbf{g} = F_{applied} \begin{bmatrix} G_x & G_y & G_z \end{bmatrix} \quad (3)$$

where \mathbf{F} is the applied force vector in pounds, m is the attached mass in slugs, \mathbf{g} is the gravity vector in ft/s², $F_{applied}$ is the applied force in pounds, and G_i is the i^{th} component of the normalized gravity vector. For the remainder of this paper the term gravity vector will signify the normalized gravity vector, a unitless, unit vector of gravity. Moments are then generated by positioning the load point of the system at a location other than BMC. The moment vector, \mathbf{M} , can be found by the cross product of the load point position, \mathbf{r} , with respect to BMC against the force vector as depicted in Figure 5:

$$\mathbf{M} = \mathbf{r} \times \mathbf{F} \quad (4)$$

From Equations 3 and 4, it can be seen that infinite load combinations can be made by varying the gravity vector and load point position. In practice, the load combinations are limited by the achievable balance orientations and the discrete load positions available. The angle measurement system (AMS) package provides knowledge of the orientation of the balance with respect to the earth frame.

Currently, NASA LaRC has two operational single-vector based systems, the Single-Vector System (SVS) and the In-Situ Load System (ILS). Illustrations of both the SVS and ILS are shown in Figures 6 and 7, respectively. The major difference between the SVS and ILS, is that the SVS can locate the load point at BMC, thus it can apply pure forces. This zero-moment case is possible, since the roll bearing of the system encompasses the entire balance and allows for the center of the bearings' axes to be collocated with BMC. It is assumed that the center of the bearings axes is the point at which the load is acting, since moments should not be transferred about the bearing axes.

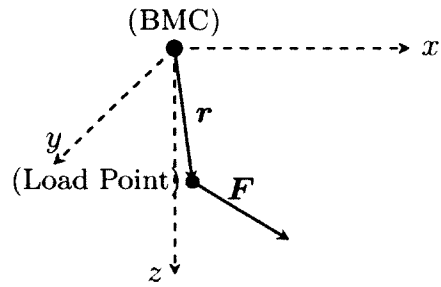


FIG. 5: Single-Vector Concept Diagram

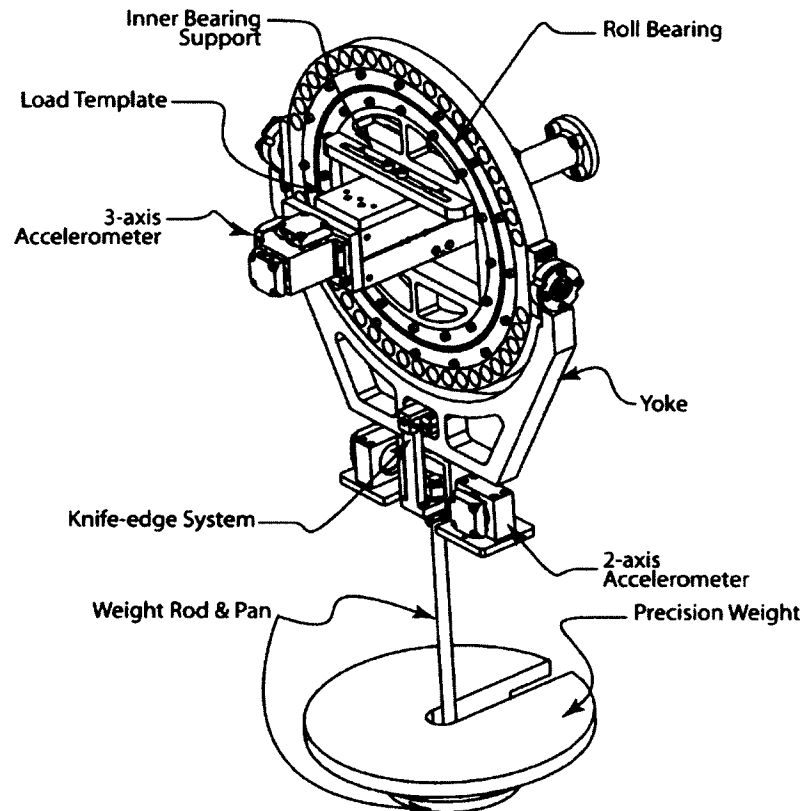


FIG. 6: Single-Vector System Mechanical Assembly (Credit: NASA)

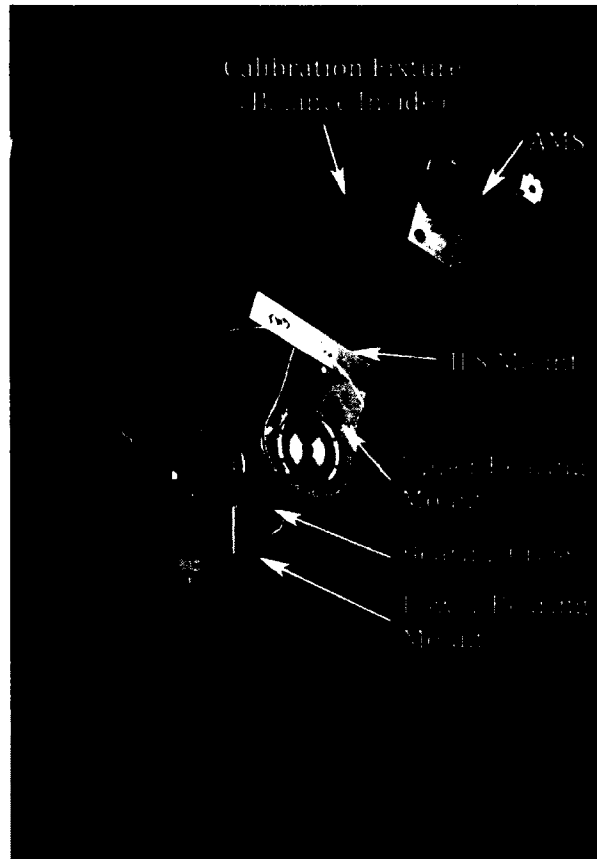


FIG. 7: In-Situ Load System Assembly (Credit: NASA)

Both the mechanical complexities of the SVS and ILS are greatly reduced from the manual stand, which helps simplify the uncertainty characterization of the systems. Since both systems are independent of the balance type and load rating, the physical properties of the systems can be quantified once, unlike the manual stand which has hardware configurations for each balance.

The SVS was originally designed for the calibration of a force balance as opposed to the ILS which was designed to apply check loads to a WTMS. For this reason the load point of the ILS is positioned away from BMC, which will always produce a moment when more than one force component is generated. There are some restrictions due to having a permanent offset load point, since the applied moments may overload the balance before the forces. It should be noted that this does not make the ILS incapable of calibrating a balance. With a carefully designed load schedule the ILS could be used for in-situ balance calibrations or full characterization of a WTMS.

A typical SVS calibration can be completed within 3 to 4 days, which is a vast improvement over a manual calibration which can take at least 4 weeks [21]. These improvements are not only due to mechanical simplicity of the system, but also due to the procedures used. RSM principles are used to help gather more information with the load points that were taken. A typical SVS calibration only comprises 64 points compared to the 729 of the OFAT manual calibration. The SVS load schedule is based on a central composite design (CCD), where every point has changes to all the components. Changing of all the components simultaneously is inefficient on a manual stand due to all the hardware changes, but since the SVS relies on balance orientation and position to change load conditions, it is efficient. One of the drawbacks of this type of load schedule is that it becomes hard to directly analyze the data, since in an OFAT design the primary sensitivities can be seen directly in load increments.

Since the balance orientation is directly measured using an AMS, it is not required to set the balance precisely as specified in a load schedule. With the measured balance orientation, the actual applied force and moment can be computed by using the mass properties and dimensions of the SVS or ILS. These computed loads and measured responses are then used to build a regression model.

The advantage of the single-vector based systems is that they reduce the hardware that is required to calibrate balances, since only one hardware set is required with

only one load basket. The system also can easily use more efficient load schedules that reduce the calibration duration, cost, and increases robustness. A complete SVS system, including a repositioning system, requires a small footprint when compared to the manual stand.

A disadvantage of the single-vector based systems is the hardware cost for both the load hardware and the repositioning system. Manufacturing costs of single-vector based systems are high due to the level of fidelity required to ensure exact placement of the load point. The repositioning system is also not common for calibration laboratories or wind-tunnel facilities, due to the range requirements of pitch and roll. The repositioning system used for the SVS at NASA LaRC has the ability to pitch and roll a balance 360 degrees. Both the current SVS and ILS have limitations on the maximum applied load, due to bearing load limits. A maximum pan weight of 3,000 and 5,000 lbs can be applied to the SVS and ILS, respectively. For balances that have high load capacities, other calibration systems must be employed.

1.1.5 AUTOMATIC SYSTEMS

Automatic balance calibration systems (ABCSs) have been developed in an effort to reduce the time and cost it takes to fully calibrate a balance by automating the process. Generally, ABCSs have been developed for high capacity balances, greater than 6,000 pounds, which are used at transonic or large-scale wind-tunnel facilities. Several ABCSs have been developed and implemented at facilities around the world, such as at Triumph Force Measurement Systems in San Diego, the European Transonic Wind-Tunnel (ETW), and at the Japanese Aerospace Exploration Agency (JAXA) [23–25]. The ABCS systems used by Triumph and JAXA are shown in Figures 8 and 9, respectively, with annotations showing the actuator layouts.

Typically, these systems rely on electrically controlled actuators to simultaneously apply loads through high-precision load cells. These load cells are placed in line with the actuator and attached to a fixed base and a calibration body via double knife-edge pivots, which are shown in Figure 10. The calibration systems can be designed to either reposition the balance back to a level position (JAXA) or measure the attitude of the balance calibration body (Triumph). These systems can also be used to calibrate lower capacity balances by using lower capacity load cells. Since the accuracies of the applied loads are a function of the load cells used, the load cells are chosen to best suit the balance design loads or the load schedule.

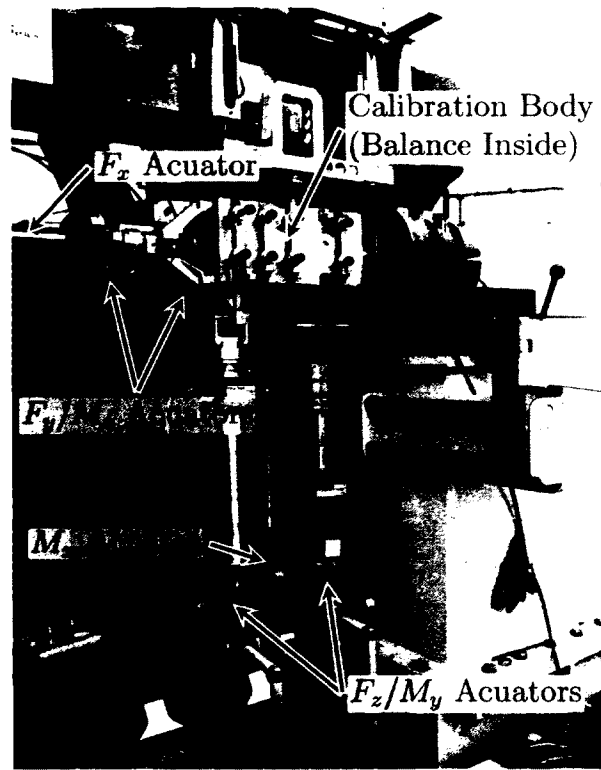


FIG. 8: Triumph ABCS (Credit: Triumph)

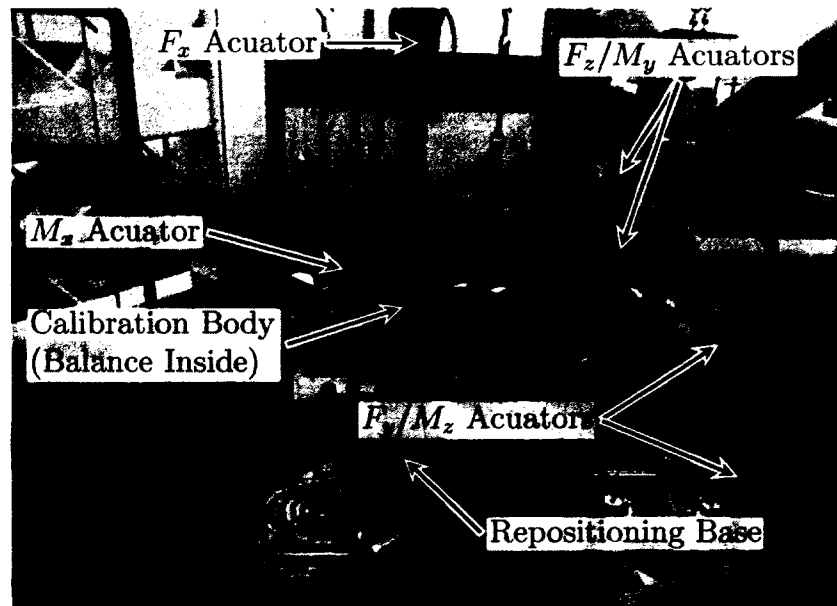


FIG. 9: Japan Aerospace Exploration Agency (JAXA) ABCS (Credit: JAXA)

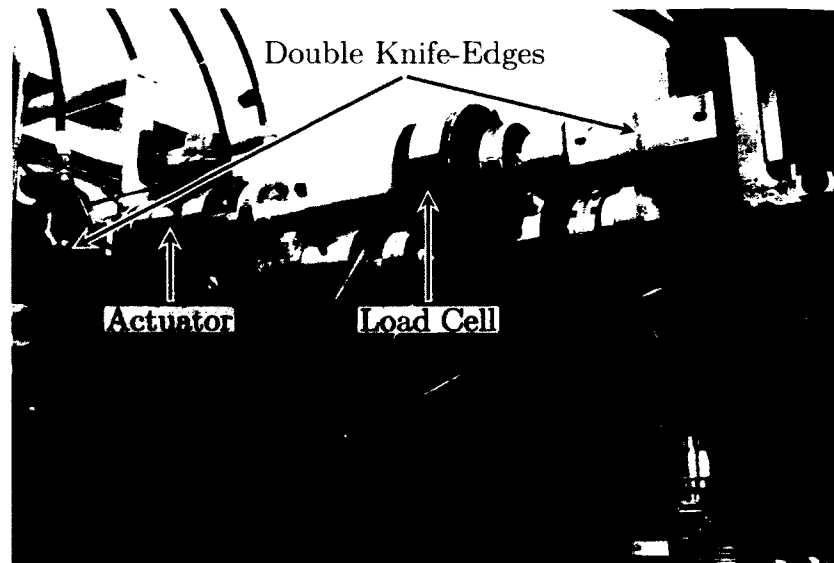


FIG. 10: Load Chain Detail (Credit: Triumph)

The advantages of an ABCS include rapid calibrations, the ability to apply pure moments, and accommodation of a range of balances. The short duration of a calibration results from automation and the lack of hardware configuration changes between load points. Pure moments are applied to the balance with the use of two-way actuators. To produce a pure moment, force coupling of two actuators is implemented.

The disadvantages of these systems include the purchase cost, maintenance, and its mechanical complexity. The ABCS uses multiple actuators and balance alignment measuring systems which all need to be precisely aligned and positioned. Any uncertainty in the positioning of the actuators or measurement devices will lead to calibration biases. Additionally, the mechanical complexity increases the initial purchase and maintenance costs.

1.1.6 OVERVIEW

From the descriptions of each of the available calibration systems, it can be seen that each system has uncertainties in the applied loads, which will affect the overall performance of a force balance. With the ever increasing need for tighter tolerances on measurement requirements to meet researchers' goals, it becomes more important

to quantify the uncertainties of balances. Quantification of calibration system uncertainty is a step to understanding the overall balance uncertainty. As discussed earlier, statistical analysis techniques can be used to provide validation of an instrument's output requirements.

CHAPTER 2

LITERATURE STUDY

From a search of relevant work, three papers were selected that best represent the research goals of this dissertation. These papers are related to the uncertainty quantification of force balances using different methods. Kammeyer and Rueger implemented propagation of error to the equations for regression coefficients [16]. Reis et al. attempt to incorporate error in the calibration process and the regression process to an overall balance output uncertainty [26]. Tripp and Tchong develop an approach which applies the regression model variance to the balance output [15]. In the following sections each of the chosen papers are reviewed in detail.

2.1 ESTIMATION OF THE UNCERTAINTY IN INTERNAL BALANCE CALIBRATION THROUGH COMPREHENSIVE ERROR PROPAGATION

2.1.1 REPORT OVERVIEW

Kammeyer and Rueger implemented error propagation in order to calculate the uncertainty of the regression coefficients. Error propagation is a common technique, standardized by several metrology organizations, to quantify the uncertainty of instrument systems [27, 28]. This method is applied to wind-tunnel balances which are multivariate precision instruments. Error propagation was used to estimate the uncertainty due to the errors in the applied load to the regression coefficients for a balance. This method was derived for the calibration and balance systems that are currently used at the Boeing facilities in St. Louis, Missouri, as shown in Figure 11. The calibration setup uses cup and cone load points to align the applied loads, and moment arms for applying forces away from BMC.

2.1.2 ANALYSIS OF CONTENT

Mathematical Model

The balances that are typically used at Boeing facilities in St. Louis are multi-piece or TASK[®] type balances. These types of balances tend to exhibit a change in

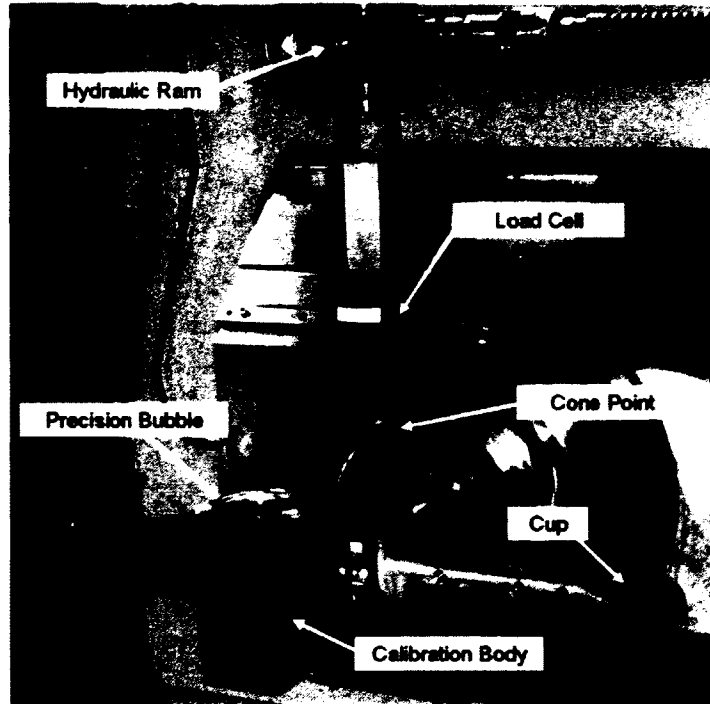


FIG. 11: Boeing St. Louis Calibration Setup

the primary sensitivities depending on the direction of an applied force, i.e. different sensitivity for positive and negative normal force. From the AIAA recommended practices for wind-tunnel balances it is suggested to use third order or absolute value terms to allow for modeling of this behavior [11]. The model that is used in this paper contains first and second order absolute value terms:

$$rF_i = \beta_0 + \sum_{i=1}^k \beta_i F_i + \sum_{i=1}^k \sum_{j=i}^k \beta_{i,j} F_{i,j} + \sum_{i=i}^k \beta_{2i} |F_i| + \sum_{i=1}^k \beta_{2i,i} F_i |F_i| \quad (5)$$

where β_0 , β_i , $\beta_{i,j}$, β_{2i} and $\beta_{2i,i}$ are the intercept, linear, quadratic, linear absolute and quadratic absolute calibration coefficients, respectively. Several model coefficients were selected to be included in the model, which included both the non-absolute linear, absolute linear and non-linear terms, and six two-factor interactions ($N_1 N_2$, $N_1 S_1$, $N_2 S_2$, $S_1 S_2$, $N_1 RM$, and $N_2 RM$). No justification for the selection of these terms was provided; previous knowledge of this balance is assumed to have been used for this model selection.

TABLE 2: Calibration Variance Inflation Factors

| Number | Term | VIF | Number | Term | VIF |
|--------|-------|------|--------|--------|------|
| 1 | N1 | 7.0 | 19 | N1 | 8.4 |
| 2 | N2 | 6.9 | 20 | N2 | 8.2 |
| 3 | S1 | 10.4 | 21 | S1 | 14.4 |
| 4 | S2 | 9.5 | 22 | S2 | 14.2 |
| 5 | RM | 13.6 | 23 | RM | 13.8 |
| 6 | AF | 13.9 | 24 | AF | 14.6 |
| 7 | N1^2 | 7.7 | 25 | N1* N1 | 6.8 |
| 8 | N2^2 | 7.5 | 26 | N2* N2 | 6.7 |
| 9 | S1^2 | 15.2 | 27 | S1* S1 | 11.2 |
| 10 | S2^2 | 15.1 | 28 | S2* S2 | 10.3 |
| 11 | RM^2 | 13.3 | 29 | RM* RM | 13.6 |
| 12 | AF^2 | 14.3 | 30 | AF* AF | 13.9 |
| 13 | N1*N2 | 1.2 | | | |
| 14 | N1*S1 | 1.1 | | | |
| 15 | N1*RM | 1.0 | | | |
| 16 | N2*S2 | 1.3 | | | |
| 17 | N2*RM | 1.0 | | | |
| 18 | S1*S2 | 2.2 | | | |

The resulting selected model coefficients with the Variance Inflation Factors (VIF) are tabulated in Table 2. The VIF is a measure of multicollinearity in the experimental design used for estimating the calibration coefficients [29]. A VIF value of unity is ideal, values below 5 indicate low correlation, and values above 10 signify moderate correlation. While a value above 10 indicates multicollinearity, a built model which includes a term with such VIF values will still provide meaningful information. From Table 2, it can be seen that multiple terms have a VIF greater than 10 which signify moderate correlation between the model terms. This signifies that the experimental design used is inadequate for estimating the selected model terms. The high VIF values can also be due to the inclusion of absolute model terms, which can be seen to automatically correlate with other terms, for example $|x_i|$ is similar to x_i^2 near the origin.

Error Propagation Method

Error propagation is a method in which the uncertainties from multiple error sources can be propagated through a data reduction equation using a Taylor series expansion. This method can be used to estimate the uncertainty of an output r from a data reduction equation with the knowledge of the elemental uncertainties u_{x_i} and correlation $\rho_{i,j}$:

$$u_r^2 = \sum_{i=1}^N \left(\frac{\partial r}{\partial x_i} u_{x_i} \right)^2 + 2 \sum_{i=1}^N \sum_{j=i+1}^N \frac{\partial r}{\partial x_i} \frac{\partial r}{\partial x_j} \rho_{i,j} u_{x_i} u_{x_j} \quad (6)$$

As noted in the paper, one of the issues with using error propagation methods is that the correlation between terms must be known or assumed. For example, when a force is applied to the balance offset from balance moment center, a moment will be generated. Any uncertainty in the location of the load will result in an uncertainty in the moments, since:

$$\mathbf{M} = \mathbf{r} \times \mathbf{F} \quad (7)$$

where \mathbf{M} is a moment vector, \mathbf{r} is a distance vector, and \mathbf{F} is a force vector. It can also be seen that the uncertainty of the moments will scale with the magnitude of the applied loads. Thus, there exists a correlation between moments if they are quantified as separate elements:

$$u_r^2 = \left(\frac{\partial r}{\partial M_1} u_{M_1}^2 \right)^2 + \left(\frac{\partial r}{\partial M_2} u_{M_2}^2 \right)^2 + \rho_{12} \frac{\partial r}{\partial M_1} \frac{\partial r}{\partial M_2} u_{M_1} u_{M_2} \quad (8)$$

To avoid any correlations, it is proposed that the moment uncertainties are based on the applied force and position by Equation 7. With this formulation, the uncertainty for a moment can be represented by applied weights, W_1 and W_2 , and the axial-distance to the load point x , for a pitching moment case:

$$u_r^2 = \left(\frac{\partial r}{\partial W_1} u_{W_1}^2 \right)^2 + \left(\frac{\partial r}{\partial W_2} u_{W_2}^2 \right)^2 + \left(\frac{\partial r}{\partial x} u_x^2 \right)^2 \quad (9)$$

By using this approach, the balance loads are represented by the applied load pans at given distances. This removes almost all of the correlation that exists in the other derivation, such that load pan 1 does not affect load pan 2, and so forth.

In the paper, uncertainty sources are broken up into three groups: the gravity referenced balance orientation Θ , the applied loads \mathcal{L} , and the electrical outputs \mathcal{E} . The balance orientation is represented by the pitch θ , roll ϕ , and yaw ψ Euler angles of the calibration body, such that $\Theta = (\phi, \theta, \psi)$. The load \mathcal{L} is used to contain the applied load W , and x , y and z coordinates of the point at which the load is placed, such that $\mathcal{L} = (W, x, y, z)$. It should be noted that only the applied load magnitude is accounted for since the applied loads are assumed to act only in the z-direction. In the case that is presented, up to three load pans can be applied for a given load

TABLE 3: Boeing St. Louis Calibration System Uncertainty Estimates

| Variable | Description | Range or nom. value | Standard uncertainty | | Units | Correlation |
|---|----------------------------------|------------------------|----------------------|--------|-------|-------------|
| | | | Systematic | Random | | |
| Orientation | | | | | | |
| θ, φ | Pitch/roll of cal body | 0/±90, 180 | 0.0048 | 0.0048 | deg | None |
| θ | Pitch alignment of bell crank | 0 | 0.0048 | | deg | SLS |
| φ | Roll of extended bar | 0, ±45 | 0.06 | | deg | SLS |
| ψ | Yaw alignment of bell crank | 0 | 0.06 | | deg | SLS |
| Applied loads | | | | | | |
| W1, W2, W3 | Dead weight | 0 to 600 | 0.005 %Rdg | | lbf | None |
| W1, W2, W3 | Load cell | 0 to 2000 | | 1 | lbf | None |
| Point of application | | | | | | |
| x, y | Loc. of cup on cal body | 0, ±3 | 0.002 | | in | SLS |
| z | Loc. of cup on cal body | -1.25, -5.9 | 0.03 | | in | SLS |
| x, z | Loc. of cup on roll arms | 0, -1 | 0.03 | | in | SLS |
| y | Loc. of cup on roll arms | 10 | 0.01 | | in | SLS |
| x, y, z | Loc. of cup on extended bar | -6, 6 | 0.004 | | in | SLS |
| x, y | Loc. of extended bar on cal body | 0 | 0.005 | | in | SLS |
| Electrical response and excitation | | | | | | |
| N1...AF | Output | -20 to +20 | 0.015 %Rdg | | mV | None |
| e1...e6 | Excitation | 10 | 0.015 %Rdg | | V | None |

* SLS: Similar load series

point. The electrical outputs \mathcal{E} contain up to six bridge voltages each representing a single-component of the balance (rF_1, \dots, rF_6) and the respective excitation voltages (E_1, \dots, E_6).

Uncertainty Estimates

The uncertainties of each variable in the data reduction equation must be quantified prior to implementing the error propagation methods. These were either directly measured, by taking multiple measurements, or estimated using engineering judgment. A summary of the uncertainties and their estimated values that are taken into account in this paper are tabulated in Table 3.

From Table 3, it can be seen that all the sources have a systematic value, but only pitch/roll of the calibration body have values for random error. The uncertainty of the body pitch and roll angles are considered to be on the order of magnitude of the resolution of the bubble level used. The systematic component is due to manufacturing and assembly errors in the calibration body, which remain the same for the entirety of the calibration. The random component originates from the re-leveling of the calibration body for each load point in the load schedule.

Most of the other quantities are assumed to only have systematic uncertainty, since it is assumed that the experimental setup does not change during the course of the calibration. For example the location of the load point should not change and

therefore is a constant offset from the nominal value due to machining and assembly errors.

Error Propagation Implementation

The error propagation method, as described earlier, was implemented by the authors on the calibration coefficients for each of the six balance components. In this paper, the partial derivatives in the error propagation were not evaluated directly, instead the jitter method was implemented which estimates the partial derivative numerically [28]. This method requires that each uncertainty source is perturbed by a small amount, Δx_i , and the partial derivative is estimated by:

$$\frac{\partial r}{\partial x_i} \approx (r_{x_i + \Delta x_i} - r_{x_i}) / \Delta x_i \quad (10)$$

where r is the output of the data reduction equation that is a function of x_i , r_{x_i} is the computed r value at $(x_i + \Delta x_i)$, and r_0 is the r value at x_i . This method of estimating the partial derivatives allows for complex data reduction equations that may have non-linear or trigonometric terms. After all the partial derivatives have been estimated they can be entered into an overall uncertainty estimation of a variable r using a formulation similar to Equation 6. Since applying error propagation to the calibration coefficients is of interest, these coefficients, $\hat{\beta}$, can be estimated by least squares [29]:

$$\hat{\beta} = (X'X)^{-1}X'Y \quad (11)$$

where $\hat{\beta}$ is the estimated coefficients, X and Y are applied loads and recorded voltages, respectively:

$$X = \begin{bmatrix} F_{1,1} & F_{2,1} & \cdots & F_{6,1} & F_{1,1}^2 & F_{1,1}F_{2,1} & \cdots & F_{6,1}^2 \\ \vdots & \vdots & \ddots & \vdots & \vdots & \vdots & \ddots & \vdots \\ F_{1,N} & F_{2,N} & \cdots & F_{6,N} & F_{1,N}^2 & F_{1,N}F_{2,N} & \cdots & F_{6,N}^2 \end{bmatrix} \quad (12)$$

$$Y = \begin{bmatrix} rF_{1,1} & \cdots & rF_{6,1} \\ \vdots & \ddots & \vdots \\ rF_{1,N} & \cdots & rF_{6,N} \end{bmatrix} \quad (13)$$

where $F_{i,j}$ is the i^{th} load component at the j^{th} load point, and similarly for $rF_{i,j}$ voltages. By substituting Equations 12 and 13 into Equation 11, the coefficients

become a function of the applied forces, moments and balance voltages. As previously discussed, if the error propagation is applied to the force and moments directly, correlation will exist. The $F_{i,j}$ terms can be rewritten such that they are only a function of the most basic variables, which were defined earlier:

$$F_{i,j} = F(\mathcal{L}_1, \mathcal{L}_2, \dots) = F(W_1, W_2, \dots, x_1, x_2, \dots, z_3) \quad (14)$$

Equations 12, 13 and 14 are substituted into 11 in order to reduce $\hat{\beta}$ to the simplest variables. With this formulation, the partial derivatives can be taken with respect to the individual uncertainty sources, so that no correlation exists. Note that it is not recommended to expand Equation 11 to the variables of Equation 14, since a properly written computer script can be used to propagate through the equations and ultimately estimate the partial derivatives.

After the uncertainties of the calibration coefficients have been estimated, they can be recast as intervals about $\hat{\beta}$. The half-width of the interval about $\hat{\beta}$ can be expressed as ku , where k is a coverage factor and $u_{\hat{\beta}}$ is the combined uncertainty of $\hat{\beta}$. Typically the coverage factor k can be expressed simply as 2, which is approximately a 95% confidence interval, although a t-statistic which is a function of the desired confidence level and the appropriate degrees of freedom is more appropriate.

Results

The uncertainties for each of the calibration coefficients were calculated for each of the six-components of the balance. Kammeyer and Rueger stated that a calibration coefficient can be deemed insignificant if $|\hat{\beta}| < ku_{\hat{\beta}}$, essentially that the interval about $\hat{\beta}$ contains zero. This method is compared against the standard 95% statistical confidence interval, which is used for significance testing. Tables 4 and 5 contain a summary of the results from the jitter and the standard statistical methods for both the forces and moments, respectively. In these tables, the first column contains the estimate for each respective coefficient, the second and third columns are highlighted in black if the respective method found the coefficient to be significant, and the fourth column contains the ratio of the two uncertainty methods.

From Table 4, it can be seen that the jitter intervals are larger than the statistical intervals only for three coefficients, signified by a u_j/u_r ratio greater than unity. This shows that the jitter method allows for more coefficients to be labeled as significant

TABLE 4: Comparison of Jitter and Regression Uncertainties for Forces

| Term | Normal | | | | Side | | | | Axial | | | |
|--------|----------|--------|-------|-------|----------|--------|-------|-------|----------|--------|-------|-------|
| | Coeff | Jitter | Regr. | Uj/Ur | Coeff | Jitter | Regr. | Uj/Ur | Coeff | Jitter | Regr. | Uj/Ur |
| N1 | 1.8E-01 | | | 0.82 | -2.3E-03 | | | 0.16 | 7.3E-04 | | | 0.39 |
| N2 | 1.5E-01 | | | 0.99 | -9.0E-04 | | | 0.17 | 3.8E-04 | | | 0.41 |
| S1 | -1.1E-03 | | | 0.22 | 5.0E-02 | | | 0.89 | 5.3E-05 | | | 0.24 |
| S2 | -3.5E-04 | | | 0.22 | 4.8E-02 | | | 0.86 | 9.0E-05 | | | 0.24 |
| RM | 3.1E-04 | | | 0.11 | -1.1E-03 | | | 0.03 | 2.4E-08 | | | 0.27 |
| AF | 1.2E-04 | | | 0.05 | -8.2E-05 | | | 0.03 | 2.1E-02 | | | 0.12 |
| N1*2 | -4.4E-08 | | | 0.88 | -2.9E-08 | | | 0.48 | -1.7E-08 | | | 0.48 |
| N2*2 | 3.7E-09 | | | 0.90 | -3.3E-09 | | | 0.33 | -1.6E-08 | | | 0.49 |
| S1*2 | 5.7E-09 | | | 0.30 | -3.3E-08 | | | 0.75 | 2.0E-09 | | | 0.24 |
| S2*2 | -2.0E-08 | | | 0.28 | -5.1E-08 | | | 0.79 | -2.0E-09 | | | 0.25 |
| RM*2 | -4.8E-09 | | | 0.38 | 3.6E-08 | | | 0.06 | -5.8E-09 | | | 0.27 |
| AF*2 | 6.1E-09 | | | 0.17 | 8.2E-10 | | | 0.15 | -2.8E-09 | | | 0.14 |
| N1*N2 | 5.7E-09 | | | 1.57 | -5.1E-08 | | | 0.28 | -9.0E-08 | | | 0.69 |
| N1*S1 | 6.7E-08 | | | 0.40 | 3.6E-07 | | | 0.35 | 9.5E-09 | | | 0.22 |
| N1*RM | 2.1E-08 | | | 0.12 | -9.8E-08 | | | 0.03 | 1.6E-10 | | | 0.30 |
| N2*S2 | 9.1E-08 | | | 0.39 | 4.0E-07 | | | 0.34 | 6.1E-09 | | | 0.22 |
| N2*RM | 1.9E-08 | | | 0.12 | -1.3E-07 | | | 0.03 | -5.1E-09 | | | 0.30 |
| S1*S2 | -7.0E-10 | | | 0.16 | 3.3E-09 | | | 1.41 | -4.4E-09 | | | 0.34 |
| N1 | -1.3E-03 | | | 0.70 | 9.6E-05 | | | 0.60 | 8.2E-05 | | | 0.36 |
| N2 | -1.9E-03 | | | 0.64 | 2.6E-04 | | | 0.43 | 9.2E-05 | | | 0.37 |
| S1 | -2.1E-05 | | | 0.42 | -9.6E-04 | | | 0.83 | -1.5E-05 | | | 0.22 |
| S2 | 2.9E-04 | | | 0.40 | -8.5E-04 | | | 0.84 | 3.6E-05 | | | 0.22 |
| RM | 4.7E-04 | | | 0.55 | -8.3E-04 | | | 0.09 | -8.1E-05 | | | 0.27 |
| AF | -1.1E-04 | | | 0.25 | 1.5E-05 | | | 0.22 | -2.9E-05 | | | 0.12 |
| N1* N1 | -1.2E-07 | | | 0.89 | 1.9E-07 | | | 0.14 | 3.5E-09 | | | 0.50 |
| N2* N2 | -1.7E-07 | | | 1.05 | 1.1E-07 | | | 0.15 | -2.1E-08 | | | 0.51 |
| S1* S1 | 8.0E-09 | | | 0.17 | -1.0E-08 | | | 0.71 | 1.1E-09 | | | 0.28 |
| S2* S2 | 1.8E-08 | | | 0.17 | -2.8E-09 | | | 0.74 | -9.1E-10 | | | 0.29 |
| RM* RM | 7.5E-09 | | | 0.10 | 1.9E-08 | | | 0.02 | 1.5E-09 | | | 0.26 |
| AF* AF | -5.7E-09 | | | 0.05 | 1.3E-09 | | | 0.02 | 2.0E-09 | | | 0.13 |

than the statistical method. This result can be attributed to several possible reasons. One of these is that several uncertainty sources are omitted or underestimated. Another reason can be due to the previously stated large VIF values for the calibration model, since the presence of multicollinearity will produce wide intervals for the statistical method.

Unlike the forces, the moments show a higher regression coefficient rejection rate by the jitter method. Observation of the roll component shows only four terms left in the final model, which is sparse for calibration models. This high rejection rate for the roll and the pitch components may suggest that the jitter method produces intervals that are too wide for these two components. These wide intervals can be due to large uncertainties in the positioning of the applied load, which do not affect the force components. It is interesting to note that yaw has a smaller interval as seen in the other two moments. Without an understanding of how yawing moment is applied to the balance or the equations used to model the applied loads, it is difficult to pass judgment on this observation. One possible reason is that yawing moment may only be a function of a single load instead of multiple loads that may affect the pitch and roll components.

TABLE 5: Comparison of Jitter and Regression Uncertainties for Moments

| Term | Pitch | | | | Yaw | | | | Roll | | | |
|--------|----------|--------|-------|-------|----------|--------|-------|-------|----------|--------|-------|-------|
| | Coeff | Jitter | Regr. | Uj/Ur | Coeff | Jitter | Regr. | Uj/Ur | Coeff | Jitter | Regr. | Uj/Ur |
| N1 | 4.5E-01 | | | 9.70 | -9.1E-03 | | | 0.73 | -1.1E-04 | | | 6.37 |
| N2 | -4.4E-01 | | | 9.74 | 8.6E-05 | | | 0.74 | 1.1E-04 | | | 7.18 |
| S1 | 2.5E-03 | | | 1.23 | 1.2E-01 | | | 1.16 | -1.7E-04 | | | 3.75 |
| S2 | 3.3E-05 | | | 1.20 | -1.2E-01 | | | 1.11 | -2.1E-05 | | | 3.74 |
| RM | -3.7E-03 | | | 1.96 | -2.8E-04 | | | 0.05 | 9.4E-02 | | | 3.13 |
| AF | -1.8E-06 | | | 0.14 | 2.1E-04 | | | 1.47 | -5.2E-04 | | | 0.17 |
| N1^2 | -5.2E-08 | | | 5.22 | 4.5E-08 | | | 0.69 | -9.5E-08 | | | 7.68 |
| N2^2 | -4.8E-08 | | | 5.45 | 6.2E-08 | | | 0.59 | -5.0E-08 | | | 8.15 |
| S1^2 | -2.7E-08 | | | 1.30 | -8.9E-08 | | | 1.17 | -1.9E-09 | | | 3.85 |
| S2^2 | 1.8E-08 | | | 1.08 | 1.2E-07 | | | 1.22 | -2.4E-08 | | | 3.94 |
| RM^2 | -1.9E-08 | | | 2.47 | 9.5E-09 | | | 0.20 | 6.9E-09 | | | 5.04 |
| AF^2 | 7.3E-09 | | | 0.63 | -1.5E-08 | | | 0.16 | -8.7E-09 | | | 0.70 |
| N1*N2 | 4.4E-08 | | | 7.80 | 8.2E-08 | | | 0.87 | -2.0E-09 | | | 12.26 |
| N1*S1 | 1.1E-07 | | | 1.91 | 6.4E-07 | | | 0.83 | 1.3E-08 | | | 3.66 |
| N1*RM | -9.7E-09 | | | 2.22 | -2.6E-07 | | | 0.06 | 4.7E-08 | | | 3.56 |
| N2*S2 | -1.6E-07 | | | 1.83 | -1.1E-06 | | | 0.79 | 4.1E-08 | | | 3.67 |
| N2*RM | -6.7E-08 | | | 2.23 | 3.8E-07 | | | 0.06 | 4.8E-08 | | | 3.57 |
| S1*S2 | 3.2E-09 | | | 0.99 | -2.1E-08 | | | 1.88 | 7.0E-09 | | | 6.39 |
| N1 | -1.9E-03 | | | 4.01 | 1.3E-05 | | | 0.85 | 4.7E-04 | | | 5.83 |
| N2 | 2.5E-03 | | | 4.09 | -3.2E-04 | | | 0.81 | 1.4E-04 | | | 6.15 |
| S1 | 6.3E-05 | | | 1.82 | -2.0E-03 | | | 1.11 | 1.1E-04 | | | 3.50 |
| S2 | -1.9E-04 | | | 1.59 | 2.4E-03 | | | 1.11 | 3.9E-04 | | | 3.52 |
| RM | 1.9E-04 | | | 3.23 | -7.6E-05 | | | 0.31 | -4.0E-05 | | | 6.97 |
| AF | -9.6E-05 | | | 1.41 | 1.7E-04 | | | 0.25 | 1.3E-04 | | | 0.88 |
| N1* N1 | -8.2E-08 | | | 8.14 | 2.6E-07 | | | 0.55 | 2.9E-08 | | | 6.06 |
| N2* N2 | 8.7E-08 | | | 8.47 | -2.2E-07 | | | 0.55 | -9.5E-09 | | | 8.56 |
| S1* S1 | 1.1E-08 | | | 0.91 | -1.7E-08 | | | 1.31 | -1.9E-09 | | | 4.35 |
| S2* S2 | 1.3E-09 | | | 0.88 | 2.8E-08 | | | 1.35 | 2.0E-09 | | | 4.47 |
| RM* RM | 1.4E-09 | | | 1.93 | 2.0E-08 | | | 0.05 | -8.3E-09 | | | 3.09 |
| AF* AF | -7.2E-09 | | | 0.13 | -1.8E-08 | | | 0.03 | -3.9E-09 | | | 0.16 |

The authors investigated the effect of having correlated uncertainties using the jitter method. The ratios of the uncertainties including and excluding correlations for each of the coefficients are plotted in Figure 12. From this it can be seen that the inclusion of correlation affect the moments more than forces. Additionally, it can be seen that correlated uncertainties have negligible effect on axial force. Axial force is unaffected by the correlation in the uncertainties, since it is insensitive to load point position and balance angle, which are the uncertainties where correlation is assumed.

2.1.3 SUMMARY AND CONCLUSIONS

It was demonstrated that error propagation can be applied to the calibration coefficients of a balance. The results from the uncertainty analysis provided similar coefficient selection when compared against a standard statistical method for the force components. The error propagation method appeared to be too aggressive for pitch and roll moments, by rejecting most of the model terms. This can be attributed to the uncertainties on the load position being too large. Typically, the uncertainty of the load point should be much smaller than the values documented in this paper. NASA LaRC performs quality assurance measurements using a coordinate measurement machine with an uncertainty of 0.0003 in., which is an order of

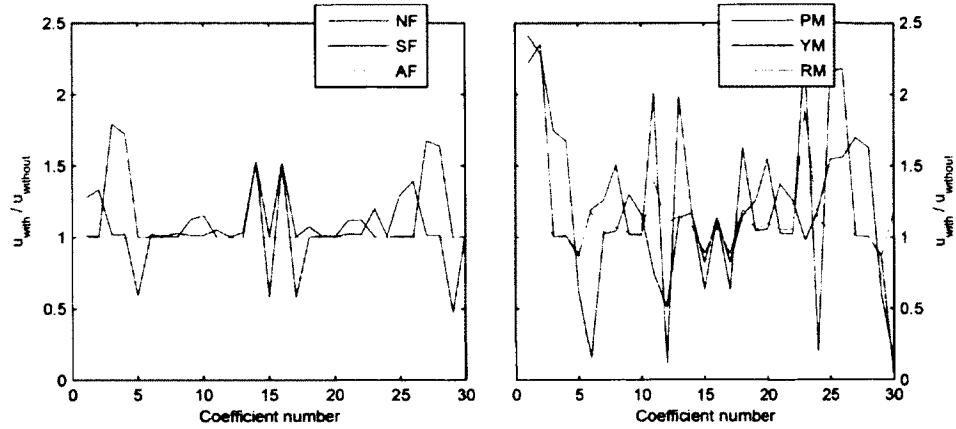


FIG. 12: Ratio of Including and Excluding Correlation

magnitude better than the value quoted in this paper for positional accuracy. The correlation which was assumed was shown to affect the moment components more than the forces, which can also be attributed to having large uncertainties on the load point. Without inspecting the equations which represent the forces and moments, it is difficult to pass judgment of the true contributor to the observed large moment uncertainties.

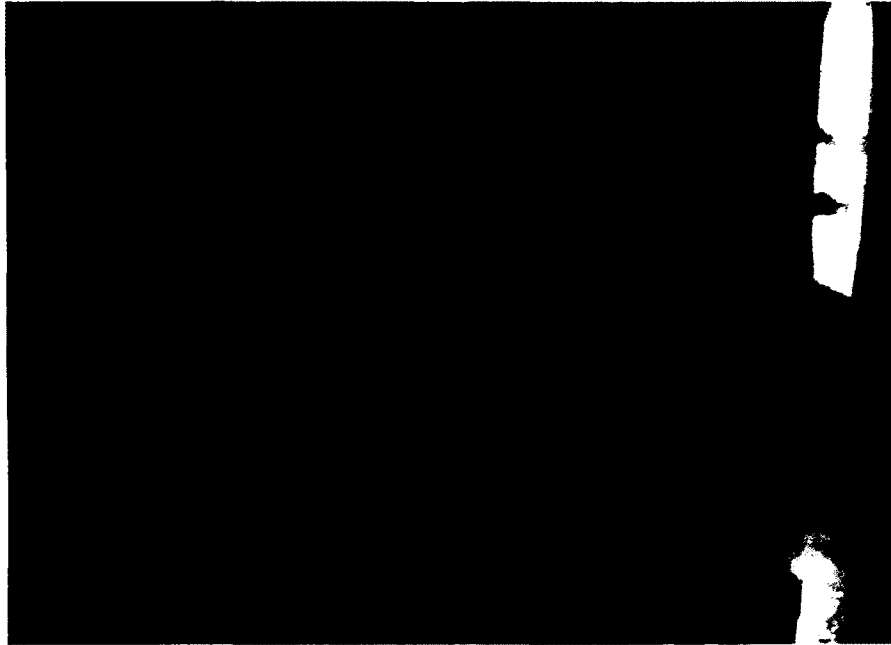


FIG. 13: TA-2 Balance Calibration Setup

2.2 CALIBRATION UNCERTAINTY ESTIMATION OF A STRAIN-GAGE EXTERNAL BALANCE

2.2.1 REPORT OVERVIEW

Reis builds upon research that was previously developed to estimate the uncertainty of the estimated load of a balance [30]. The method proposed in this paper uses generalized least squares to integrate uncertainty from the applied calibration loads into the regression model and balance output. The method was developed to be used for an external force balance used at the TA-2 wind-tunnel in Brazil. The calibration experiment performed used a series of pulleys and weight pans to apply loads to the balance as shown in Figure 13. The calibration setup to apply the loads will introduce errors into the regression process and overall balance output. The uncertainties of this system are investigated and integrated into the regression process.

2.2.2 ANALYSIS OF CONTENT

Calibration Estimation

Prior to using an external balance, a calibration model must be assumed and estimated. A mathematical model is used to represent the relationship of the applied forces, F_i , to the balance voltages, rF_i . Force balances have been found to exhibit slight nonlinearities and are generally modeled with a second-order Taylor series:

$$F = \sum_{i=1}^k \beta_i(rF_i) + \sum_{i=1}^k \sum_{j=i}^k \beta_{ij}(rF_i)(rF_j) + \epsilon \quad (15)$$

From Equation 15, it can be seen that the relationship formed sets the applied force to be a function of the balance voltages. This is generally considered to be an inverse regression method, where the roles of the factors and responses are reversed. It is widely accepted that the mathematical model used for balances relate the balance output voltage, the measured value, as a function of the applied load [11]. Research in the properties of inverse regression showed that for a simple one-component linear case, negligible differences were found between the inverse and classical method for precise instruments [31]. For a multivariate case of inverse regression it can be argued that this method sums and multiplies noise sources, assuming that the noise in the voltages rF_i are larger than the loads F_i , since the loads were the controlled variable in the calibration experiment. Furthermore, it is difficult to conceptualize and control the design space for inverse regression, since the experimental design is built using the load and not the voltages. This may lead to non-orthogonal design matrices X , which may lead to high multicollinearity. Using the inverse regression method, the X and Y matrices can be defined as:

$$X = \begin{bmatrix} rF_{1,1} & rF_{2,1} & \cdots & rF_{6,1} & rF_{1,1}^2 & rF_{1,1}rF_{2,1} & \cdots & rF_{6,1}^2 \\ \vdots & \vdots & \ddots & \vdots & \vdots & \vdots & \ddots & \vdots \\ rF_{1,N} & rF_{2,N} & \cdots & rF_{6,N} & rF_{1,N}^2 & rF_{1,N}rF_{2,N} & \cdots & rF_{6,N}^2 \end{bmatrix} \quad (16)$$

$$Y = \begin{bmatrix} F_{1,1} & \cdots & F_{6,1} \\ \vdots & \ddots & \vdots \\ F_{1,N} & \cdots & F_{6,N} \end{bmatrix} \quad (17)$$

where $rF_{i,j}$ is the i^{th} voltage component at the j^{th} load point in the calibration table, and $F_{i,j}$ follows the same logic but with the forces. Note that the X matrix has

TABLE 6: Sample Load Table

| Loading number | F_1 | F_2 | F_3 | F_4 | F_5 | F_6 |
|----------------|-------|-------|-------|-------|-------|-------|
| 1 | 0 | 0 | -80 | 0 | -40 | 0 |
| 27 | 80 | 0 | 0 | -40 | 0 | 0 |
| 46 | 0 | -80 | 0 | 0 | 0 | -48 |
| 58 | 0 | -80 | 0 | 0 | 40 | 0 |
| 69 | 0 | 0 | 80 | 0 | 0 | 48 |

TABLE 7: Sample Load Schedule

| Loading number | Weights (kg) | | | | | | | | | | | | | |
|----------------|--------------|-------|-------|-------|-------|-------|-------|-------|-------|----------|----------|----------|----------|----------|
| | T_1 | T_2 | T_3 | T_4 | T_5 | T_6 | T_7 | T_8 | T_9 | T_{10} | T_{11} | T_{12} | T_{13} | T_{14} |
| 1 | 0 | 0 | 0 | 0 | 0 | 0 | 0 | 0 | 0 | 20 | 20 | 20 | 60 | 0 |
| 27 | 80 | 0 | 0 | 0 | 0 | 0 | 40 | 0 | 0 | 0 | 0 | 40 | 0 | 0 |
| 46 | 0 | 0 | 0 | 80 | 0 | 0 | 0 | 0 | 0 | 0 | 0 | 0 | 0 | 0 |
| 58 | 0 | 0 | 0 | 40 | 0 | 40 | 0 | 0 | 0 | 40 | 0 | 0 | 40 | 0 |
| 69 | 0 | 0 | 40 | 0 | 0 | 40 | 20 | 20 | 20 | 20 | 0 | 0 | 0 | 0 |

the voltages expanded as a second-order Taylor series to satisfy Equation 15. A portion of the load table and schedule which were used to calibrate the external balance are tabulated in Tables 6 and 7, respectively, where the load table is the ideal resultant applied load and the schedule is the actual loads applied to the load pans. With generalized least squares (GLS) the regression coefficients were estimated using experimental data by:

$$\hat{\beta} = (X'V^{-1}X)^{-1} (X'V^{-1}Y) \quad (18)$$

where V is the variance-covariance matrix, such that $\text{Var}(\epsilon) = \sigma^2V$ [29], ϵ is the zero-mean random error, and σ^2 is the variance of ϵ . For the case of ordinary least squares V is assumed to be the identity matrix I , since it is assumed that there is no heteroskedasticity or serial correlation in the data points. GLS is generally used when heteroskedasticity and/or correlation exist in the error structure of the data. When V is an unequal diagonal matrix, the data is assumed to have unequal variance, but if the off-diagonal terms are non-zero then correlation is also assumed. In Equation 18 the variance-covariance structure of the random error essentially applies a weight of $1/V$ to the data, in turn applying more emphasis on the points with the lowest variance. The variance-covariance matrix of the estimated calibration coefficients $\hat{\beta}$ is found by:

$$V_{\hat{\beta}} = \text{Var}(\hat{\beta}) = \sigma^2 (X'V^{-1}X)^{-1} \quad (19)$$

After the $\hat{\beta}$ are estimated from the calibration data using Equation 18, a new voltage measurement x can be used to estimate a corresponding load \hat{y} :

$$\hat{y} = x\hat{\beta} \quad (20)$$

Applying the variance operator on Equation 20 and the results of Equation 19 results in:

$$V_{\hat{y}} = XV_{\hat{\beta}}X' = \sigma^2 X (X'V^{-1}X)^{-1} X' \quad (21)$$

Equation 21 can be used to represent the variance in \hat{y} , but this must not be confused with a confidence or prediction interval. $V_{\hat{y}}$ only represents one σ or 67% of the sample population.

Variance Matrix Derivation

Ideally, the covariance matrix V is known prior to estimating $\hat{\beta}$ and based on known trends in the random error. It is proposed in this paper that V can be estimated using both prior knowledge and regression results after an initial estimation of $\hat{\beta}$. The covariance matrix was represented as a combination of the uncertainty in the applied load V_W and the uncertainties in the balance readings V_X :

$$V = V_W + CV_XC' \quad (22)$$

where C is a matrix of the coefficient sensitivities, which allow for the units of V_X to be converted to the units of V_W . The C matrix was formed by taking the partial derivatives of Equation 18 for a given response as shown in Equation 23. This equation is simplified from the full Jacobian where all the elements are partial derivatives, since the off-diagonal derivatives are zeros as shown.

$$C = \begin{bmatrix} \frac{\partial Y_{1,1}}{\partial X_{1,1}} & 0 & \cdots & 0 & \frac{\partial Y_{1,1}}{\partial X_{2,1}} & \cdots & 0 \\ 0 & \frac{\partial Y_{1,2}}{\partial X_{1,2}} & \cdots & 0 & 0 & \cdots & 0 \\ \vdots & \vdots & \ddots & \vdots & \vdots & \ddots & \vdots \\ 0 & 0 & \cdots & \frac{\partial Y_{1,N}}{\partial X_{1,N}} & 0 & \cdots & \frac{\partial Y_{1,N}}{\partial X_{6,N}} \end{bmatrix} \quad (23)$$

The V_W matrix is of dimension N by N , where N is the number of load points, and is only comprised of diagonal terms. Each element along the diagonal represents the uncertainty that each load point acquires due to the calibration system uncertainty. This was set to include the frictional forces in the pulleys, cable misalignment, and the uncertainty of the applied weights.

The V_X matrix represents the uncertainties in the balance readings for a given load point. This was said to be estimated by performing three identical calibrations to the balance in quick succession. It should be noted that three samples is generally not considered to be sufficient to provide an estimate of variation. The V_X matrix was built by computing the variance and covariance for each voltage combination at every data point, as shown:

$$V_X = \begin{bmatrix} u(X_{1,1}X_{1,1}) & u(X_{1,1}X_{1,2}) & \cdots & u(X_{1,1}X_{1,N}) & u(X_{1,1}X_{2,1}) & \cdots & u(X_{1,1}X_{6,N}) \\ u(X_{1,2}X_{1,1}) & u(X_{2,1}X_{1,2}) & \cdots & u(X_{2,1}X_{1,N}) & u(X_{2,1}X_{2,1}) & \cdots & u(X_{2,1}X_{6,N}) \\ \vdots & \vdots & \ddots & \vdots & \vdots & \ddots & \vdots \\ u(X_{1,N}X_{1,1}) & u(X_{1,N}X_{1,2}) & \cdots & u(X_{1,N}X_{1,N}) & u(X_{1,N}X_{2,1}) & \cdots & u(X_{1,N}X_{6,N}) \\ u(X_{2,1}X_{1,1}) & u(X_{2,1}X_{1,2}) & \cdots & u(X_{2,1}X_{1,N}) & u(X_{2,1}X_{2,1}) & \cdots & u(X_{2,1}X_{6,N}) \\ \vdots & \vdots & \ddots & \vdots & \vdots & \ddots & \vdots \\ u(X_{6,N}X_{1,1}) & u(X_{6,N}X_{1,2}) & \cdots & u(X_{6,N}X_{1,N}) & u(X_{6,N}X_{2,1}) & \cdots & u(X_{6,N}X_{6,N}) \end{bmatrix} \quad (24)$$

Since the second terms of Equation 22 requires $\hat{\beta}$, an initial regression with $V = V_W$ must be performed. After the initial regression is built a second regression is made with the full Equation 22.

2.2.3 RESULTS AND DISCUSSION

Variance Matrix Estimation

The V_W matrix was calculated using type B analysis, which uses methods other than the statistical analysis of repeated observations [27]. The uncertainty of the dead weights was estimated from the maximum possible error of the weight and a rectangular distribution. The quoted maximum error for a 10 kg weight is around 1 gram, which is 0.01% and is equivalent to precision weights. Using 1 gram as the limits of the rectangular distribution the uncertainty can be calculated from [28]:

$$u = A/\sqrt{3} \quad (25)$$

TABLE 8: Friction Estimates

| Load Cell | Applied Weight (g) |
|-----------|--------------------|
| X_1 | 2 |
| X_2 | 2 |
| X_3 | 32 |
| X_4 | 5 |
| X_5 | 8 |
| X_6 | 5 |

where u is the uncertainty, and A is the limits of the rectangular distribution. The resulting uncertainty for the applied weights is 0.58 grams for a 10 kg applied load. If two or more 10 kg weights are used in a stack to apply a load, the uncertainties from each individual weight are combined into a total uncertainty.

A second uncertainty source added to the V_W matrix was the resolution of the calibration system. The resolution was the ability to overcome friction in the pulleys used to apply several load components. Reis accomplished this by applying load increments of 1 gram to corresponding load pans and detecting significant differences in the load cell output. This method was conducted for each of the six load cells in the calibration system and determined the worst case and the results are tabulated in Table 8. From the results, X_3 displays the highest required load before a perceptible change in the output occurred. The method used to determine the friction in the system is shown in Figure 14. In this figure, every five readings was a load series of 8 grams. Using Equation 25 the uncertainty for X_3 due to friction was calculated to be 18.5 grams. Once the two sources of uncertainties were estimated, they were summed together to form the V_W matrix.

The V_X matrix was calculated using the methods described earlier, where the variance and covariance were calculated for all the terms in Equation 24. After V_W and V_X were defined, the total variance matrix was found by using Equation 22. With an estimated V , a second regression was performed to calculate the final estimate of $\hat{\beta}$, which includes the variance structure of the calibration system.

Regression Results

The calibration coefficients and uncertainties for the final calibration are tabulated in Table 9. Note that \hat{p} and $u_{\hat{p}}$ are the estimated calibration coefficients $\hat{\beta}$ and

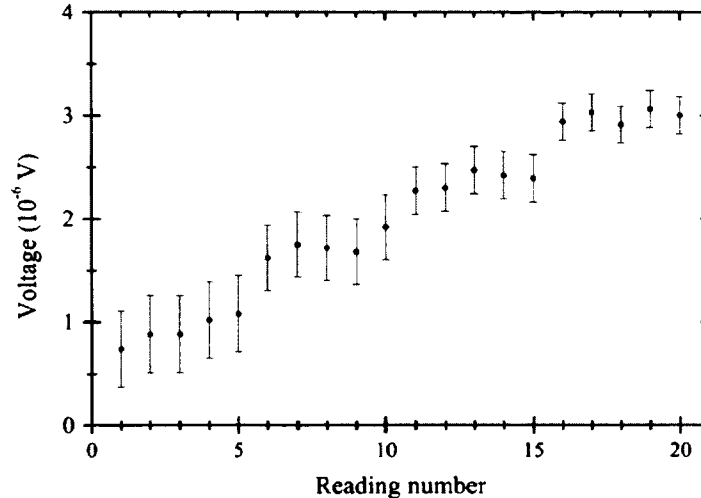


FIG. 14: Calibration Resolution for X_6

the coefficient uncertainty, respectively. The coefficient uncertainty $u_{\hat{p}}$ was defined as the square root of the diagonals of $V_{\hat{\beta}}$, from Equation 19. The ratio $u_{\hat{p}}/\hat{p}$ was used to determine the significance of terms for the model. If $u_{\hat{p}}/\hat{p}$ was less than unity, then the term was insignificant, since an interval of $u_{\hat{p}}$ about \hat{p} contained zero. From this, it can be seen that several terms were insignificant, namely a_4 , a_{14} , a_{16} , a_{18} , a_{19} , and a_{25} .

The applied forces were estimated using Equation 20 from the recorded balance voltages. Additionally, the uncertainties for these measurements were estimated using Equation 21. The results from these calculations on five points from the calibration are tabulated in Table 10, which are loads listed in Table 6. Note that this is Table 8 from the paper, which was labeled to have units of Newtons and Newton-meters, but it seems that those unit conversions were never made. From a quick comparison between the estimated and the desired loads, it can be seen that the estimates were very close to the desired loads in Table 6. Furthermore, the uncertainties that were quoted are relatively constant despite different load conditions for each load point. Assuming that 80 kg is the full scale load for F_1 , F_2 and F_3 , the uncertainties are around 0.02% of full scale, which is typical for modern wind-tunnel force balances.

Chi-squared, χ^2 , and reduced chi-squared, χ_{red}^2 , statistics were calculated from the results of the regression. The χ^2 is a measure of goodness of model fit to the calibration data. The χ^2 is equal to the number of degrees of freedom in the model;

TABLE 9: Regression Estimates for Y_1

| Parameter | $\hat{\rho}$ | $u_{\hat{\rho}}$ | $u_{\hat{\rho}}/\hat{\rho}$ |
|-----------|--------------|------------------|-----------------------------|
| a_1 | 3.525849 | 0.001298 | 2717.01 |
| a_2 | 0.011648 | 0.001295 | 8.99 |
| a_3 | -0.008513 | 0.001440 | -5.91 |
| a_4 | -0.000051 | 0.000649 | -0.08 |
| a_5 | 0.001620 | 0.000534 | 3.04 |
| a_6 | 0.004485 | 0.000501 | 8.95 |
| a_7 | 0.000557 | 0.000058 | 9.53 |
| a_8 | -0.000234 | 0.000163 | -1.43 |
| a_9 | -0.001408 | 0.000185 | -7.60 |
| a_{10} | -0.000242 | 0.000082 | -2.92 |
| a_{11} | -0.000164 | 0.000067 | -2.43 |
| a_{12} | -0.000087 | 0.000064 | -1.35 |
| a_{13} | 0.000862 | 0.000364 | 2.36 |
| a_{14} | -0.000599 | 0.000864 | -0.69 |
| a_{15} | 0.000705 | 0.000383 | 1.84 |
| a_{16} | 0.000283 | 0.000309 | 0.91 |
| a_{17} | 0.000658 | 0.000290 | 2.27 |
| a_{18} | 0.000080 | 0.000447 | 0.17 |
| a_{19} | -0.000127 | 0.000430 | -0.29 |
| a_{20} | -0.000369 | 0.000350 | -1.05 |
| a_{21} | -0.000635 | 0.000328 | -1.93 |
| a_{22} | -0.000197 | 0.000088 | -2.23 |
| a_{23} | 0.000177 | 0.000155 | 1.13 |
| a_{24} | 0.000583 | 0.000144 | 4.04 |
| a_{25} | -0.000001 | 0.000057 | -0.02 |
| a_{26} | 0.000250 | 0.000117 | 2.13 |
| a_{27} | 0.000443 | 0.000058 | 7.63 |

TABLE 10: Estimated Applied Forces and Uncertainties, kg (Force) or kg m (Moments)

| Load | F_1 | u_{F1} | F_2 | u_{F2} | F_3 | u_{F3} | F_4 | u_{F4} | F_5 | u_{F5} | F_6 | u_{F6} |
|------|--------|----------|---------|----------|---------|----------|---------|----------|---------|----------|---------|----------|
| 1 | 0.011 | 0.012 | -0.016 | 0.013 | -79.816 | 0.013 | -0.044 | 0.030 | -39.928 | 0.015 | 0.044 | 0.012 |
| 27 | 79.914 | 0.016 | 0.019 | 0.015 | -0.014 | 0.014 | -39.903 | 0.014 | -0.039 | 0.020 | 0.008 | 0.014 |
| 46 | 0.042 | 0.013 | -79.855 | 0.014 | 0.021 | 0.012 | 0.002 | 0.014 | 0.017 | 0.013 | -47.835 | 0.015 |
| 58 | 0.031 | 0.013 | -79.776 | 0.013 | -0.041 | 0.013 | -0.069 | 0.035 | -39.977 | 0.013 | -0.065 | 0.013 |
| 69 | 0.012 | 0.013 | 0.095 | 0.016 | 79.786 | 0.014 | 0.036 | 0.014 | -0.036 | 0.013 | 47.841 | 0.013 |

TABLE 11: Regression Goodness of Fit Results

| Load cell | χ^2 | χ_{red}^2 |
|-----------|----------|----------------|
| F_1 | 232.33 | 5.05 |
| F_2 | 271.65 | 5.91 |
| F_3 | 453.91 | 9.87 |
| F_4 | 67.69 | 1.47 |
| F_5 | 165.99 | 3.61 |
| F_6 | 529.83 | 11.52 |

in this case the degrees of freedom is $\nu = N - N_p$, where N_p is the number of estimated parameters. The reduced chi-square is simply defined as $\chi_{red}^2 = \chi^2/\nu$, thus a number near unity is desired. The χ^2 and χ_{red}^2 values for the resulting calibration are tabulated in Table 11. Both goodness of fit values were larger than what is desired, which indicate that a poor model fit was made. A poor model fit could have resulted from underestimates of the uncertainties of the load points were made or the inappropriate assumptions of the mathematical model.

2.2.4 SUMMARY AND CONCLUSIONS

A method for estimating and applying the uncertainty of the applied loads during a calibration to estimated loads and the regression process was developed. This method included the use of inverse regression, which simplifies the calibration problem but also may introduce unknown regression properties. The properties of multivariate inverse regression have not been well documented in the literature and violates several basic assumptions of methods of least squares and generalized least squares.

Calculated loads were computed from the estimated regression and the balance voltages showed results close to the applied loads. This signifies that the regression model provided reasonable residuals, but only points used to estimate the model were included in the estimate. It would be beneficial to have results from confirmation points that are different than the points used for the calibration, since they will exercise the prediction ability of the regression model. Additionally, other regression statistics could be useful to diagnosis the high χ^2 values that were calculated.

TABLE 12: Load Component Notations

| F_i | Component | Description |
|-------|-----------|-----------------|
| F_1 | F_x | Axial Force |
| F_2 | F_y | Side Force |
| F_3 | F_z | Normal Force |
| F_4 | M_x | Rolling Moment |
| F_5 | M_y | Pitching Moment |
| F_6 | M_z | Yawing Moment |

2.3 DETERMINATION OF MEASUREMENT UNCERTAINTIES OF MULTI-COMPONENT WIND TUNNEL BALANCES

2.3.1 REPORT OVERVIEW

Tripp and Tchong investigate and develop a method to calculate the uncertainty of the estimated loads that are applied to a force balance. Their method calculates an estimate of the uncertainty based on the results from a multivariate regression [15]. Tripp derives an interval about the measured balances voltages using the regression data and then converts the interval on the balance voltages into units of force and moments. This method required the derivation of a Jacobian matrix, which takes into account the non-linear terms present in the model.

2.3.2 ANALYSIS OF CONTENT

Calibration Model

Typically, wind-tunnel balances are capable of estimating forces and moments about all the major axes, i.e. six total components. A load vector can be formed to represent the six load components that are applied to the force balance:

$$F = [F_1, F_2, F_3, F_4, F_5, F_6] = [F_1, \dots, F_k] \quad (26)$$

where F_i is an individual force component and k is the total number of individual components. For this analysis we can define the first three terms as the forces and the latter three terms as the moments, as shown in Table 12.

Generally, force balances are primarily linear, but they are modeled with higher order functions to increase the overall accuracies. From previous balance history, it was determined that a second-order Taylor series fit the characteristics of a force balance to acceptable accuracy levels. Due to the second-order modeling, the load vector F must be expanded to represent this:

$$G(F) = [F_1^2, F_1F_2, \dots, F_1F_6, F_2^2, F_2F_3, \dots, F_6^2] \quad (27)$$

The entire expansion of the load vector is not shown due to length, but the expansion pattern can be seen. Expansion of the load vector results in k_{exp} terms which is equal to $\frac{k^2+k}{2}$, which is 21 for a k equal to 6. The load vector F and expanded load vector $G(F)$ can be combined into a single vector:

$$x = [1, F_i, G(F_i)] \quad (28)$$

where the 1 is included for estimation of an intercept of the model, or the balance voltage at zero-load. The x vector represents the factors, applied loads, to a balance and is used in the regression process and data processing. The balance output voltages can be represented as:

$$y = [rF_1, rF_2, rF_3, rF_4, rF_5, rF_6] = [rF_1, \dots, rF_k] \quad (29)$$

A mathematical relationship between the applied loads, x , and the output voltages, y , is assumed to represent the instrument behavior. As previously mentioned the assumed mathematical model for a balance is a second-order Taylor series:

$$y = x\beta + \epsilon = C_0 + FC_1 + G(F)C_2 + \epsilon \quad (30)$$

$$\beta = [C_0, C_1, C_2]$$

where β is a $(1 + k + k_{exp})$ by k matrix of coefficients that can be broken down into intercepts, linear terms and non-linear terms. The intercept terms are placed into the C_0 vector which is a k column vector. The linear C_1 is a k by k matrix comprised of pure linear and linear interactions coefficients, such that the C_1 matrix is only multiplied by linear load terms (i.e. F_i). The non-linear matrix C_2 is comprised of all the pure quadratics (F_i^2) and two-factor interactions (F_iF_j).

From Equation 30, it can be seen that when the balance is used to determine the applied loads, when voltages are known, no closed-form solution exist. For this

reason, the applied loads must be estimated by an iterative method, such as Newton-Raphson which is implemented in this paper.

Calibration Estimation

Prior to the use of a force-balance, the characteristics of the balance, the model coefficients β , are estimated experimentally. A well designed experiment can be used to estimate the coefficients. The matrices X and Y represent the design matrix and the balance response from the calibration experiment, respectively:

$$X = [x_1, \dots, x_N]' = \begin{bmatrix} 1 & F_1 & G(F_1) \\ \vdots & \vdots & \vdots \\ 1 & F_n & G(F_n) \end{bmatrix} \quad (31)$$

$$Y = [y_1, \dots, y_n]' = \begin{bmatrix} rF_{1,1} & \dots & rF_{k,1} \\ \vdots & \ddots & \vdots \\ rF_{1,n} & \dots & rF_{k,n} \end{bmatrix} \quad (32)$$

where n is the number of points in the experimental design. Substituting Equations 31 and 32 into Equations 30 results in:

$$Y = X\beta + E \quad (33)$$

where E is the zero-mean error associated with each load point in the calibration experiment. Due to the assumption that E has a mean of zero, it is assumed to be zero and the coefficients can be solved for by methods of least squares:

$$\hat{\beta} = (X'X)^{-1}X'Y \quad (34)$$

where $\hat{\beta}$ is an estimate of β . In order to calculate $\hat{\beta}$, the inverse of $(X'X)$ must exist, where the inverse will exist if the X matrix is of full column rank, i.e. rank 28 when k equals 6. An estimate of the residual error E for the data points is solved from Equation 33 and replacing β with the estimate $\hat{\beta}$:

$$\hat{E} = Y - X\hat{\beta} \quad (35)$$

The covariance matrix \hat{S} of the calibration is estimated from the residual errors \hat{E} :

$$\hat{S} = \frac{\hat{E}\hat{E}'}{n - (1 + k + k_{exp}) - 1} \quad (36)$$

where the denominator is the residual degrees of freedom. The diagonal of \hat{S} are the mean square error for each regression component of the balance. The covariance between any two calibration coefficient columns, such as $\hat{\beta}_m$ and $\hat{\beta}_n$ can be estimated by:

$$\Sigma_{\beta mn} = \text{Cov}(\hat{\beta}_m, \hat{\beta}_n) = \sigma_{mn}(X'X)^{-1} \quad (37)$$

where σ_{mn} is the (m, n) th element of the covariance matrix that is estimated by \hat{S} . The covariance $\Sigma_{\beta mn}$ for the coefficients are only a function of the design matrix X and scaled by the σ_{mn} . The uncertainty of the calibration coefficients $\delta\hat{\beta}_{i,j}$ is estimated by:

$$\delta\hat{\beta}_{i,j} = \sqrt{\sigma_{ii}[(X'X)^{-1}]_{jj}} \quad (38)$$

Output Vector Prediction and Interval

A new load x_e , not from the calibration schedule, can be applied to the force balance after the calibration experiments are completed. These new loads can be confirmation points, check loads, or aerodynamic forces applied to the balance. The actual voltage output of the balance from the load x_e is:

$$y_e = x_e\beta \quad (39)$$

This formulation assumes that β represents the true behavior of the balance, and that there are no error sources in the voltage. Typically voltage measurement systems have uncertainties and errors, which alter the true voltage y_e :

$$y_v = y_e + \epsilon_v = x_e\beta + \epsilon_v \quad (40)$$

where ϵ_v is the zero-mean measurement error in the voltage. The balance voltages can be forecast using the estimated model coefficients $\hat{\beta}$ from the calibration experiments by:

$$\hat{y}_e = x_e\hat{\beta} \quad (41)$$

It should be noted that there are no errors assumed, since the calibration coefficients were estimated assuming a zero-mean error. The difference between the

forecast output \hat{y}_e and the actual output y_v is the residual error e or error in the forecast:

$$e = \delta y = \hat{y}_e - y_v = x_e \hat{\beta} - x_e \beta - \epsilon_v = x_e (\hat{\beta} - \beta) - \epsilon_v \quad (42)$$

From this it is seen that the error in the forecast output is a combination of the difference between the estimated and true model of the balances and the measurement error. The covariance matrix of the estimated response can be found by:

$$\text{cov}(\hat{y}) = \text{cov}(x_0 \hat{\beta}) = x_0 \text{cov}(\hat{\beta}) x_0' = \sigma^2 x_0 (X'X)^{-1} x_0' \quad (43)$$

where $\text{cov}(\beta) = \sigma^2 (X'X)^{-1}$ and assumes homoscedasticity, which is the assumption that variance of the regression data is constant across all independent values. Alternatively, the covariance matrix δy for the residual of the response can be found by:

$$\text{cov}(\delta y) = \text{cov}(y - \hat{y}) = \text{cov}(x_0 \hat{\beta}) = \sigma_v^2 + x_0 \text{cov}(\hat{\beta}) x_0' = \sigma_v^2 + \sigma^2 x_0 (X'X)^{-1} x_0' \quad (44)$$

where σ_v^2 is the covariance matrix for the measured balance voltages. The value of σ_v^2 represents error associated with measuring a voltage, ϵ_v , and is independent of σ^2 . As mentioned before, the term σ contains errors both from the measurement of Y and the modeling error in the estimation of $\hat{\beta}$. A confidence interval formed using the covariance of \hat{y} from Equation 43 and a proper coverage factor. Since there are six balance components, six new predictions are made simultaneously and the coverage factor should be adjusted accordingly. Tripp and Tchong used a coverage factor that was estimated from a F-distribution with degrees of freedom of $(k, n - k - p)$, where p is the number of simultaneous estimates, at a $1 - \alpha$ confidence level. It is proposed that a confidence interval about the estimated voltage δy_n can be written as:

$$\delta y_n \equiv |y_n - x_e \hat{\beta}_n| < \sqrt{\hat{S}_{nn} (x_0 (X'X)^{-1} x_0') \frac{pK}{K - r - p} F_{p, K-r-p}} \quad (45)$$

where \hat{S}_{nn} is the n^{th} diagonal term of \hat{S} , and x_0 is the applied load. Equation 45 shows that the residual error should be less than the radical term and can be recast as:

$$\delta y_n = \sqrt{\hat{S}_{nn} (x_0 (X'X)^{-1} x_0') \frac{pK}{K - r - p} F_{p, K-r-p}} \quad (46)$$

where the interval δy_n should have a capture rate equivalent to the level of significance used.

Placing the Interval on Loads

The computed interval on the balance voltages δy_n does not provide useful information to the balance users. An interval on the estimated load of the balance is desired. Tripp and Tchong begin the development of such intervals by first letting the estimated load be denoted by \hat{F}_e , which is the inverse solution of Equation 30 for a given measured balance voltage y_v . With this, the interval based on the estimated load $\delta \hat{F}_e$ can be defined as:

$$\delta \hat{F}_e = F_e - \hat{F}_e$$

where F_e is the true applied load. Thus, $\delta \hat{F}_e$ contains uncertainties from the measurement error of the balance voltage and the error associated with estimating calibration coefficients. An interval on the expanded loads δx_e can be defined as:

$$\delta x_e = [0, \delta F_e, \delta G(F_e)] \quad (47)$$

The interval δx_e can be substituted into Equation 30, yielding:

$$\delta y_e = \delta x_e \beta = \delta F_e C_1 + \delta G(F_e) C_2 \quad (48)$$

Equation 48 does not have a closed-form solution for $\delta \hat{F}_e$, which is the desired quantity. It is proposed that the $\delta G(F_e)$ term can be differentiated with respect to δF_e to provide local linearization by:

$$\delta G(F) = \frac{\partial G(F)}{\partial F} \delta F = W \delta F = W \delta F \quad (49)$$

where the W is a Jacobian matrix, that can be expanded as:

$$W = \frac{\partial G(F)}{\partial F} = \begin{bmatrix} \frac{\partial F_1^2}{\partial F_1} & \frac{\partial F_1 F_2}{\partial F_1} & \dots & \frac{\partial F_k^2}{\partial F_1} \\ \vdots & \vdots & \ddots & \vdots \\ \frac{\partial F_1^2}{\partial F_k} & \frac{\partial F_1 F_2}{\partial F_k} & \dots & \frac{\partial F_k^2}{\partial F_k} \end{bmatrix} \quad (50)$$

where k equals 6, the Jacobian matrix becomes:

$$W = \begin{bmatrix} 2F_1 & 0 & 0 & 0 & 0 & 0 \\ F_2 & F_1 & 0 & 0 & 0 & 0 \\ F_3 & 0 & F_1 & 0 & 0 & 0 \\ F_4 & 0 & 0 & F_1 & 0 & 0 \\ F_5 & 0 & 0 & 0 & F_1 & 0 \\ F_6 & 0 & 0 & 0 & 0 & F_1 \\ 0 & 2F_2 & 0 & 0 & 0 & 0 \\ 0 & F_3 & F_2 & 0 & 0 & 0 \\ 0 & F_4 & 0 & F_2 & 0 & 0 \\ 0 & F_5 & 0 & 0 & F_2 & 0 \\ 0 & F_6 & 0 & 0 & 0 & F_2 \\ 0 & 0 & 2F_3 & 0 & 0 & 0 \\ 0 & 0 & F_4 & F_3 & 0 & 0 \\ 0 & 0 & F_5 & 0 & F_3 & 0 \\ 0 & 0 & F_6 & 0 & 0 & F_3 \\ 0 & 0 & 0 & 2F_4 & 0 & 0 \\ 0 & 0 & 0 & F_5 & F_4 & 0 \\ 0 & 0 & 0 & F_6 & 0 & F_4 \\ 0 & 0 & 0 & 0 & 2F_5 & 0 \\ 0 & 0 & 0 & 0 & F_6 & F_5 \\ 0 & 0 & 0 & 0 & 0 & 2F_6 \end{bmatrix}$$

Since the Jacobian matrix provides local linearization, caution should be taken for systems that have strong second-order terms. From observation of Equation 49, it can be seen that if the ∂F_e is large, the estimate of δG can be erroneous depending on the local curvature of the system. Generally, balances are primarily linear, where the primary coefficients are a multiple order of magnitude larger than the non-linear terms. Since linear coefficients typically dominate, linearization of the model provides acceptable results. Substituting Equation 49 into 48 provides the voltage interval as a function of only $\delta \hat{F}_e$:

$$\delta y_e = \delta F_e C_1 + \delta F_e W C_2 = \delta F_e (C_1 + W C_2) = \delta F_e J \quad (51)$$

where J is defined by $(C_1 + W C_2)$. Equation 51 can be solved for δF_e to provide the desired interval on the estimated loads:

$$\delta F_e = \delta y_e J^{-1} \quad (52)$$

where the J term in this equation has to be computed at the estimated load F_e . It is also assumed that the inverse of J exists; for most metrology instruments, the inverse of J will exist since the C_1 matrix will be invertible.

Experimental Results

Calibration data from two NASA LaRC balances, UT61B and 748, were used to validate the methods that were developed. The two balances were calibrated using a manual stand system at NASA LaRC. A one-factor-at-a-time (OFAT) experimental design was used to calibrate both balances with 729 individual load points. Note that all the following graphs present the balance forces as a percentage of full-scale loads.

The residuals errors for the normal force component are plotted as a histogram in Figures 15 and 16 for both the 748 and UT61B, respectively. Illustrated in the histograms are a fitted normal distribution with a mean and standard deviation from the residual data. Tripp and Tchong used a chi-squared goodness of fit to test how well the normal distribution fits the data. The calculated chi-squares were much larger than the critical value of 55.8, for a 95% confidence level, which signifies that the residuals do not follow a normal distribution and may be caused by systematic errors in the calibration process.

From the paper, the residuals from the calibrations of the two balances were computed and plotted in Figures 17 and 18 for the 748 and UT61B respectively. These plots included overlays of the intervals due to the modeling error and the total error computed by Equation 52, separately. A 3σ , or 99.7%, confidence level was used for both overlaid intervals.

From Figures 17 and 18, it can be seen that the interval width changes with the load point. This is to be expected, since Equation 45 is a function of the current load point, x_0 . From observation, it can be seen that the majority of the data points were captured by the overlaid intervals. Due to the lack of a stated capture rate by the authors, it is difficult to make comparisons against the assumed confidence level, 3σ or 99.7%.

Proof loads were applied to the balance as confirmation points following calibration. These proof loads include several different load combinations which were

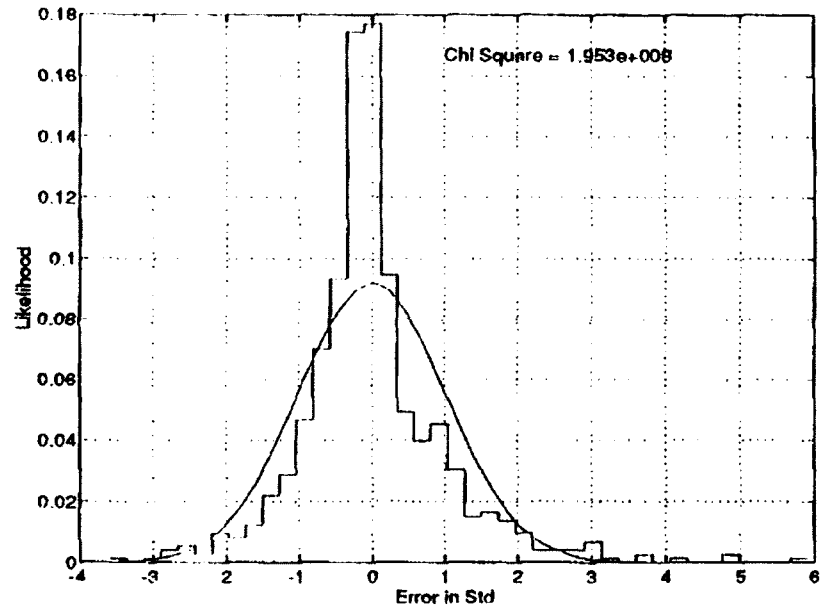


FIG. 15: 748 Histogram of Residuals in F_z

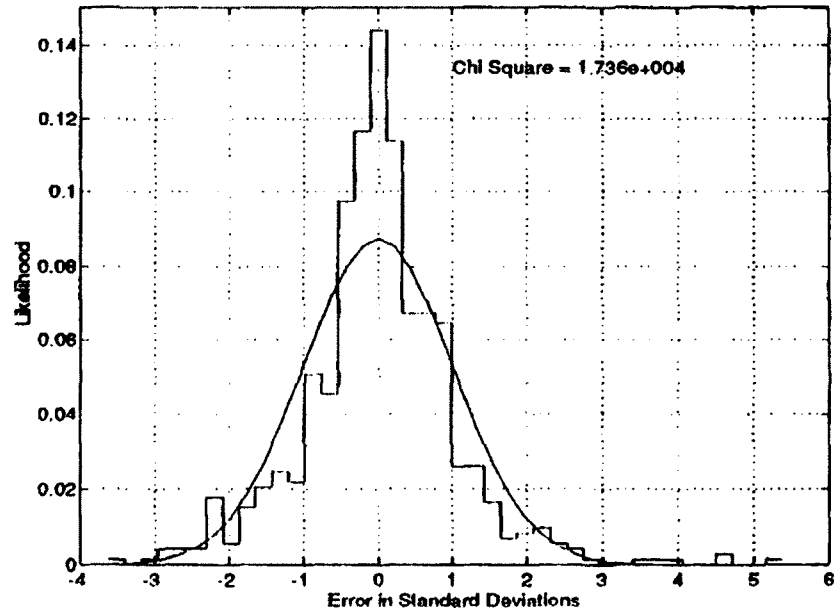


FIG. 16: UT61B Histogram of Residuals in F_z

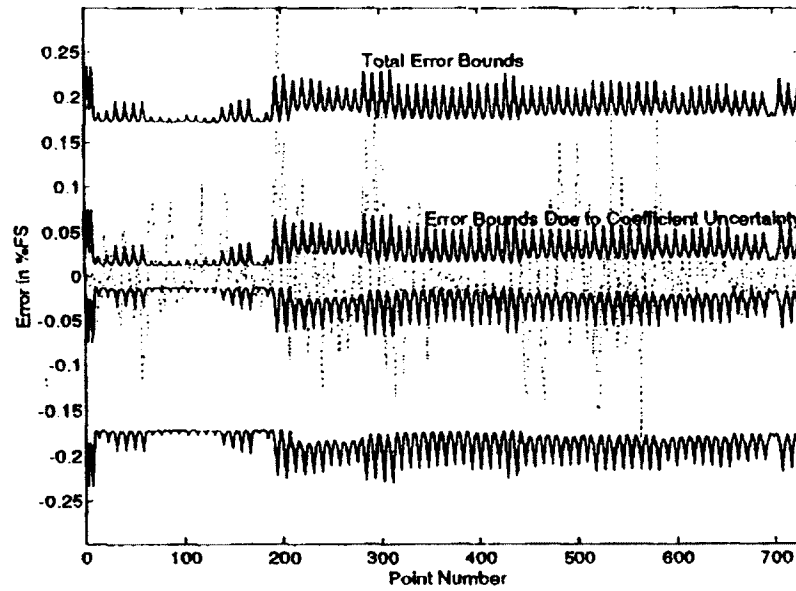


FIG. 17: 748 Predicted Error in F_z

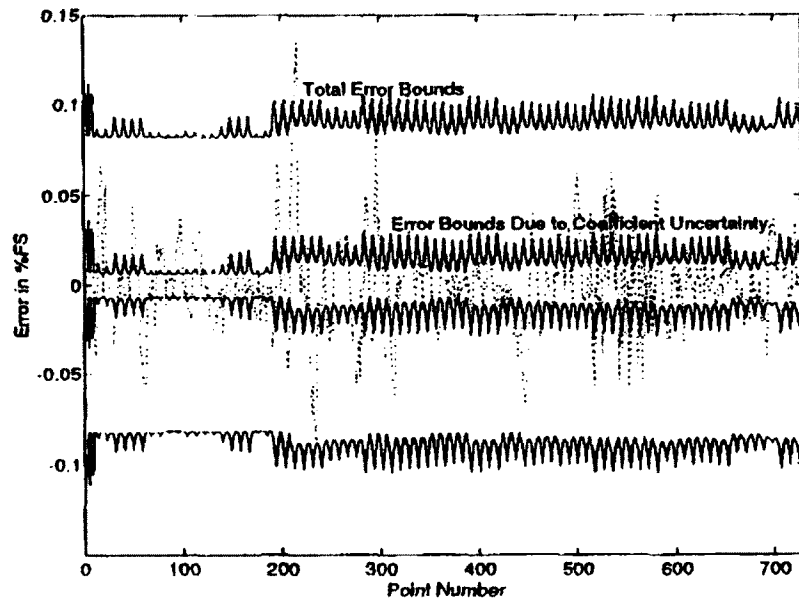


FIG. 18: UT61B Predicted Error in F_z

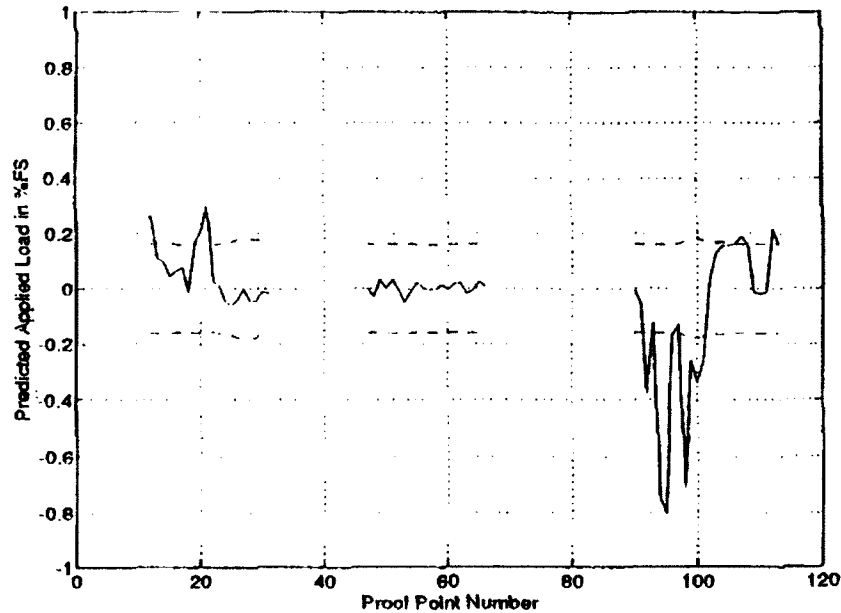


FIG. 19: 748 Proof Load Residuals in F_z

broken up into three sets: 1. normal, pitch and roll, 2. side, yaw and roll, and 3. all six components. The residual error from these loads are plotted as solid lines in Figures 19 and 20. The dashed lines in these figures represent the (3σ) uncertainty intervals.

From Figures 19 and 20, it can be seen that only the second set of loads were well behaved and the majority were within the intervals. It can be said that either the uncertainty intervals were too narrow for the proof load data or that there were errors in the applied loads. Both of these statements can be combined such that the interval calculation for a check load should include the errors due to the applied load, which would result in a larger interval.

2.3.3 SUMMARY AND CONCLUSIONS

It was shown that an uncertainty interval can be calculated for the estimated loads of a balance. This derived interval only included uncertainties from the modeling error of the regression process. It was shown that the interval performs well at capturing the calibration data used to model the system, but performed poorly for proof load points. This can be attributed to the lack of accounting for uncertainties from the calibration system and the applied check loads in the calculated interval.

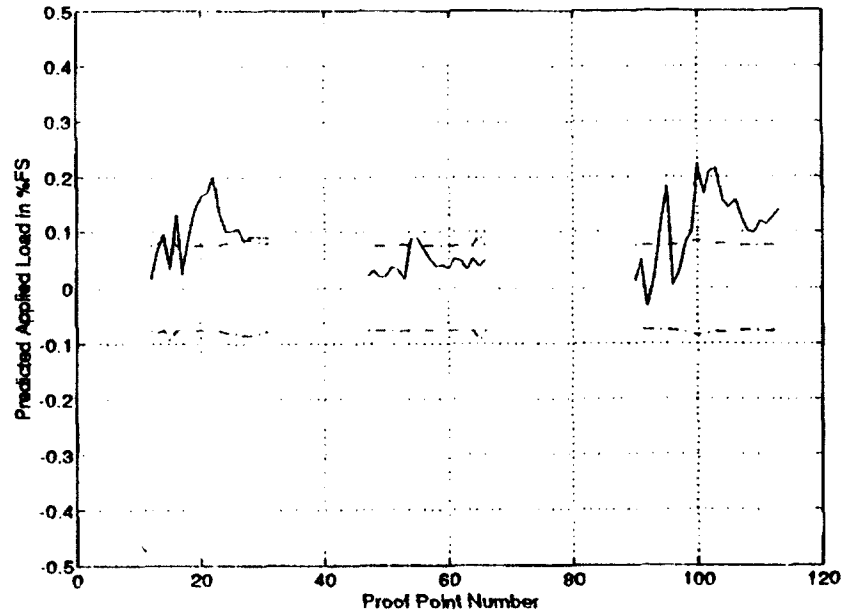


FIG. 20: UT61B Proof Load Residuals in F_z

Further work can be done to integrate the uncertainty characteristics of the calibration system to build a complete understanding of variability in the estimated load of a force balance.

CHAPTER 3

PREDICTION INTERVAL DEVELOPMENT

Typically, before a measurement system is employed for experimental data collection, checks are performed to ensure the performance of the instrument. Generally, this is accomplished by using the system to measure known quantities and cross validating them with the results estimated by the instrument's regression model. Researchers have defaulted to using the standard deviations from the characterization experiment to check the instruments functionality. This is done by verifying if the response of the check measurement is within two standard deviations (2σ) of the mean response, as mentioned in Chapter 1. The use of standard deviations for this process only considers modeling error and ignores the variability of equipment used to calibrate the instrument.

Statistics-based intervals can be used to provide an interval about a predicted value which can represent the uncertainty or lack of information in the estimate. These intervals are derived from the variance that exists in the mathematical model used to characterize a system. Typically, the method of least squares is used to estimate the coefficients of an assumed mathematical model, such as the assumed model for force balances in Equation 2. By the Gauss-Markov theorem, least squares provides the Best Linear Unbiased Estimator (BLUE) for the coefficients of a mathematical model, since it is assumed that the errors are uncorrelated, have a zero mean and variance of σ^2 [29]. For this reason it has been widely used to characterize or calibrate a range of measurement systems.

There are three different major types of statistical intervals in current literature that are derived using least squares: confidence, prediction and tolerance [32]. Each of the interval types have different purposes and applications. A confidence interval (CI) is used to find where the true calibration characteristic or parameter would lie about an estimated parameter. For modeling applications, a CI could be used to provide an interval about the calibration coefficients, which could be compared to known values or the coefficients from a previous calibration model. A prediction interval (PI) is used to find where a single future prediction of a value should lie about the mean prediction. For example, a PI will be used to find where a single

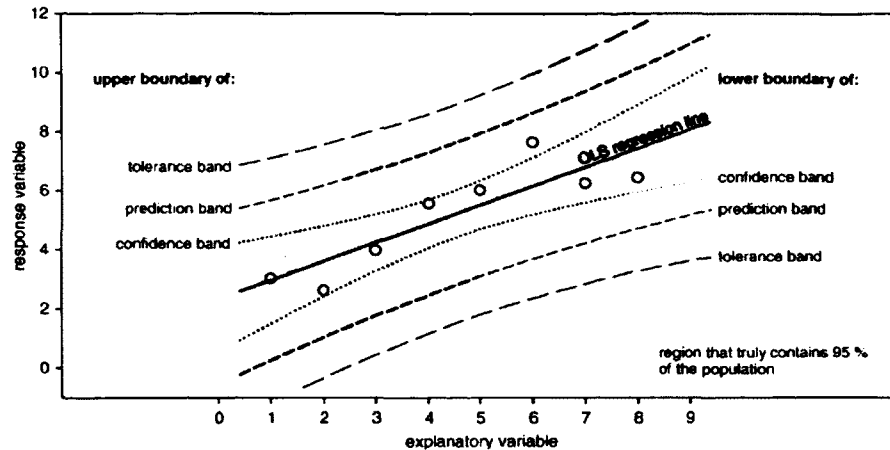


FIG. 21: Example of Statistical Intervals

new response should be observed based on the calibration model. A tolerance interval (TI) is used to determine an interval in which a large portion of a future response would reside. The TI differs from the PI, since the TI will form an interval which will contain a percentage of all future response observations instead of one observation for the PI.

An example of the different types of intervals is illustrated in Figure 21. It can be seen that the width of the intervals increases from the confidence interval to the tolerance interval. Additionally, it is shown that a CI does not capture the points used to build the regression. By definition, the CI should behave in this manner, since it is not derived to capture the points, but to provide an indication of where the mean value.

As shown by the Figure 21, the intervals have a bow-tie shape where the ends have larger widths than the center. This behavior differs greatly from using a constant standard deviation to form an interval. The inflation of the interval width near the ends is due to increasing uncertainty of the regression model at the edges of the design space. For this reason, it is cautioned to only predict within the design space, used for modeling, and not to extrapolate outside of the space.

From the several approaches presented in Chapter 2, the most defensible and complete is the work presented in Section 2.3. The method presented by Tripp and Tcheng incorporates a CI with a novel routine to provide an inverse solution to the calibration problem. This method can be modified to include sources of variability

which are presented by the calibration system, which were discussed in Sections 2.1 and 2.2.

3.1 FORWARD PREDICTION INTERVAL

From the prior discussion, for the application of ensuring the performance of an instrument through check measurements, a prediction interval should be implemented. A prediction interval should be used since it forms an interval within which a new predicted value should lie. A two-sided prediction interval about the observed residual can be expressed by the following probability function:

$$\Pr [|y - \hat{y}| \leq I_P] = 1 - \alpha \quad (53)$$

where y is the measured response, \hat{y} is the predicted response, I_P is the prediction interval width, and $1 - \alpha$ is the confidence level. It can be seen that $y - \hat{y}$ is the residual error of a measurement, where the error should be less than I_P for the set confidence level and a two-sided interval. If a one-sided interval was desired, the absolute value function should be removed from the equation. For the purpose of providing verification checks of an instrument, a two-sided interval should be used, since the residual can fall on either side of the mean response. Note, that y and \hat{y} should be measured and evaluated at a new point x_0 , which is not part of the calibration experiment but a new observed point. An interval I_P , which would satisfy Equation 53, is found by first computing the variance of the residual error [33]:

$$\text{Var}(y - \hat{y}) = \text{Var}(y) + \text{Var}(\hat{y}) = \sigma_y^2 + \sigma^2 x_0 (X'X)^{-1} x_0' \quad (54)$$

This equation shows that the variance of the measured response, y , is a constant, since the measurement error of the response should have a zero mean random error with a variance of σ_y^2 , assuming normal distribution and independence. The variance of the estimated response is a function of the noise in the response and the variance of the regression model used. The σ^2 term is an estimate of unexplainable noise seen in the calibration model, but ideally should represent the possible variance in the response, i.e. σ^2 equal to σ_y^2 . The $x_0 (X'X)^{-1} x_0'$ term is the variation which exists due to modeling and is a function of the location in the design space, x_0 , and the design model used, X . Note that the variance of \hat{y} that is formulated above, derived in Equation 43, only holds for the method of least squares and would differ for other

methods. The classical prediction interval can be developed from Equation 54 and a t-distribution by:

$$\left| \frac{y - \hat{y}}{\sqrt{\sigma_y^2 + \sigma^2 x_0 (X'X)^{-1} x_0'}} \right| \leq t_{\nu, \alpha/2} \quad (55)$$

where $t_{\nu, \alpha}$ is the t-statistic at $1 - \alpha$ percentile of the t-distribution with ν degrees of freedom. Equation 55 is similar to the form of the t-test, which is a statistical hypothesis test used to verify if a population mean is equal to a given value with a certain confidence level. In this case, the t-test is used to check if the residual error is significantly different than zero, assuming a normal distribution. The denominator in Equation 55 is the estimated standard error for the residuals, Equation 54. Assuming that σ_y^2 and σ^2 are equivalent, the mean square error (MSE) from the calibration experiment can be substituted and the prediction interval width I_P can be written as:

$$I_P = t_{\nu, \alpha/2} \sqrt{\text{MSE} (1 + x_0 (X'X)^{-1} x_0')} \quad (56)$$

The interval width derived assumes all the assumptions of the method of least squares, namely that variability only exists in the response and the explanatory variables are known with no errors. It is known that the application of the explanatory variable during the calibration experiment is done so with a measurable error. For most applications the explanatory variable error is much smaller than the measurement error in the response, which allows for the zero-error assumption to be justified. For complex calibration processes which have several possible uncertainty sources, the errorless explanatory variable assumption may break down.

During the calibration of an instrument, known explanatory variables are transformed to responses by the instrument, i.e. producing a voltage response for a given measurement. These known explanatory variables are the control in the calibration experiment, where the variability of these variables are minimized. Generally, the known explanatory variable, such as a weight or length, is calibrated or compared to a known standard. These standards are controlled by international and/or national organizations to maintain uniformity and value of the measure. These known explanatory variables used for the calibration process have uncertainty, since they are not the standard but the calibrated against one. This type of error in the explanatory variable can be regarded as a set point error, since it is an error in the set conditions.

Additional errors will exist from the instrument itself and from the measurement of the response. The errors due to the instrument are due to changes in its behavior usually from environmental changes. These errors and the response measurement are both captured in the estimate of MSE from the calibration experiment.

The measurement errors that may exist in the explanatory variables can either be a random or bias errors. Bias measurement errors are not easily detectable in collected data, since it is hidden from the statistical properties of least squares due to being a constant offset of the response. In the assumptions of least squares, only random error is assumed, and a bias error will then fall into the estimate of the intercept or other coefficients. Thus, biases in a system must be estimated by other means, such as modeling the system or by directly measuring the bias with other instruments. The latter can be done by using an instrument that has been calibrated on another system to check for any disparities in the data [34]. However, it would be difficult to know the true bias of the calibration system, since there is no unbiased instrument available to provide a true measurement.

A bias in a calibration system is an additional uncertainty which should be included in the total variance of the system. The bias and random error due to the calibration hardware can be represented as a variance σ_{Cal} , which must be in units of the response variable. This added variance represents the total possible variance which exists due to a calibration system. For force measurement calibration systems, this additional variance can arise from weights, manufacturing errors, balance moment center dimensions, etc. Given two different and independent variances, they can be combined to represent the total system:

$$s_{\text{system}} = \sqrt{s_{\text{measurement}}^2 + s_{\text{bias}}^2} \quad (57)$$

where $s_{\text{measurement}}^2$ and s_{bias}^2 are the assumed variance due to the measurement and bias errors. Since the additional calibration system variance is independent of the MSE, by Equation 57 the calibration variance can be added to the prediction interval in Equation 56 by assuming that the term under the radical represents the residual variance:

$$I_P = t_{\nu, \alpha/2} \sqrt{\text{MSE}(1 + x_0'(X'X)^{-1}x_0) + \sigma_{\text{Cal}}^2} \quad (58)$$

During an instrument's checks, the equipment that is employed may differ from the calibration, thus having different uncertainties or biases. When applying a prediction interval to check measurements, the calibration and check apparatus uncertainties should both be taken into account. The prediction interval as shown in Equation 58 is only valid if the same system is used for both calibration and check measurements, since it assumes only one additional variance source. Without the inclusion of the two individual system uncertainties, the prediction interval can be too narrow and may not capture the correct percentage of points. The potential of under- or over-capture of points may lead to misinformed decisions to be made in regards to the performance of the instrument.

Similar to the calibration system, the bias due to the check system can be represented by a variance σ_{Check}^2 . This additional variance is added to the total variance of the system, including the variance of the calibration system, since it's effect will still be present in the calibration model. The total variance will then include the prediction variance, and calibration and check biases. Using the same method for the calibration system, the final prediction interval can be written as:

$$I_P = t_{\nu, \alpha/2} \sqrt{\text{MSE}(1 + x_0'(X'X)^{-1}x_0) + \sigma_{\text{Cal}}^2 + \sigma_{\text{Check}}^2} \quad (59)$$

Equation 59 will provide the interval width of a single new prediction given MSE, design matrix, x_0 , and calibration and check system variances. For multi-component systems, multiple predictions are made simultaneously for the number of responses. Due to simultaneous predictions, the t-statistic should be adjusted to reflect simultaneous predictions. The Bonferroni correction can be used to adjust the confidence level α to maintain the overall Type I error rate [35]. A Type I error is where a false positive is made, such as stating that a value is not within the interval when in fact it is. This correction is applicable when a known number of p predictions are made, and the confidence level is adjusted by:

$$\alpha^* = \alpha/p \quad (60)$$

where the adjusted confidence level α^* replaces α in the derived prediction interval equations. With this correction, the prediction intervals will be the correct distance from the predicted values, given a set of calibration and check system variances. These additional variances need to be estimated either by statistical analysis of observations or by mathematical estimation. Typically, it is preferred to perform this

analysis by mathematical means due to the cost of performing multiple measurements in order to build a population of data samples large enough to make statistical inferences. The uncertainties for both the SVS and ILS systems were estimated using numerical methods with estimates of the input variable uncertainties [22, 36].

Propagation of error or a Monte Carlo Simulation (MCS) are two examples of numerical methods which can be used to mathematically determine the variance of a system, which can include systems biases. Both of these approaches require building a mathematical model of the system and should include all the known error sources. The propagation of error method is a mathematical approach, which assembles the individual input uncertainties to an overall output uncertainty. A first-order Taylor series expansion is used to expand the desired output uncertainty as a function of the input variable uncertainties. Since only a first-order series is used, it is assumed that the higher-order partial derivatives are much smaller than the first-order terms and are negligible. Due to these assumptions, the system model should be linearized to satisfy the first-order assumptions.

MCS is a computational method used to estimate distributional properties of an output variable of a system. This method builds a simulated population of an output variable by randomly sampling the input variables from statistical distributions. Depending on the input error sources, the assumed statistical distribution may differ, such as a normal or uniform distribution. Many iterations are performed, upwards of several thousand, to build a large enough distribution of the output variable. This standard deviation then is used to represent an estimate of the output variance. Since a Monte Carlo simulation calculates the output directly from each random input combination, with no linearization or simplification applied, the output of complex systems can be modeled.

3.2 REVERSAL OF THE PREDICTION INTERVAL

As shown in the previous section, a prediction interval can be developed around the estimated response of a system. In the case of most measurement systems, the response is generally a voltage. Formulating an interval about the response in this case provides little practical information for the user of the instrument. Users generally want to know the confidence of the measured variable or in these cases the explanatory variable.

For a simple linear calibration case, the conversion between units of the explanatory and response variables is straight forward. The inverse of the regression model is used to convert between the two units, if the inverse exists. Since closed form solution existing for the explanatory variable as a function of the response. Calibration models that include non-linear terms, such as that of a force balance, do not have a closed form solution for the explanatory variable, thus a direct function does not exist for the explanatory variable with respect to the response.

A basic solution to the inversion problem, for a non-linear model, is to ignore the non-linear terms in the model to reduce the problem so that a closed-form solution will exist. This approach is only applicable for models where second-order terms are small, in order to reduce the possible error. But for any models that have large second-order terms, it would be inappropriate to use such an approach since the effects are unknown.

A non-linear calibration matrix $\hat{\beta}$ can be broken up into the linear and non-linear components:

$$\hat{\beta} = \begin{bmatrix} C_0 & C_1 & C_2 \end{bmatrix} \quad (61)$$

where C_0 , C_1 and C_2 are the intercepts, linear and non-linear terms of the calibration matrix. Note that C_1 should be a k by k square matrix, where k is number of responses. The response of the system due only to the linear matrix can be estimated by $\hat{\mathbf{y}} = C_0 + \mathbf{x}C_1$. Note that $\hat{\mathbf{y}}$ and \mathbf{x} are row arrays, which are size 1 by k . If the inverse of C_1 exists, an estimate for the explanatory variable array for a measured response can be found by:

$$\hat{\mathbf{x}} = (\mathbf{y} - C_0) C_1^{-1} \quad (62)$$

Note that the hat accent was removed from the response and applied to the explanatory variable, since what is being estimated has be reversed. Since this equation is linear, the response term can be exchanged with an interval width to convert it over to the explanatory variable units. Assuming a response interval width of I_{P_y} , the width of the explanatory interval I_{P_x} can be estimated by:

$$I_{P_x} = I_{P_y} C_1^{-1} \quad (63)$$

A more complete approach which does not simplify the problem, is to solve for the explanatory variables at the corresponding response interval limits. The high and

low limits of the response interval are found by adding and subtracting the interval width, from prediction interval equations, to the measured response:

$$\mathbf{y}_{high/low} = \mathbf{y} \pm I_{P_y} \quad (64)$$

With the interval limits, an iterative method such as Newton-Raphson can be used to solve Equation 65 for the interval limit values in units of the explanatory variable, or $\hat{\mathbf{x}}$, with the full regression matrix $\hat{\beta}$:

$$\mathbf{y} = \hat{\mathbf{x}}\hat{\beta} \quad (65)$$

This process is identical to the routine that is used to compute the explanatory variables from the measured response when the instrument is used experimentally. A risk of this method is that it may not converge to a solution for wide intervals or for highly non-linear models. Non-convergence may occur when the interval on the responses generates a point that does not have a unique solution for the explanatory variable. Another drawback is that this method can be computationally intensive due to the iterative process. Typically, force measurement systems can converge to a solution rapidly, within five iterations, since they are primarily linear. Other systems may require more iteration to achieve a certain convergence criterion.

A method that does not require numerical iterations or have issues with convergence was developed by Tripp and Tchong. The method developed by Tripp inverts the response interval width to the explanatory variable through local linearization. The development of this method is thoroughly discussed in Section 2.3.2. The advantages of this method is that it retains second-order effects and does not require an iterative routine. Equation 66 provides a direct solution for the explanatory variable interval for a given response interval, calibration matrix, and mean explanatory variable:

$$I_{P_x} = I_{P_y} (C_1 + W(\hat{\mathbf{x}})C_2)^{-1} = I_{P_y} J(\hat{\mathbf{x}})^{-1} \quad (66)$$

In this equation, W is a Jacobian that is defined in Section 2.3.2, for a force balance application, and is function of the current explanatory variable or load point for a force measurement case. Note that the Jacobian, W , must be computed at the explanatory variable under investigation, which is an estimate based on the measured response. The explanatory variables are estimated by the use of Equation 65 and a numerical method.

With the inversion processes established above, an interval on the response variable can be converted to the explanatory variable. The inversion process in combination with the prediction interval that is derived in Section 3.1 can be used to apply statistically rigorous intervals to an instrument's estimated explanatory variable. These intervals can be used to validate the performance of an instrument prior to experimentation in the form of check loads. Additionally, a prediction interval can be used to provide information on an instrument's accuracy instead of the commonly used standard deviation values.

As shown, the derived prediction intervals requires estimation of the calibration and check system variances. For multi-component force balances, the single-vector system variances for both the SVS and ILS have been estimated using numerical methods. The variance of manual stands, such as the ones used at NASA LaRC, needs to be estimated in order to employ these methods.

CHAPTER 4

MANUAL STAND UNCERTAINTY

Manual stand calibrations have been implemented for the calibration of strain-gaged wind-tunnel balances since their inception. These systems are still in use for the calibration of large-scale balances, when other calibration systems are inadequate for the load ratings of the balance. Manual stands currently lack a rigorous uncertainty analysis due to the scale and complex hardware attributes of these systems. Several studies were conducted to evaluate the uncertainty of manual stand calibration systems, but with simplifications to the system [16,26]. Some of the uncertainties related to the manual stand are:

- applied Weight*
- knife Edges (x,y) *
- moment Arm Position (x,y,z) *
- balance Angle (ϕ,θ,ψ) *
- cable Misalignment*
- angle Measurement*
- cable/Rod Catenary
- moment Arm Deflections
- balance Anelastic Effects
- balance Temperature
- calibration Body Deflections
- data Acquisition Uncertainty



FIG. 22: NASA LaRC 20K Manual Stand (Credit: NASA)

Uncertainty sources marked with the asterisk (*) are already considered in other systems. Due to the large number of possible uncertainties, the significance of each uncertainty source should be determined prior to constructing an overall system uncertainty. This approach will reduce the complexity of the system uncertainty to only those that have a significant influence on the balance's performance. A combination of actual measurements and engineering judgment are used to quantify the effects of each the considered uncertainty sources. Engineering judgment is required to bound these uncertainties that cannot be directly measured. One example is the practice of cable alignment for axial or side force, which relies on the voltage readings of the balance for the alignment and not an actual measurement of the cable's orientation.

4.1 INDIVIDUAL UNCERTAINTY SOURCES

The following subsections detail the individual uncertainty sources for the NASA LaRC 20K manual stands, which are similar to other manual systems used at other facilities. An photograph of the 20K manual stand is shown in Figure 22. The goal of each subsection is to understand the impact of each source of uncertainty. With an end goal of incorporating all the individual uncertainty sources into a final uncertainty estimate.

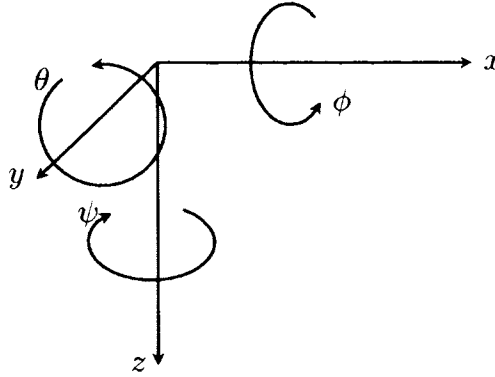


FIG. 23: Balance Coordinate System, with Rotations

4.1.1 CALIBRATION BODY ANGLE AND MISALIGNMENT

Repositioning of the balance calibration body to a level position after loads are applied is required for manual stand calibrations. At every recorded data point, the body should be nominally level to ensure that there is minimal transfer of loads between the force vector components. Leveling of the body is done using calibrated electrolytic tilt sensors or traditional bubble levels placed on the calibration body. With this, there are several sources of uncertainty, such as the sensor accuracy and bias, calibration body flatness, and the angular offset between the calibration body and the balance. The latter two potential uncertainty sources are considered to be relatively small due to the high level of fidelity used to manufacture the calibration hardware and balance. It is generally assumed that the primary source for angle uncertainty lies in the angle measurement system, but for this study all the considered sources will be analyzed and vetted.

The manual stand at NASA LaRC employs a pair of electrolytic bubble levels, manufactured by Spectron Glass and Electronics Inc., which are arranged with their sensing axis perpendicular to one another, i.e. one measuring the pitch angle and the other for the roll angle of the calibration body. These sensors are placed on the top surface of the calibration body in a region close to the tip of the balance, if a moment balance is used. This placement, for a moment balance, would reduce any errors that may arise due to deflections of the calibration body, since the balance tip is where the two bodies are mated and pinned. These sensors have a sensing range of $\pm 1^\circ$ and a quoted null repeatability of 0.0008° .

The rotation convention about the three primary axes of the balance coordinate system is illustrated in Figure 23. Where ϕ , θ , and ψ are the rotations about the x , y , and z axes, also are the roll, pitch and yaw angles of the calibration body, respectively. This coordinate system and rotation convention will be used exclusively, and is similar to the convention of an aircraft body axis coordinate system [37]. A vector \mathbf{r} can be transformed between two different coordinate systems that share the same origin, with one rotated about the three major axes, using a Euler rotation matrix [38]:

$$\mathbf{r}_{new} = \begin{bmatrix} C_\psi C_\theta & S_\psi C_\theta & -S_\theta \\ S_\psi S_\theta S_\phi + S_\psi C_\phi & S_\psi S_\theta S_\phi + C_\psi C_\phi & C_\theta S_\phi \\ C_\psi S_\theta C_\phi + S_\psi S_\phi & S_\psi S_\theta C_\phi - C_\psi S_\phi & C_\theta C_\phi \end{bmatrix} \mathbf{r} \quad (67)$$

where C_θ and S_θ represent the cosine and sine values for a given angle θ , and \mathbf{r}_{new} is the vector \mathbf{r} represented in the new rotated coordinate system. With this Euler rotation matrix, a force with magnitude P that is aligned with the gravity vector, i.e. an original force vector of $[0 \ 0 \ P]'$, is applied to the balance, the resultant force vector \mathbf{F} in a misaligned coordinate system can be represented as:

$$\mathbf{F} = P \begin{bmatrix} -S_\theta & S_\phi C_\theta & C_\phi C_\theta \end{bmatrix} \quad (68)$$

From Equation 68, it can be seen that any misalignment of the calibration body in the pitch and roll axes will allow for a hanger load to apply forces in undesired axes. For example, a normal force hanger can apply an axial or side force if the calibration body is not level. It should be noted that the yaw angle ψ does not have any contributions to the applied force vector, since it is assumed that the applied gravity load acts through the z -axis.

An illustration of side force inadvertently applied by a normal force load due to a balance roll angle is shown in Figure 24. Depicted is a misaligned calibration body, in gray, with a load applied via knife-edge on the top surface. The variables F_y and F_z represent the force components that are applied to the calibration body in the y - and z -axis of the balance coordinate system. From this it can be seen that the force is applied at a half-width, $w/2$, away from the balance moment center. Thus, a rolling moment will be generated with a magnitude of $(wF_y)/2$, for this example. A moment vector \mathbf{M} generated by an applied force vector, \mathbf{F} , is resolved by the cross product between a distance vector \mathbf{r} from the BMC and the applied force vector:

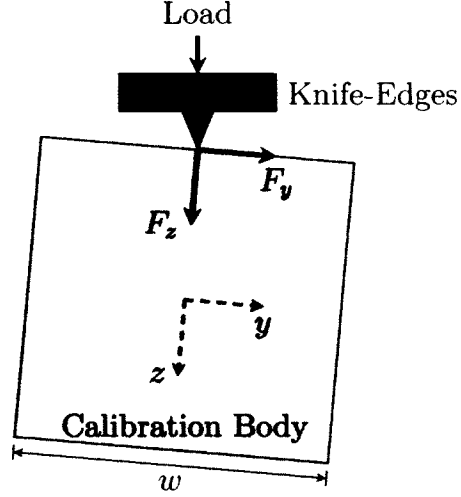


FIG. 24: Misaligned Fixture with Applied Load

$$\mathbf{M} = \mathbf{r} \times \mathbf{F} = \begin{bmatrix} \hat{i} & \hat{j} & \hat{k} \\ x & y & z \\ F_x & F_y & F_z \end{bmatrix} \quad (69)$$

Substituting Equation 68 into Equation 69 resolves the moment vector into a function of applied load, balance angles, and load position:

$$\mathbf{M} \approx P \begin{bmatrix} C_\phi C_\theta y - S_\phi C_\theta z \\ -C_\phi C_\theta x - S_\theta z \\ S_\phi C_\theta x + S_\theta y \end{bmatrix}' \quad (70)$$

Equation 70 results in a non-linear formula for the moments due to the non-linear force vector. Due to the small uncertainty range of the angle sensors, small angle approximations can be used, which will allow for linearization of the force and moments equations. Linearization will help reduce the complexity of the uncertainty process and allow for error propagation methods, since these methods require linearization. The small angle approximations for a sine and cosine function about zero angle are:

$$\sin(\phi) \approx \phi \quad (71)$$

$$\cos(\phi) \approx 1 - \phi^2/2 \quad (72)$$

For a 1 percent error in the linearized Equations 71 and 72 to occur, an angle of 14° and 38° for sine and cosine is required, respectively. Note that this linearization

is only valid for angles in units of radians. The angle term in Equation 72 can be seen to provide little contribution for very small angles due to being squared. By simply equating cosine to a value of unity, the angle at which a 1 percent error will occur is reduced to 8° . The expected maximum error for both pitch and roll angles is less than 0.1° , thus the small angle approximations are acceptable for this application. Implementing the small angle approximation for Equations 68 and 70 yields the following simplified force and moment equations:

$$\mathbf{F} \approx P \begin{bmatrix} -\theta & \phi & 1 \end{bmatrix} \quad (73)$$

$$\mathbf{M} = P \begin{bmatrix} y - \phi z \\ -x - \theta z \\ \phi x + \theta y \end{bmatrix}' \quad (74)$$

From Equation 73, it can be inferred that in order to not exceed 1 lb of incidental axial force with a 6,000 lb normal force load, an angle setting better than 0.01° is required. These loads are based on the NTF-113 balance, which has a normal and axial force design load of 6,500 and 400 lbs, respectively. For these balance design loads, a 0.25% error in axial force is 1 lb. An applied side or axial force can also be said to affect the other two orthogonal computes, but in lower magnitudes due to the lower applied loads. This shows that the level of precision that the balance angle is set to plays a major part in the uncertainty of the applied forces. Using methods of error propagation, or Taylor series expansion, the overall uncertainty in the forces and moments can be estimated by Equations 75 and 76, respectively [28]:

$$s_{\mathbf{F}}^2 = \left(\frac{\partial \mathbf{F}}{\partial P} \right)^2 s_P^2 + \left(\frac{\partial \mathbf{F}}{\partial \phi} \right)^2 s_\phi^2 + \left(\frac{\partial \mathbf{F}}{\partial \theta} \right)^2 s_\theta^2 \quad (75)$$

$$s_{\mathbf{M}}^2 = \left(\frac{\partial \mathbf{M}}{\partial P} \right)^2 s_P^2 + \left(\frac{\partial \mathbf{M}}{\partial \phi} \right)^2 s_\phi^2 + \left(\frac{\partial \mathbf{M}}{\partial \theta} \right)^2 s_\theta^2 + \left(\frac{\partial \mathbf{M}}{\partial x} \right)^2 s_x^2 + \left(\frac{\partial \mathbf{M}}{\partial y} \right)^2 s_y^2 + \left(\frac{\partial \mathbf{M}}{\partial z} \right)^2 s_z^2 \quad (76)$$

Equations 75 and 76 are the root-sum square (RSS) of all the partial derivatives that exist in Equations 73 and 74 with respect to the individual error sources. The propagation of error presented lacks the correlation terms between uncertainties. It is assumed that correlation between the individual terms is negligible or zero.

Correlation would only exist for uncertainties that are measured using the same measurement device, i.e. two uncertainty sources using the same measurement devices. This correlation will exist between two sources, since knowledge of one source will influence another due to the two sources having the same possible bias. With the force and moment equations written in the most fundamental variables as shown in Equations 73 and 74 it is assumed that the individual variables do not exhibit correlations.

Substituting Equation 73 into the error propagation Equation 75 and evaluating the partial derivatives yields the expanded uncertainty for the force components:

$$s_{\mathbf{F}}^2 = \begin{bmatrix} \theta^2 \\ \phi^2 \\ 1 \end{bmatrix}' s_P^2 + \begin{bmatrix} 0 \\ P^2 \\ 0 \end{bmatrix}' s_\phi^2 + \begin{bmatrix} P^2 \\ 0 \\ 0 \end{bmatrix}' s_\theta^2 \quad (77)$$

From this equation, the angle contributions, s_ϕ and s_θ , to the force uncertainties are proportional to the square of the applied load P_{F_z} . The applied load uncertainty s_P primarily affects the z -component, with very low contributions to the x - and y -components. This low contribution is due to the use of small angles, which are nominally zero, and are much smaller in magnitude than 1 or the applied load P_{F_z} . With the assumption that all angles are nominally zero, the force uncertainty equation is simplified:

$$s_{\mathbf{F}}^2 = \begin{bmatrix} 0 \\ 0 \\ 1 \end{bmatrix}' s_P^2 + \begin{bmatrix} 0 \\ P_{F_z}^2 \\ 0 \end{bmatrix}' s_\phi^2 + \begin{bmatrix} P_{F_z}^2 \\ 0 \\ 0 \end{bmatrix}' s_\theta^2 \quad (78)$$

From Equation 78, it is seen that with the zero angle assumption, the applied load uncertainty only applies to the primary component, but the other two components have uncertainties due to the angle terms. Substituting in Equation 74 into 76 yields the expanded uncertainty for the moment components:

$$\begin{aligned}
s_M^2 = & \begin{bmatrix} (y - \theta z)^2 \\ (-x - \theta z)^2 \\ (\phi x + \theta y)^2 \end{bmatrix}' s_P^2 + \begin{bmatrix} (P_{F_z} z)^2 \\ 0 \\ (P_{F_z} x)^2 \end{bmatrix}' s_\phi^2 + \begin{bmatrix} 0 \\ (P_{F_z} z)^2 \\ (P_{F_z} y)^2 \end{bmatrix}' s_\theta^2 + \begin{bmatrix} 0 \\ P_{F_z}^2 \\ (P_{F_z} \phi)^2 \end{bmatrix}' s_x^2 + \\
& \begin{bmatrix} P_{F_z}^2 \\ 0 \\ (P_{F_z} \theta)^2 \end{bmatrix}' s_y^2 + \begin{bmatrix} (P_{F_z} \phi)^2 \\ (P_{F_z} \theta)^2 \\ 0 \end{bmatrix}' s_z^2
\end{aligned} \tag{79}$$

By applying the same zero angle assumption that was implemented in the force uncertainty equation, Equation 79 is simplified to only the significant terms:

$$\begin{aligned}
s_M^2 = & \begin{bmatrix} y^2 \\ x^2 \\ 0 \end{bmatrix}' s_P^2 + \begin{bmatrix} (P_{F_z} z)^2 \\ 0 \\ (P_{F_z} x)^2 \end{bmatrix}' s_\phi^2 + \begin{bmatrix} 0 \\ (P_{F_z} z)^2 \\ (P_{F_z} y)^2 \end{bmatrix}' s_\theta^2 + \begin{bmatrix} 0 \\ P_{F_z}^2 \\ 0 \end{bmatrix}' s_x^2 + \begin{bmatrix} P_{F_z}^2 \\ 0 \\ 0 \end{bmatrix}' s_y^2
\end{aligned} \tag{80}$$

In this equation, it is seen that the applied force uncertainty contribution scales with the x - and y -position of the load, which suggest that small distances should be used in order to minimize the moment uncertainty. Although, if the applied force uncertainty is represented as a percentage of full scale u_P^2 , where $s_P = P_{F_z} u_P$, the terms in the array change to the applied moments M_x and M_y for the y and x terms, respectively. With this conversion, the applied load contribution, in percent of full-scale load, will be constant for a given applied moment. Thus, to reduce the overall uncertainty of the moments, reductions must be made with other terms. From the positional uncertainty terms, s_x and s_y , a reduction in the applied load will yield a reduction in the moment uncertainties. With this, large x and y values with a low applied load, P_{F_z} , reduce the overall moment uncertainty.

With these derivations, the force and moment uncertainties become a function of the applied load (P) and load point (x, y, z), which are the fundamental variables of the system (for this load case). In order to compute a final overall uncertainty the individual variables and their corresponding uncertainties or standard deviations, s_i , must be quantified. These uncertainty values will be estimated using engineering judgment, known sensor accuracies and dimensional tolerances. Several of the

TABLE 13: Position Uncertainty Sources

| Source | Description | Uncertainty Estimate | Impact |
|--------------------------|--|----------------------|-----------|
| Calipers | Set point error of vernier calipers | 0.001-.002 in. | x |
| Knife Edge | Geometric tolerance of the knife edge blocks | 0.0002 in. | x, y |
| Knife Edge Groove | Groove location on fixture | 0.0025 in. | y |
| Balance | | | |
| Dowel Hole (CMM) Fixture | CMM measurement of the pin location w.r.t. BMC | 0.0002 in. | x |
| Dowel Hole (CMM) | CMM measurement of dowel hole location | 0.0002 in. | x |
| Fixture QA (CMM) | CMM measurements of the calibration fixture | 0.0002 in. | x, y, z |

uncertainty sources in Equations 78 and 80 are a composite of multiple individual error sources. For example, s_x will be based on the root-sum square (RSS) of the uncertainties of the vernier caliper, the measurements of the balance moment center, dowel-pin fitting, and the knife-edge groove tolerance.

Position Uncertainty (x, y, z)

The specific uncertainty contributors for the load point position that are considered in this study are tabulated in Table 13. This table provides details of each contributor such as its origin, estimated uncertainty, and the variables that it affects. Since these uncertainties are for the load point position, the contributors are primarily from manufacturing and coordinate measurement machine (CMM) errors. For the majority of the calibration hardware that is built for NASA LaRC, quality assurance (QA) checks are performed via CMM measurements. These CMM results are generally used to first ensure that the hardware is built to specification and secondarily used to know the measured lengths with high precision.

The x location of the load point can be represented as an offset between the measured BMC and the location of the knife-edges. These knife-edges are placed along the x -axis of the calibration body to apply a pure normal force or with a pitching

moment, when knife-edges are not located at BMC. Knife-edges are positioned along the calibration body by using a vernier caliper, which is set to a distance based on the assumed location of the BMC with respect to the calibration body front face. With this, the x -offset of the load point is defined by:

$$x = x_{\text{Pin,Bal}} + x_{\text{Pin,Fixture}} - x_{\text{Calipers}} - x_{\text{KnifeEdge}} \quad (81)$$

An estimate of the x -position uncertainty is derived by implementing propagation of error on Equation 81. From observation of the equation above, it is seen that the results from the propagation of error will be a summation of the contributing factor uncertainties, due to all the partial derivatives equating to unity.

$$s_x^2 = s_{\text{Pin,Bal}}^2 + s_{\text{Pin,Fixture}}^2 + (s_{\text{Calipers}}^2 + s_{\text{FixtureQA}}^2) + s_{\text{KnifeEdge}}^2 \quad (82)$$

where the s_{Calipers} and $s_{\text{FixtureQA}}$ terms are inside parenthesis to represent that the fixture QA term was added due to the calipers. This can be done since the errors from both the caliper setting and the fixture QA are independent of each other, thus the caliper uncertainty can be a composite of the two sources as shown. The same derivations can be done for both the y - and z -terms that are in the moment calculations, with some modification. Calipers are not used for locating the knife-edges in the y - or z -directions when in the F_z orientation, since the knife edge groove runs along the x -direction of the calibration body. Therefore, the load point y - and z -position is represented by:

$$y = y_{\text{FixtureQA}} - y_{\text{KEGroove}} \quad (83)$$

$$z = z_{\text{FixtureQA}} \quad (84)$$

From Equations 83 and 84, it can be seen that there is a large reduction in complexity from Equation 81, which is mainly due to the y - and z -positions being fixed by physical constrains. Both the y and z positions are dependent on a fixture QA term, which is how well the balance bore hole is centered about the fixture. The y -position has an additional term, y_{KEGroove} , due to the knife edge groove, since the machined groove, which runs along the x -axis, will not be perfectly centered on the fixture body. As was done with the x -position equation, propagation of error is applied to Equations 83 and 84 to derive the uncertainties for these variables:

TABLE 14: Load Position Uncertainty Estimates

| Variable | Estimate, in. |
|----------|---------------|
| s_x | 0.0011 |
| s_y | 0.0025 |
| s_z | 0.0002 |

$$s_y^2 = s_{\text{FixtureQA}}^2 + s_{\text{KEGroove}}^2 \quad (85)$$

$$s_z^2 = s_{\text{FixtureQA}}^2 \quad (86)$$

Note, that these equations are derived for the case of a normal force hanger load. For the case of a side force hanger load, the roles of the y and z variables are exchanged, since the balance fixture is rotated 90-degrees about the x -axis. Additionally, special care should be used to ensure the proper final signs of x , y and z , since during a rotation of the calibration body the signs of the y - and z -positions can change.

Entering the estimated uncertainties from Table 13 into Equations 82, 85 and 86 yields the uncertainty estimates for the x , y and z variables. The estimated values for the load position uncertainties are tabulated in Table 14. From these values, it is seen that the uncertainty estimates are approximately equal to the largest uncertainty value in their respective equations. For example, s_x is near the largest uncertainty value of 0.001 inches.

Angle Uncertainty (ϕ , θ)

The specific contributors to the angle uncertainties that are considered in this study are tabulated in Table 15. Similar to the position uncertainty table, listed are the descriptions of each contributor, uncertainty estimate, and which variables that it affects. The contributors that are listed are due to manufacturing and fixture leveling errors. Note that the last dowel pin and fixture surface uncertainty estimates are based on the CCM accuracies over a distance of 1 inch.

The total angles, ϕ and θ , of the calibration body for a load point can be represented as a function of the error contributors, which will result in an offset from level

TABLE 15: Angle Uncertainty Sources

| Source | Description | Uncertainty Estimate | Impact |
|-------------------|--|----------------------|----------------|
| Angle Measurement | Error due to angle measurement device | 0.0007 Deg. | ϕ, θ |
| Dowel Pin | Dowel pin manufacturing error and pin slop | 0.0086 Deg. | ϕ |
| Fixture Surface | Surface angularity and irregularities | 0.0086 Deg. | ϕ, θ |

TABLE 16: Body Angle Uncertainty Estimates

| Variable | Estimate, Deg. |
|------------|----------------|
| s_ϕ | 0.0122 |
| s_θ | 0.0087 |

balance coordinate system. A series of angle transformations are not a linear operation, but linearization is implemented due to the small offset angles. To simplify the angle transformation problem, the final measured angle is assumed to be the sum of the small offsets from the balance coordinate system to the sensor:

$$\phi = \phi_{\text{Sensor}} + \phi_{\text{Surface}} + \phi_{\text{Dowel}} \quad (87)$$

$$\theta = \theta_{\text{Sensor}} + \theta_{\text{Surface}} \quad (88)$$

Applying propagation of error to Equations 87 and 88 to yield the uncertainty estimates of the measured calibration body angles:

$$s_\phi^2 = s_{\phi_{\text{Sensor}}}^2 + s_{\phi_{\text{Surface}}}^2 + s_{\phi_{\text{Dowel}}}^2 \quad (89)$$

$$s_\theta^2 = s_{\theta_{\text{Sensor}}}^2 + s_{\theta_{\text{Surface}}}^2 \quad (90)$$

With the estimates of the load point and angle uncertainties, they are entered into the force and moment uncertainty equations 78 and 80, respectively. Unlike the

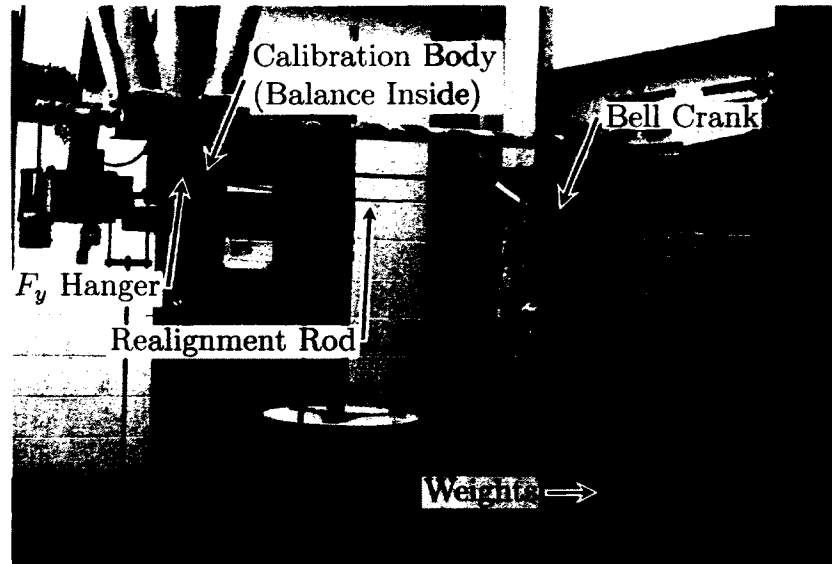


FIG. 25: F_y Cable Load Example

load point and angle uncertainties, the force and moment uncertainties are not a constant value and will vary for each particular load case.

4.1.2 BELL CRANKS AND PULLEYS

When the application of a side and/or axial force is desired to be in combination with a normal force, the axial and side forces must be applied in the horizontal plane of the calibration body as shown in Figure 25. In this figure a F_y load is applied via cables and a M_y load is applied by a pitch arm. It is typical to not rotate a balance for application of a side or axial force to align one with gravity, since a normal force load is generally of higher magnitude and it is undesirable to apply large loads via cables. Generally at NASA LaRC, bell cranks and pulleys are used to transfer a load from the horizontal plane to the vertical plane.

An example of the load path for a horizontal loading is illustrated in Figure 26. In this figure, it can be seen that the gravity load is attached to one end of the bell crank and the other is attached to a cable which then applies the load to the calibration body via a hanger and knife-edges. The use of a bell crank is preferred over a pulley, since the bell crank provides near frictionless movement which reduces the uncertainties. The pivot point of a bell crank is a knife-edge which is fixed to a movable platform for cable alignment. As discussed prior, knife-edges provide

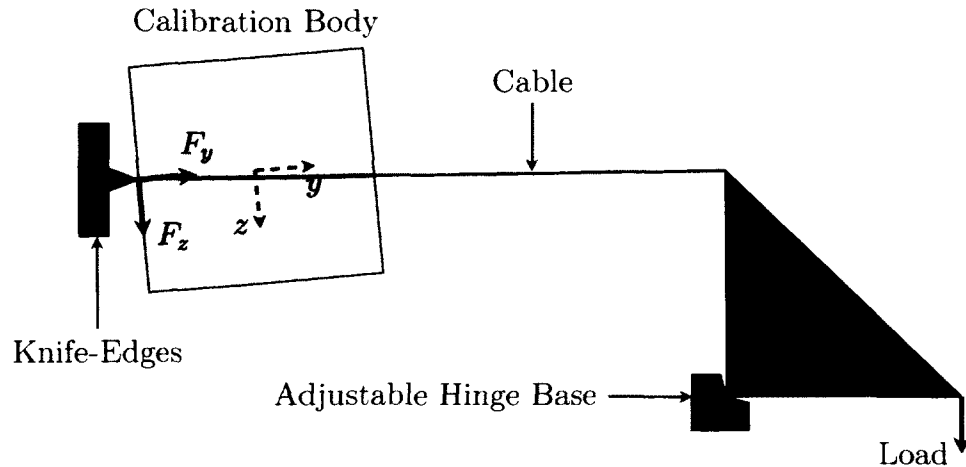


FIG. 26: Typical Bell Crank Arrangement

a means to transfer loads without a transfer of moments due to friction, whereas bearings in a pulley may result in frictional losses in the cable tension. Cable loads can be seen as similar to a pure hanger load, which was discussed in Section 4.1.1, but with the hanger aligned horizontally instead of vertically. Due to this analog, the derivations and process used for the hanger load uncertainties can be modified for the cable loads case.

The alignment of the horizontally pulled cables presents a challenge for the calibration of force balances. Unlike a hanger load, which is aligned with gravity, there are no simple references for alignment of the cable in the x -direction, for a side force load. At NASA LaRC, a cathetometer is used for vertical z -alignment, where the bell crank end of the cable is set to the same height as the knife-edge groove on the calibration fixture. At other facilities, simple bubble levels have been used to set the cable to level for the z -alignment.

At NASA LaRC, the alignment of the cable in the x -direction is achieved with “line-up” numbers; these line-up numbers use prerecorded balance outputs of a pure hanger load for the component under alignment. For example, a side force cable load will reference to the delta balance outputs of a side force hanger load. The cable is considered to be aligned once the delta outputs of the balance are equal. Note that the delta outputs are the difference between a tare point with the calibration hardware attached and a fully loaded point, which will account for the difference in tare hardware between the pure hanger and cable load. The cable alignment is only

TABLE 17: Angle Uncertainty Sources

| Source | Description | Uncertainty Estimate | Impact |
|-----------------|-----------------------------------|----------------------|----------------|
| Cathetometer | Vertical cable alignment | 1/64 in. | F_y, F_z |
| Line Up Numbers | Initial horizontal alignment | 0.0005 mV/V | F_x, F_y |
| Realignment | Realignment after line up numbers | 1/64 in. | ϕ, θ |

done with a single load applied at a time, whether it be side or axial force. Once these numbers are met, the end of a flexible metal rod is adjusted to mark where the cable has to be for it to be aligned properly. On subsequent loads, the alignment of the cable loads are made by adjusting the bell crank until the flexible rod end is within visual tolerance to the cable.

It can be seen from the alignment process described that there are opportunities for large uncertainties to exist. Additionally, the uncertainties or biases in the alignment process are highly dependent on the calibrator, since many of the steps and processes are based on observations and not direct measurements, such as the position of the cable with respect to the adjusted rod for cable alignments.

The additional source of uncertainty from the cable loads that are considered in addition to the hanger loads are tabulated in Table 17. Note that the bell crank friction is not listed, since it is assumed to provide negligible friction to the system. From this table it can be seen that uncertainty estimates are not in the units of the impacted variables, lbs or in-lbs. Thus, the uncertainty estimates must be converted over to force and moment units via physics-based equations or characteristics of the balance.

The line-up numbers that are used for the cable alignments are in units of the balance output, microvolts per volt. The balance output is normalized by the bridge excitation voltage to reduce the output sensitivity to the excitation voltage level. Since the line-up numbers rely on the balance, these number will have different uncertainties due to differences in balance sensitivities. The line-up number uncertainty estimate can be converted directly to units of force and moment by using the primary sensitivities of a balance. This can be done since a balance is fundamentally linear, since second order effects relatively small.

TABLE 18: Balances Sensitivities and Uncertainty Estimates

| | NTF-118A | | SS12 | |
|-------|--|---------------------------------|--|----------------------------------|
| | Sensitivity lbs/mV/V or in-lbs/mV/V. | Uncertainty lbs or in-lbs | Sensitivity lbs/mV/V or in-lbs/mV/V. | Uncertainty lbs or in-lbs. |
| F_x | 366.47 | 0.18 | NA | NA |
| F_y | 2037.82 | 1.02 | 15.5 | 0.0078 |
| F_z | 3175.84 | 1.59 | 37.7 | 0.0189 |
| M_x | 14576.89 | 7.29 | 45.56 | 0.0228 |
| M_y | 9225.33 | 4.61 | 50.63 | 0.0253 |
| M_z | 5785.42 | 2.89 | 11.3 | 0.0057 |

The primary sensitivities and line-up uncertainty estimates for two NASA LaRC balances are tabulated in Table 18. The two balances that are listed are of two different sizes and load capacities. The NTF-118A is a 2.375 inch diameter NTF internal balance with a normal force capacity of 6,500 lbs; the SS-12 is a 0.6 inch internal balance with a normal force capacity of 100 lbs. These two balances represent a range of balance ranges available, but this study will focus on larger scale balances such as the NTF-118A. Note that the SS-12 does not have a F_x component due to being a flow through balance.

In Table 18 a voltage uncertainty of 0.0005 mV/V is used to estimate the uncertainty for the line-up numbers with the balance sensitivities. Note that the units of the balance sensitivity listed are lb/mV/V or in-lb/mV/V for the force and moment components, respectively. Since the uncertainty estimate is proportional to the balance sensitivity, the uncertainty remains nearly constant if represented in terms of balance design loads. From the two balances listed, the uncertainty of the line-up numbers are on the order of 0.02 to 0.08 percent of design loads. With the values presented in terms of balance design loads and the results of Table 18, it is shown that the line-up number method has a small influence on the overall uncertainty of the applied load.

The other two uncertainties that are listed in Table 17 must have the units converted by applying physical trigonometric relations to the values. Both values were presented in units of inches, which represents the vertical or horizontal offset of the bell crank end of the cable with respect to a level condition. Knowing the length of

the cable and the vertical offset, the roll angle ϕ_c at which cable tension acts is found by:

$$\phi_c = \sin^{-1} \left(\frac{\delta z}{l} \right) \approx \frac{\delta z}{l} \quad (91)$$

where δz is the vertical offset of the bell crank cable end from a level condition, and l is the distance from the knife-edges to the bell crank cable end. Since δz is much smaller than l , small angle approximations can be used, as represented by the approximation in the equation above. For misalignment in the x -direction, a small change, δx , can be exchanged for δz to provide the yaw angle ψ_c of the cable's attitude. These small perturbations of the cable end will change the force vector which is applied to the knife-edges with respect to the balance coordinate system. This force vector definition is due to the assumption that the cable tension acts through a line formed by the two fixed cable ends.

A horizontal cable that is simply supported, has zero moment at the ends, where the cable will deform or sag due to gravity. The shape which such a constrained cable will form is called a catenary, a shape that is proportional to a hyperbolic cosine [39]. An illustration of the catenary shape of a tensioned flexible-cable is shown in Figure 27. As shown in Figure 27, a flexible cable will sag under its own weight, where the maximum vertical displacement is at the mid-length of the cable, if the two ends are at the same height. Since the lowest point of the cable is at the mid-length distance between the free ends, half the weight of the cable is shared equally between each fixed end of the cable, assuming constant material properties. During the alignment process of the cable loads, preloads are added to keep the hardware in place and to prevent significant sag of the system. Assuming that the height difference of the cables ends are small, as shown in the uncertainty estimates, the catenary of the cables will have negligible effects on the cable tension.

The 20K stand at NASA LaRC employs rods between the hanger and the bell crank, instead of cables. A rod will change the end support constraints to cantilever, which will change the free hang shape to having zero slope at the fixed ends. Similar to the catenary of the cables, any sag in the rods used will be assumed to have negligible affects on the overall uncertainties.

With the cable angular offset found by Equation 91, the force vector applied to a level calibration body can be estimated. Using an Euler rotation matrix, Equation

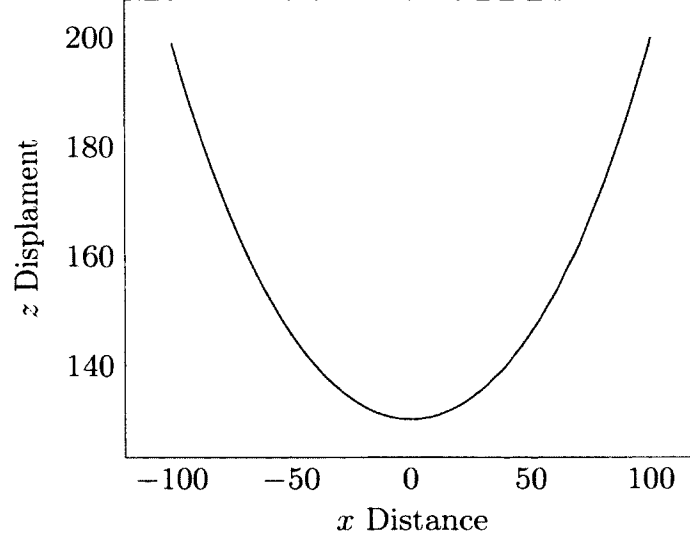


FIG. 27: Catenary Shape Example

67, the tension in the cable can be represented as a function of the pitch, roll and yaw angles of the cable with respect to a level balance coordinate system:

$$\mathbf{F}_{F_y} = P_{F_y} \begin{bmatrix} c_{\theta_c} s_{\psi_c} \\ c_{\phi_c} c_{\psi_c} + s_{\phi_c} s_{\psi_c} s_{\theta_c} \\ c_{\phi_c} s_{\psi_c} s_{\theta_c} - c_{\psi_c} s_{\phi_c} \end{bmatrix} \quad (92)$$

where ϕ_c , θ_c and ψ_c are rotations about the x , y and z axes, respectively, and P_{F_y} is the applied tension to the cable. Small angle approximation can be applied to simplify the derived side force vector. Assuming that the pitch angle θ_c is zero, the force vector can be further approximated as:

$$\mathbf{F}_{F_y} \approx P_{F_y} \begin{bmatrix} \psi_c \\ 1 \\ -\phi_c \end{bmatrix} \quad (93)$$

The assumption of zero pitch angle is due to pitch causing a rotation about the y -axis or about the primary axis of the cable load, thus resulting in no affect on the force vector. From Equation 93, it can be seen that the load is primarily along the y -axis with only small magnitudes in the two other axes. From observation, the magnitude of the force vector \mathbf{F}_{F_y} , if ψ_c or ϕ_c are non-zero, will be greater than the applied load P_{F_y} due to the small angle approximation error, but only by a small percentage. As

previously noted, the error due to the small angle approximation is acceptable for the angles that are expected in a manual calibration.

The derived force vector \mathbf{F}_{F_y} (Equation 93) is only applicable for a side force cable load and can not be used for an axial force cable load. For an axial force cable load, the cable will misaligned in the y - and z -directions, which will result in errors in the pitch and yaw angles of the cable's alignment. Using the Euler rotation matrix, the applied load due to an axial force cable load is converted to a force vector \mathbf{F}_{F_x} :

$$\mathbf{F}_{F_x} = P_{F_x} \begin{bmatrix} c_{\psi_c} c_{\theta_c} \\ s_{\psi_c} s_{\theta_c} s_{\phi_c} + s_{\psi_c} c_{\phi_c} \\ c_{\psi_c} s_{\theta_c} c_{\phi_c} + s_{\psi_c} s_{\phi_c} \end{bmatrix} \quad (94)$$

Similar to the side force case, a rotation about the cable axis, will result in no affect on the force vector, in this case the roll angle ϕ_c . As was done to the side force vector derivation, small angle approximation and zero roll angle assumption is used to simplify Equation 94:

$$\mathbf{F}_{F_x} \approx P_{F_x} \begin{bmatrix} 1 \\ \psi_c \\ \theta_c \end{bmatrix} \quad (95)$$

With Equations 93 and 95, the cable load uncertainty can be finalized with the same processes that were used in the hanger load section. Unlike the hanger loads where the applied load was aligned with gravity, i.e. single-component, the misalignment of the cable loads may result in a multicomponent applied load. Conversion of this multicomponent load to a non-level balance coordinate system requires the full Euler rotation matrix:

$$\begin{bmatrix} F_x \\ F_y \\ F_z \end{bmatrix}_{bal} = \begin{bmatrix} c_{\psi} c_{\theta} & s_{\psi} c_{\theta} & -s_{\theta} \\ c_{\psi} s_{\theta} s_{\phi} + s_{\psi} c_{\phi} & s_{\psi} s_{\theta} s_{\phi} + c_{\psi} c_{\phi} & c_{\theta} s_{\phi} \\ c_{\psi} s_{\theta} c_{\phi} + s_{\psi} s_{\phi} & s_{\psi} s_{\theta} c_{\phi} - c_{\psi} s_{\phi} & c_{\theta} c_{\phi} \end{bmatrix} \begin{bmatrix} F_x \\ F_y \\ F_z \end{bmatrix}_{app} \quad (96)$$

where $F_{i_{bal}}$ and $F_{i_{app}}$ are the force vector components of the balance and the applied load, respectively. Applying the small angle approximation and equating the yaw angle ψ to zero, the force vector in the balance coordinate system is simplified to:

$$\begin{bmatrix} F_x \\ F_y \\ F_z \end{bmatrix}_{bal} \approx \begin{bmatrix} F_{x_{app}} - F_{z_{app}}\theta \\ F_{y_{app}} + F_{x_{app}}\phi\theta + F_{z_{app}}\phi \\ F_{x_{app}}\theta - F_{y_{app}}\phi + F_{z_{app}}\phi \end{bmatrix} \quad (97)$$

The yaw angle is assumed to be zero in Equation 97, since the method used to align the cable loads will account for any calibration body yaw angle. The derivations for both the side and axial force, Equations 93 and 95, are substituted into Equation 97 to provide the final estimate of the applied force vector in the balance coordinate system:

$$\mathbf{F}_{F_y bal} = P_{F_y} \begin{bmatrix} \psi_c - \phi_c\theta \\ 1 + \psi_c\phi\theta + \phi_c\phi \\ \psi_c\theta - \phi + \phi_c \end{bmatrix} \quad (98)$$

$$\mathbf{F}_{F_x bal} = P_{F_x} \begin{bmatrix} 1 - \theta_c\theta \\ \psi_c + \phi\theta + \theta_c\phi \\ \theta - \psi_c\phi + \theta_c \end{bmatrix} \quad (99)$$

With the derived force vectors for a side and axial force cable load in the balance coordinate system, the applied moments to the balance are estimated by substituting Equations 98 and 99 into the moment Equation 69. Assuming that the hanger, which is attached to the cable, is placed at a position vector \mathbf{r} , the applied moment is found by the cross product taken between the position vector and the derived force vector:

$$\mathbf{M}_{F_y bal} = P_{F_y} \begin{bmatrix} (\psi_c\theta - \phi + \phi_c)y - (1 + \psi_c\phi\theta + \phi_c\phi)z \\ (\psi_c - \phi_c\theta)z - (\psi_c\theta - \phi + \phi_c)x \\ (1 + \psi_c\phi\theta + \phi_c\phi)x - (\psi_c - \phi_c\theta)y \end{bmatrix} \quad (100)$$

$$\mathbf{M}_{F_x bal} = P_{F_x} \begin{bmatrix} (\theta - \psi_c\phi + \theta_c)y - (\psi_c + \phi\theta + \theta_c\phi)z \\ (1 - \theta_c\theta)z - (\theta - \psi_c\phi + \theta_c)x \\ (\psi_c + \phi\theta + \theta_c\phi)x - (1 - \theta_c\theta)y \end{bmatrix} \quad (101)$$

Error propagation can be used to estimate the force and moment uncertainty of the cable loads. Using a Taylor series expansion, similar to the hanger load section, the force and moments are expanded to approximate the uncertainties. The general form for the force and moment uncertainties, $s_{F_{bal}}^2$ and $s_{M_{bal}}^2$, for the cable loads are written as:

$$\begin{aligned}
s_{F_{bal}}^2 &= \left(\frac{\partial F_{bal}}{\partial P_{F_x}} \right)^2 s_{P_{F_x}}^2 + \left(\frac{\partial F_{bal}}{\partial \phi_c} \right)^2 s_{\phi_c}^2 + \left(\frac{\partial F_{bal}}{\partial \psi_c} \right)^2 s_{\psi_c}^2 \\
&\quad + \left(\frac{\partial F_{bal}}{\partial \phi} \right)^2 s_{\phi}^2 + \left(\frac{\partial F_{bal}}{\partial \theta} \right)^2 s_{\theta}^2
\end{aligned} \tag{102}$$

$$\begin{aligned}
s_{M_{bal}}^2 &= \left(\frac{\partial M_{bal}}{\partial P_{F_x}} \right)^2 s_{P_{F_x}}^2 + \left(\frac{\partial M_{bal}}{\partial \phi_c} \right)^2 s_{\phi_c}^2 + \left(\frac{\partial M_{bal}}{\partial \psi_c} \right)^2 s_{\psi_c}^2 \\
&\quad + \left(\frac{\partial M_{bal}}{\partial \phi} \right)^2 s_{\phi}^2 + \left(\frac{\partial M_{bal}}{\partial \theta} \right)^2 s_{\theta}^2 + \left(\frac{\partial M_{bal}}{\partial x} \right)^2 s_x^2 \\
&\quad + \left(\frac{\partial M_{bal}}{\partial y} \right)^2 s_y^2 + \left(\frac{\partial M_{bal}}{\partial z} \right)^2 s_z^2
\end{aligned} \tag{103}$$

From Equations 102 and 103, it is seen that the propagation of error method expands the force and moment equations as a series of partial derivatives for each contributor to the overall uncertainties. The total uncertainty of the force vector due to a side force load is found by substituting Equation 98 into Equation 102 and taking all the partial derivatives:

$$\begin{aligned}
s_{F_{F_{bal}}}^2 &= \begin{bmatrix} (\psi_c - \phi_c \theta)^2 \\ (1 + \psi_c \phi \theta + \phi_c \phi)^2 \\ (\psi_c \theta - \phi + \phi_c)^2 \end{bmatrix} s_{P_{F_y}}^2 + \begin{bmatrix} P_{F_y}^2 \theta^2 \\ P_{F_y}^2 \phi^2 \\ P_{F_y}^2 \end{bmatrix} s_{\phi_c}^2 \\
&\quad + \begin{bmatrix} P_{F_y}^2 \\ P_{F_y}^2 \phi^2 \theta^2 \\ P_{F_y}^2 \theta^2 \end{bmatrix} s_{\psi_c}^2 + \begin{bmatrix} 0 \\ P_{F_y}^2 (\psi_c \theta + \phi_c)^2 \\ P_{F_y}^2 \end{bmatrix} s_{\phi}^2 \\
&\quad + \begin{bmatrix} P_{F_y}^2 \phi_c^2 \\ P_{F_y}^2 (\psi_c \phi)^2 \\ P_{F_y}^2 \psi_c^2 \end{bmatrix} s_{\theta}^2
\end{aligned} \tag{104}$$

After the partial derivatives are evaluated, the uncertainty equation is evaluated at the nominal values of each variable. As was done with the hanger load uncertainty, all the angles in the uncertainty equation should be zero, since the cables should be perfectly aligned and the calibration body should be level. Setting all the angle values in the force equation to zero, while keeping the P_{F_y} term as it is, results in a simplified uncertainty equation for the force vector:

$$s_{\mathbf{F}_{y_{bal}}}^2 = \begin{bmatrix} 0 \\ 1 \\ 0 \end{bmatrix} s_{P_{F_y}}^2 + \begin{bmatrix} 0 \\ 0 \\ P_{F_y}^2 \end{bmatrix} s_{\phi_c}^2 + \begin{bmatrix} P_{F_y}^2 \\ 0 \\ 0 \end{bmatrix} s_{\psi_c}^2 + \begin{bmatrix} 0 \\ 0 \\ P_{F_y}^2 \end{bmatrix} s_{\phi}^2 \quad (105)$$

From Equation 105, several observations are made of the properties of the force uncertainties. One observation is that the applied load uncertainty only affects the y -component of the force vector due to the zero angle assumption. If the zero angle condition was not enforced, the angle terms will have little to no contribution. The uncertainty of the pitch angle θ of the balance does not contribute to the overall force uncertainty, since all the terms preceding s_{θ} in Equation 104 have angles. Generally, for a large scale balance, similar to the NTF-118A, side force loads can be in the order of several thousand pounds, whereas the angles are on the order of several arc seconds. Thus, the side force load terms dominate the uncertainty equation and any angle term is negligible. The uncertainty of the applied moments due to a side force cable load is estimated by substituting Equation 100 into 103 and evaluating all the partial derivatives:

$$s_{M_{F_{y_{bal}}}}^2 = \begin{bmatrix} z^2 \\ 0 \\ x^2 \end{bmatrix} s_{P_{F_y}}^2 + \begin{bmatrix} P_{F_y}^2 y^2 \\ P_{F_y}^2 x^2 \\ 0 \end{bmatrix} s_{\phi_c}^2 + \begin{bmatrix} 0 \\ P_{F_y}^2 z^2 \\ P_{F_y}^2 y^2 \end{bmatrix} s_{\psi_c}^2 + \begin{bmatrix} P_{F_y}^2 y^2 \\ P_{F_y}^2 x^2 \\ 0 \end{bmatrix} s_{\phi}^2 \quad (106)$$

$$+ \begin{bmatrix} 0 \\ 0 \\ P_{F_y}^2 \end{bmatrix} s_x^2 + \begin{bmatrix} P_{F_y}^2 \\ 0 \\ 0 \end{bmatrix} s_z^2$$

The derived moment equation for the side force cable load is similar to that of the one derived for the hanger load derived, Equation 80. The two equations differ in the placement of the terms, such as the x and z variables for the applied load uncertainty, and the inclusion of the cable angle uncertainties. Similar to the hanger moment uncertainty, in order to minimize the total uncertainty, the lowest load should be used with large arms if an applied moment is required. For a case where a moment is not required and only a side force load, the x - and z -positions are nominally zero. With both x and z set to zero, only the y -position will remain with the angle uncertainty terms. Since the y -position can never be zero and is equal to half the width of the calibration body due to the placement of the knife-edges, the

contributions of the s_{ϕ_c} , s_{ψ_c} and s_{ϕ} can only be minimized by reduction of the side force load. This reduction is not preferred, since the required side force load must be applied at the proper magnitude.

The same methodology that was used to simplify the force and moment uncertainties for the side force cable loads is used for the axial force equations:

$$s_{F_{bal}}^2 = \begin{bmatrix} 1 \\ 0 \\ 0 \end{bmatrix} s_{P_{F_x}}^2 + \begin{bmatrix} 0 \\ 0 \\ P_{F_x}^2 \end{bmatrix} s_{\theta_c}^2 + \begin{bmatrix} 0 \\ P_{F_x}^2 \\ 0 \end{bmatrix} s_{\psi_c}^2 + \begin{bmatrix} 0 \\ 0 \\ P_{F_x}^2 \end{bmatrix} s_{\theta}^2 \quad (107)$$

$$s_{M_{bal}}^2 = \begin{bmatrix} 0 \\ z^2 \\ y^2 \end{bmatrix} s_{P_{F_x}}^2 + \begin{bmatrix} P_{F_x}^2 y^2 \\ P_{F_x}^2 x^2 \\ 0 \end{bmatrix} s_{\theta_c}^2 + \begin{bmatrix} P_{F_x}^2 z^2 \\ 0 \\ P_{F_x}^2 x^2 \end{bmatrix} s_{\psi_c}^2 + \begin{bmatrix} P_{F_x}^2 y^2 \\ P_{F_x}^2 x^2 \\ 0 \end{bmatrix} s_{\theta}^2 \quad (108)$$

$$+ \begin{bmatrix} 0 \\ 0 \\ P_{F_x}^2 \end{bmatrix} s_y^2 + \begin{bmatrix} 0 \\ P_{F_x}^2 \\ 0 \end{bmatrix} s_z^2$$

Equations 107 and 108 are both similar to those of the side force loads, only with several of the terms reordered and/or exchanged. The same properties of the side force equations apply to the axial force equations, namely, that the moment uncertainty is minimized when long arms and low loads are used. With the set of uncertainty equations for both side and axial force cable loads, the applied load, positional and angular uncertainties that were quantified in Section 4.1.1 can be used to provide uncertainty estimates.

4.1.3 MOMENT ARM UNCERTAINTY

For the application of moments on a manual stand, arms are attached to the calibration body where free weights are hung. The inclusion of these arms leads to several sources of uncertainty over the previous uncertainty derivation; namely load position, and arm deflections. Generally, manual stand calibrations rely on lengthy arms which are called “long arms”. The term long arm relates how low magnitude loads are applied to a long arm to generate a pseudo pure moment. This is done to reduce the amount of load that is required to be applied at the end of the arm and the uncertainty of the applied moment. From the derivations of the moment

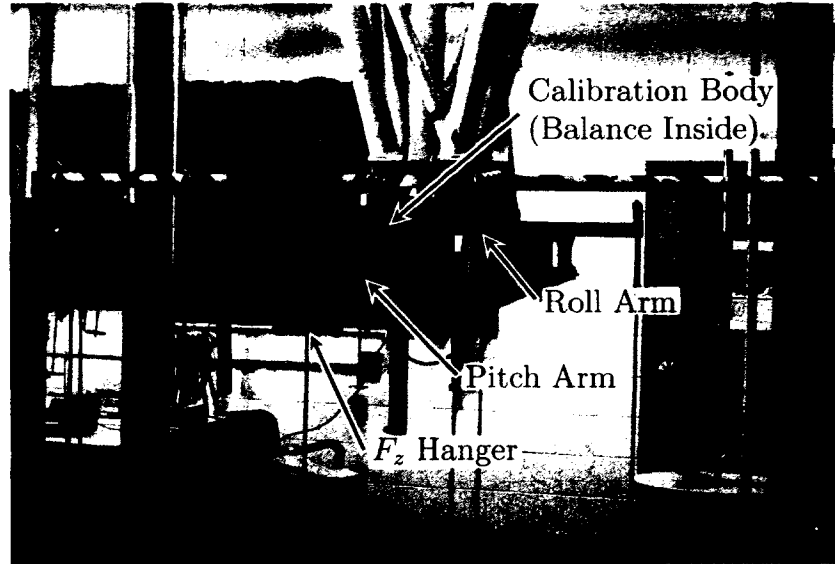


FIG. 28: M_x and M_y Arm Load Example

uncertainties in a hanger load, it was shown that it is desired to use low loads with long arms to reduce the uncertainties.

These arms that are attached to the calibration body provide locations to apply hanger loads via knife-edges at fixed moment arm lengths. Since the arm loads rely on the use of a hanger and knife-edges, the derived force and moment equations in Section 4.1.1 will represent the arm loadings after some modifications are made to the equations. These modifications will only pertain to the positioning of the applied hanger load, which only affects the moment equation. With the attachment of these arms, additional positioning offsets are introduced, since the arm is attached mechanically with some error. Under load, these arms will deform and cause a change in the position at which the load is applied.

The attached arm behaves as a cantilever beam, due to the assumption of rigid attachment to the calibration body. The deformation shape of cantilever beams with a constant cross section are well understood and documented in literature [40]. The vertical deflection of the free-end is estimated with the knowledge of the material and cross sectional properties of the beam under load:

$$\delta_z = \frac{PL^3}{3EI} \quad (109)$$

TABLE 19: NTF-113C Moment Arm Properties

| Component | L , in. | P , lbs. | I , in. ⁴ | δ_z , in. |
|-----------|-----------|------------|------------------------|------------------|
| M_x | 38 | 225 | 0.677 | 0.209 |
| M_y | 38 | 320 | 0.677 | 0.298 |
| M_z | 38 | 162 | 0.677 | 0.151 |

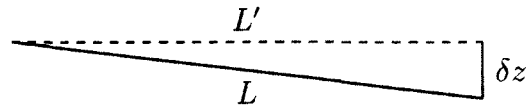


FIG. 29: Triangle Analog for Deflected Beam

where P is the applied load at L distance from the fixed end, E is the Young's modulus of elasticity of the beam's material, and I is the moment of inertia of the beam. From this it can be seen that the load point deflection will be exponentially increased by the length L . From the properties of the moment uncertainty equation, it was desired to have lengthy arms which will increase the possibility of deflection. Although for a constant applied moment, the increase in arm length will require a decreased applied load that will in turn reduce final deflections. The properties of the beams used for the NTF-113C calibration are tabulated in Table 19.

In Table 19, the estimated deflection calculations assume a modulus of elasticity of 29,000 ksi, which is typical for carbon steel. From these results it is seen that the arms do not deflect significantly for their lengths, with the largest deflection being for pitching moment. Due to the relatively small deflections, the load point will not significantly change along the long axis of the beam, which is the desired property of a moment arm. This is shown by equating the beam to a triangle with a hypotenuse equal to the beam length L and the opposite side equal to the deflection δz , as shown in Figure 29. With this triangle analog, the adjacent side will signify the load position along the long axis of the beam L' ; for the largest computed deflection, the beam length would decrease by 0.0012 inches ($L' - L$). Assuming that the arm deflection will have no affect on the load position, the following equations represent the load point:

$$x = x_{FixtureQA} + x_{arm} + x_{KnifeEdge} \quad (110)$$

TABLE 20: Arm Load Position Uncertainty Estimates

| Variable | Estimate, in. |
|----------|---------------|
| s_x | 0.00065 |
| s_y | 0.00065 |
| s_z | 0.00042 |

$$y = y_{FixtureQA} + y_{Arm} + y_{KnifeEdge} \quad (111)$$

$$z = z_{FixtureQA} + z_{Arm} \quad (112)$$

Since the moment arms can be used for all three moment types, the x , y and z terms can be interchanged depending on the placement of the arms and balance orientation. For the equations shown, it is assumed that x represents the long axis of the beam, y represents the lateral axis of the beam, and z represents the normal or load direction of the beam. Similar to the previous section, propagation of error can be used to estimate the uncertainties for each of the three position terms:

$$s_z^2 = s_{z_{FixtureQA}}^2 + s_{z_{Arm}}^2 \quad (113)$$

$$s_y^2 = s_{y_{FixtureQA}}^2 + s_{y_{Arm}}^2 + s_{y_{KnifeEdge}}^2 \quad (114)$$

$$s_x^2 = s_{x_{FixtureQA}}^2 + s_{x_{arm}}^2 + s_{x_{KnifeEdge}}^2 \quad (115)$$

With the uncertainty derivations, the values from Table 13 can be used to estimate the total uncertainty of the load position. Note that the arm uncertainties $s_{i_{arm}}$ are assumed to have the same level of uncertainty of the fixture QA, since the arm length is measured with a CMM. From Table 20 it is seen that the uncertainty estimates for the arm load position is much smaller than the values presented in Table 14 due to the lack of certain uncertainty factors, such as calipers.

4.1.4 CALIBRATION BODY DEFLECTION

The deflection or torsion of the calibration body may occur while the balance is subjected to loads. The calibration body for a balance is generally a hardened steel

shell with loads applied to the outside. These calibration bodies are long square cross section beams, which have a circular bore to house the balances. For moment balances such as the NTF-113C, the calibration body only makes contact with the balance at the forward end, thus the calibration body can be assumed to be a cantilever beam. A beam with constant cross section and subjected to a moment T will result in an angular twist of ϕ at some distance L away from the fixed end [40]:

$$\phi = \frac{TL}{GI_p} \quad (116)$$

where G is the shear modulus for the beam's material, and I_p is the polar moment of inertia of the beam's cross section. Assuming that the cross section of the NTF-113C calibration body is a 4 inch square with a 2.75 inch bore, the polar moment of inertia can be found by:

$$I_p = \frac{h^4}{6} - \pi d^4/32$$

where h is the height of the faces of the calibration body and d is the diameter of the central bore hole. For the NTF-113C calibration body, the polar moment of inertia is assumed to be 37.05 in⁴. Assuming that the balance is subjected to the maximum rolling moment, $T = 9,000$ in-lbs, at the BMC, $L = 5.7$ in., and has a shear modulus of 12,000 ksi, which is typical for hardened steels, the maximum angular rotation is 0.0066 deg. Note that the calibration body for the NTF-113C is PH17-4 stainless steel and is hardened to H915. From this result it is shown that the calibration body does not deform significantly to warrant any additional uncertainty accounting.

4.1.5 DATA ACQUISITION

The balance voltages are considered to be the response of the calibration experiment, although the uncertainty can be combined with the overall uncertainty of the manual stand. Measurement of the balance voltages will have errors associated with noise and drifts in the data acquisition system. The entire data system consists of an electrical connection box, cabling, multiplexer, and a digital multimeter. Each of these components adds electrical junctions where thermocouple effects may be present. At these junctions two or more dissimilar metals may make contact and result in a small electrical voltage being generated, which may influence the voltage measured.

TABLE 21: Data Acquisition Uncertainty Estimates

| Component | NTF-113C | SS-12 |
|-----------------|----------|--------|
| F_x , lbs. | 0.18 | NA |
| F_y , lbs. | 1.02 | 0.0078 |
| F_z , lbs. | 1.59 | 0.0189 |
| M_x , in-lbs. | 7.29 | 0.0228 |
| M_y , in-lbs. | 4.61 | 0.0253 |
| M_z , in-lbs. | 2.89 | 0.0057 |

Other sources of electrical uncertainty exists in the stability of the electrical components used for voltage supply, voltage measurement and channel switching. Each of these components used are susceptible to thermal drift in the systems which can affect the bias in the final voltage measurement. These thermal drifts tend to occur over long periods of time and may affect day-to-day absolute measurements. During a balance calibration, the data system is left on overnight, or longer, to let the system reach this stable period.

From several years of knowledge, the stability of the data acquisition system is around 0.0005 mV/V. This value includes all the noise from the wires, thermal couple effects of the connectors and thermal stability of the data acquisition system. Similar to line-up numbers described in Section 4.1.2, the uncertainty of the measured voltages are a function of the balance sensitivities. The conversion of the voltage uncertainty can be accomplished by multiplying the known uncertainty by the balance's primary sensitivity, which was done for the line-up numbers. Using this approach, the uncertainty estimates for the NTF-113C and SS-12 balances are tabulated in Table 21.

The results in Table 21 are similar to the values of the line-up number uncertainty due to the similar uncertainty value used for the voltages. Note that the units are lbs and in-lbs for the force and moment components, respectively. The converted values for the data acquisition uncertainty can be directly used to estimate the overall uncertainty of the calibration system.

4.2 OVERALL SYSTEM UNCERTAINTY

From the previous sections, the uncertainties in the applied forces and moments were derived from the assumed uncertainty sources. These separate sources can be

combined to yield an overall applied load uncertainty. Since each uncertainty source is assumed to be independent of each other, the overall uncertainty is found by the root-sum square of all the separate load cases:

$$s_{\mathbf{F}_{Total}}^2 = \sum_{i=1}^N s_{\mathbf{F}_i}^2 \quad (117)$$

where $s_{\mathbf{F}_{Total}}$ is the total force vector uncertainty and $s_{\mathbf{F}_i}$ is the contribution to the force vector uncertainty from each uncertainty source. From this equation it is seen that the total uncertainty will increase with every additional uncertainty source or load applied to the calibration body. For example, if two F_z hangers are applied, one for pure F_z and another for a moment arm, the uncertainty in F_z will increase by about $\sqrt{2}$ times the individual hanger load uncertainty, since this would include two separate applied hanger loads. Though, for a case where both a F_z and F_y are applied to the calibration body, the increase in overall uncertainty will differ from the double F_z load case due to the difference in the uncertainty equations for F_z and F_y .

The total uncertainty estimates for the manual stand are not constant values for any load that is applied. From the equations presented in the previous sections, the uncertainties are based on the properties of the individual load case, such that the uncertainty estimates would change based on having or not having an applied F_x term. To further complicate the matter, every load point in a calibration schedule has different sets of load combination which will toggle on and off the added uncertainties. Thus, the uncertainty estimates from the components that are not loaded will have to be neglected. While computing uncertainties, a case structure can be added to each individual uncertainty source checking whether or not the uncertainty should be included in the overall estimate. For example, the uncertainty of an applied F_z load will be assumed to be zero if no F_z is applied to the balance:

$$s_{F_z} = \begin{cases} 0 & P_{F_z} = 0 \\ s_{SF} & P_{F_z} \neq 0 \end{cases}$$

The same logic is applied to each of the possible loads that can be applied to the balance, including applied moments. Furthermore, special care must be taken to ensure that the correct component is in the gravity direction, since this will change

TABLE 22: Manual Stand Load Combinations

| Load Combinations | Active Uncertainties | Balance Orientation |
|-------------------|--|---------------------|
| $F_z \times F_x$ | $s_{P_{F_z}}$ (Hanger) and $s_{P_{F_x}}$ (Cable) | F_z |
| $F_z \times F_y$ | $s_{P_{F_z}}$ (Hanger) and $s_{P_{F_y}}$ (Cable) | F_z |
| $F_z \times M_x$ | $s_{P_{F_z}}$ (Hanger) and $s_{P_{F_z}}$ (Roll Arm) | F_z |
| $F_z \times M_y$ | $s_{P_{F_z}}$ (Hanger) and $s_{P_{F_y}}$ (Pitch Arm) | F_z |
| $F_z \times M_z$ | $s_{P_{F_z}}$ (Hanger) and $s_{P_{F_y}}$ (Cable) | F_z |
| $F_y \times F_x$ | $s_{P_{F_y}}$ (Hanger) and $s_{P_{F_x}}$ (Cable) | F_y |
| $F_y \times M_x$ | $s_{P_{F_y}}$ (Hanger) and $s_{P_{F_y}}$ (Roll Arm) | F_y |
| $F_y \times M_y$ | $s_{P_{F_z}}$ (Pitch Arm) and $s_{P_{F_y}}$ (Cable) | F_z |
| $F_y \times M_z$ | $s_{P_{F_y}}$ (Hanger) and $s_{P_{F_y}}$ (Yaw Arm) | F_y |
| $F_x \times M_x$ | $s_{P_{F_z}}$ (Roll Arm) and $s_{P_{F_x}}$ (Cable) | F_z |
| $F_x \times M_y$ | $s_{P_{F_z}}$ (Pitch Arm) and $s_{P_{F_x}}$ (Cable) | F_z |
| $F_x \times M_z$ | $s_{P_{F_y}}$ (Yaw Arm) and $s_{P_{F_x}}$ (Cable) | F_y |
| $M_x \times M_y$ | $s_{P_{F_z}}$ (Pitch Arm) and $s_{P_{F_z}}$ (Roll Arm) | F_z |
| $M_x \times M_z$ | $s_{P_{F_y}}$ (Roll Arm) and $s_{P_{F_y}}$ (Yaw Arm) | F_y |
| $M_y \times M_z$ | $s_{P_{F_z}}$ (Pitch Arm) and $s_{P_{F_y}}$ (Cable) | F_z |

depending on the applied F_z . A manual calibration is based on a OFAT calibration schedule, which was discussed in Section 1.1.3. With an OFAT design, only combinations of two component loads are used to build the regression model. Since a manual calibration is broken up into these different combinations of loads, the uncertainties can be estimated for each of the possible load combinations. All the two-component load combinations that are used during the calibration are tabulated in Table 22. This table also includes which uncertainty terms will be active for the desired combination and the balance orientation. From this table it is seen that there is a hierarchy of which force component takes the gravity direction, such as when a F_z load is required it will be the component loaded via a hanger followed by the F_y component loaded by cable. Note that the balance orientation column defines which load is applied in-line with gravity, such as a notation of F_z meaning that the balance z -axis is aligned with gravity.

Estimates of the total uncertainty for the listed combinations can be made using the full-scale design loads of a balance. These uncertainties will assume that the balance is loaded to 100% of full scale for the listed combinations, which will result in the worst case load combinations. Note that these load levels are actually applied during a manual stand calibration for the listed combinations. For this research,

TABLE 23: NTF-113C Design Loads

| Components | F_x , lbs | F_y , lbs | F_z , lbs | M_x , in-lbs | M_y , in-lbs | M_z in-lbs |
|--------------|-------------|-------------|-------------|----------------|----------------|--------------|
| Design Loads | 400 | 4,000 | 6,500 | 9,000 | 13,000 | 6,500 |

TABLE 24: NTF-113C Calibration Properties

| | |
|------------------------|--------|
| Pitch Arm Length | 40 in. |
| Roll Arm Length | 40 in. |
| Yaw Arm Length | 40 in. |
| Calibration Body Width | 4 in. |
| Side Cable Length | 8 ft |
| Axial Cable Length | 7 ft |

the considered balance is the NTF-113C and the design loads for this balance are tabulated in Table 23.

With the applied calibration loads defined by the load combinations and the balance design loads, the other variables in the uncertainty equations need to be defined. These variables are the lengths of the pitch, roll and yaw arms; F_x and F_y cable lengths; and load point information. The values for these variables for the 20K manual stand at NASA LaRC and the NTF-113C balance are tabulated in Table 24. The listed values only pertain to the NTF family of balances calibrated specifically on the 20K stand; the results from this balance/stand combination may be used for other balance/stand combinations with similar load ranges and hardware arrangements. However, it is cautioned that these values will not represent balances and load stands with drastically different load ranges.

Using the inputs from Table 24 and the load combination from Table 22, the uncertainty estimates and the input loads are tabulated in Table 25. The applied loads shown in this table are based on the balance design loads and the load combinations listed previously. Note that the units for both the load and the uncertainties are in lbs and in-lbs for the force and moment components, respectively. From the table it is seen that the load combinations with the largest errors are the combinations that involve F_z loads. These loads are the highest due to the heavy loads used to apply full-scale F_z . All the moment-only combinations have the lowest uncertainties due to the low loads used to provide the moment, typically under 250 lbs. Note that pure

TABLE 25: Load Combinations and Uncertainty Results

| F_x , lbs. | F_y , lbs. | F_z , lbs. | M_x , in-lbs. | M_y , in-lbs. | M_z , in-lbs. | s_{F_x} , lbs. | s_{F_y} , lbs. | s_{F_z} , lbs. | s_{M_x} , in-lbs. | s_{M_y} , in-lbs. | s_{M_z} , in-lbs. |
|-----------------|-----------------|-----------------|--------------------|--------------------|--------------------|---------------------|---------------------|---------------------|------------------------|------------------------|------------------------|
| 400 | 0 | 6500 | 0 | 0 | 0 | 1.02 | 2.00 | 2.27 | 19.5 | 9.65 | 4.24 |
| 0 | 4000 | 6500 | 0 | 0 | 0 | 1.21 | 2.01 | 2.50 | 19.5 | 9.72 | 5.86 |
| 0 | 0 | 6500 | 9000 | 0 | 0 | 0.97 | 1.68 | 1.61 | 17.5 | 8.26 | 3.19 |
| 0 | 0 | 6500 | 0 | 13000 | 0 | 0.96 | 1.68 | 1.61 | 17.5 | 8.24 | 4.00 |
| 0 | 0 | 6500 | 0 | 0 | 6500 | 1.03 | 2.00 | 2.28 | 19.5 | 9.80 | 4.25 |
| 400 | 4000 | 0 | 0 | 0 | 0 | 0.66 | 1.45 | 2.40 | 10.5 | 6.53 | 6.09 |
| 0 | 4000 | 0 | 9000 | 0 | 0 | 0.60 | 1.04 | 1.78 | 7.5 | 4.80 | 5.04 |
| 0 | 4000 | 0 | 0 | 13000 | 0 | 0.70 | 1.45 | 2.48 | 10.4 | 6.65 | 6.48 |
| 0 | 4000 | 0 | 0 | 0 | 6500 | 0.61 | 1.04 | 1.78 | 7.5 | 4.81 | 5.10 |
| 400 | 0 | 0 | 9000 | 0 | 0 | 0.26 | 1.44 | 2.24 | 10.3 | 6.67 | 4.24 |
| 400 | 0 | 0 | 0 | 13000 | 0 | 0.26 | 1.44 | 2.24 | 10.3 | 6.54 | 5.06 |
| 400 | 0 | 0 | 0 | 0 | 6500 | 0.26 | 1.44 | 2.24 | 10.3 | 6.68 | 4.25 |
| 0 | 0 | 0 | 9000 | 13000 | 0 | 0.19 | 1.02 | 1.58 | 7.4 | 4.62 | 4.22 |
| 0 | 0 | 0 | 9000 | 0 | 6500 | 0.19 | 1.02 | 1.58 | 7.3 | 5.00 | 2.92 |
| 0 | 0 | 0 | 0 | 13000 | 6500 | 0.32 | 1.44 | 2.26 | 10.3 | 6.75 | 5.07 |

moments are not applied, the application of the moment will result in an applied F_y or F_z load, which are not shown in the table but are considered in the uncertainty calculations.

The average uncertainty of all the load combinations can be used to represent the performance of the manual calibration system for the given balance/stand combination. The average values in both engineering units and percent of full scale are tabulated in Table 26 accompanied with the quoted standard deviations of a manual calibration for the NTF-113C balance. From the full scale values, the force and moment components are mostly below 0.01% of full scale with only the F_x and M_x estimates being larger. The uncertainty of F_x is expected to be larger than the other two force terms due to the lower load capacity on this component which makes the component is sensitive to errors. For the M_x term, it is seen from the balance sensitivities listed in Table 18 that this component has more sensitive than the other two moment components which results in the higher uncertainty shown. Comparison of the estimated uncertainties to the quoted standard deviations from the balance calibration shows good agreement between the two values for several of the components. For the values shown, only the F_x and M_x components have larger uncertainties than

TABLE 26: Average Uncertainty Estimates

| | s_{F_x} , lbs. | s_{F_y} , lbs. | s_{F_z} , lbs. | s_{M_x} , in-lbs. | s_{M_y} , in-lbs. | s_{M_z} , in-lbs. |
|-----------------------|---------------------|---------------------|---------------------|------------------------|------------------------|------------------------|
| Engineering Units | 0.61 | 1.48 | 2.06 | 12.35 | 6.98 | 4.67 |
| Percent of Full Scale | 0.15 | 0.04 | 0.03 | 0.14 | 0.05 | 0.07 |
| Quoted Std. Dev. | 0.12 | 0.07 | 0.03 | 0.09 | 0.05 | 0.10 |

the standard deviations due to these components having high sensitivities. Due to these high values, further checks should be made on the uncertainties used in the derivations.

From the results of the uncertainty analysis, it was shown that the equations and methods developed provide reasonable results of the applied load uncertainty. The uncertainty estimates in engineering units will be used later for use in the prediction interval equation derived in Section 3. The uncertainty estimates that are presented in a percentage of full scale could be used to get a rough estimate of the applied load uncertainty for another balance and/or manual stand, since several of the uncertainty estimates will remain constant when presented in percent of full scale. It is cautioned that this kind of rough estimate only be used for balance and stands of similar range to the NTF-113C and the NASA LaRC 20K stand.

4.3 UNCERTAINTY ESTIMATE VALIDATION

A MCS was used to validate the uncertainty estimates from the propagation of error method. In this simulation the mathematical model implemented was the unsimplified model of the manual stand system. In this way, the assumptions of linearization and small angle approximation, which were implemented in the propagation of error derivations, are tested against the full unsimplified mathematical model. For example, for a hanger load, the force applied to the balance is represented by Equation 96, where the original force vector, \mathbf{F}_{app} , is the applied weight acting solely in the gravity direction, such that if a F_z load is desired the force vector would equal $[0 \ 0 \ P]'$. Applied moments to the balance are found by taking the cross product between a position vector, \mathbf{r} and the force vector, as shown in Equation 69. Cable loads that are applied to the balance are calculated through the same

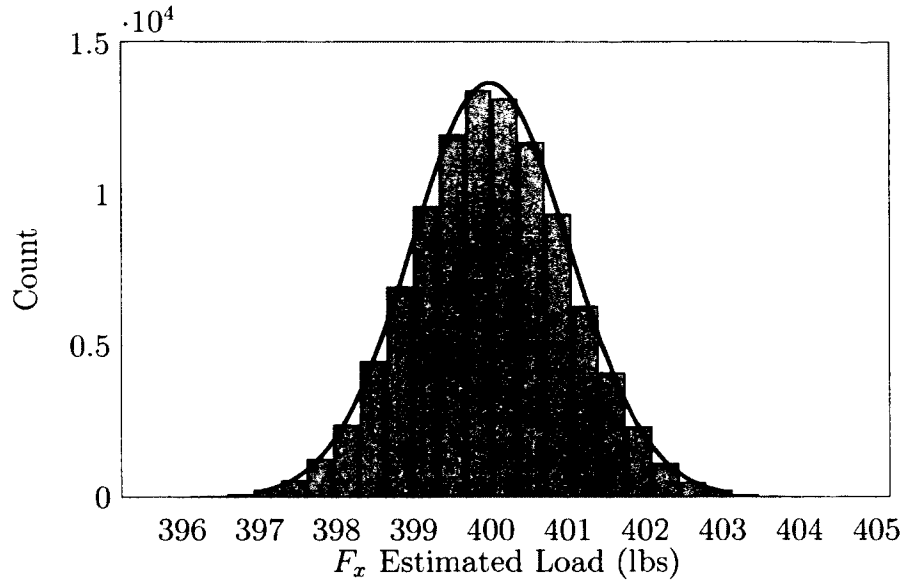


FIG. 30: F_x Histogram

routine as a hanger load, but with \mathbf{F}_{app} equal to the force vector which is the result of rotating the applied load by the cable angles.

In a MCS, the input variables to the model are randomly sampled from an assumed statistical distribution and a sample population is formed for the output variables. Many iterations of this process are made to ensure that a proper distribution is formed, in this study 100,000 iterations were made. A normal distribution was assumed for all the variables in the mathematical model, since all the variables are represented as random noise in the system. The assumed standard deviations for the variables are the values shown in the previous sections, such as Tables 13, 15 and 17.

The load schedule shown in Table 25 was used as the inputs to the MSC, where the perturbed forces in the balance coordinate system are the outputs. Figure 30 is the histogram and the normal distribution for the F_x component of the first load in the schedule. From this figure, it is shown that the sample population for the F_x component does follow a normal distribution with a mean of 400 lbs and a standard deviation of 1.02 lbs, which is the expected result from the MCS.

The standard deviation values for each of the load combinations are tabulated in Table 27. These results from the simulation are in agreement with the values that were calculated using the propagation of error method in Table 22. This agreement shows that the assumptions made for the propagation of error are valid and that

TABLE 27: MCS Standard Deviation Results

| s_{F_x} , lbs. | s_{F_y} , lbs. | s_{F_z} , lbs. | s_{M_x} , in-lbs. | s_{M_y} , in-lbs. | s_{M_z} , in-lbs. |
|---------------------|---------------------|---------------------|------------------------|------------------------|------------------------|
| 1.02 | 2.01 | 2.27 | 19.41 | 9.76 | 4.23 |
| 1.21 | 2.00 | 2.52 | 19.44 | 9.62 | 5.99 |
| 1.00 | 1.72 | 1.61 | 17.53 | 8.29 | 3.18 |
| 1.00 | 1.72 | 1.61 | 17.48 | 8.23 | 3.99 |
| 1.03 | 2.00 | 2.28 | 19.38 | 9.80 | 4.27 |
| 0.66 | 1.45 | 2.39 | 10.47 | 6.54 | 6.09 |
| 0.63 | 1.04 | 1.80 | 7.50 | 4.79 | 5.06 |
| 0.70 | 1.46 | 2.49 | 10.63 | 6.57 | 6.63 |
| 0.63 | 1.03 | 1.79 | 7.51 | 4.79 | 5.12 |
| 0.26 | 1.44 | 2.24 | 10.30 | 6.56 | 4.23 |
| 0.26 | 1.44 | 2.24 | 10.39 | 6.61 | 5.08 |
| 0.26 | 1.44 | 2.25 | 10.31 | 6.68 | 4.25 |
| 0.20 | 1.02 | 1.59 | 7.38 | 4.68 | 4.23 |
| 0.19 | 1.02 | 1.58 | 7.33 | 5.00 | 2.93 |
| 0.31 | 1.44 | 2.25 | 10.37 | 6.78 | 5.08 |

TABLE 28: Average Difference Between Error Propagation and MCS Results

| F_x , lbs. | F_y , lbs. | F_z , lbs. | M_x , in-lbs. | M_y , in-lbs. | M_z , in-lbs. |
|-----------------|-----------------|-----------------|--------------------|--------------------|--------------------|
| -0.0094 | -0.0051 | -0.0029 | -0.0131 | -0.0001 | -0.0222 |

there are no strong correlations in the system. To further depict the agreement, the average differences between the two methods are tabulated in Table 28. From the average difference values, it is shown that the MCS estimates slightly larger standard deviation values, but the difference between the two estimates are negligible. With these results, either the MCS or propagation of error can be used to mathematically determine the uncertainties of a calibration system. The propagation of error method does have added benefits over the MCS, since it provides a direct solution and allows for interpretation of the individual uncertainties' sensitivities.

CHAPTER 5

UNCERTAINTY AND PREDICTION INTERVAL

INTEGRATION

The results from the manual stand uncertainty derivations in Section 4.2 can be used to estimate the prediction interval estimates for a balance undergoing check loads. To demonstrate derived prediction interval and manual stand uncertainties, data were collected on several check loads that were applied to the NTF-113C balance in one of the preparation bays at NASA LaRC's NTF [36]. For this demonstration a manual calibration which was performed on the 20K stand is used for the estimation of applied loads, thus the prediction intervals require the estimated uncertainties for the manual stand. The ILS estimated bias for the check load system should also be entered into the equation to provide the correct total uncertainty for the prediction interval estimates.

During the demonstration the balance was loaded with the ILS with a load stack of 2,500 lbs at various angles and load positions. The characteristics and capability of the ILS were detailed in Section 1.1.4. For these loadings the balance was installed to a repositioning system, which allowed for pitch and roll authority, and mimics the model support system in the tunnel. For attachment, the ILS was mounted to the calibration body of the balance as shown in Figure 31. The loads that were applied to the balance during this demonstration are tabulated in Table 5, and are based on the physics of the ILS. These load combinations were chosen to provide several multi-component loads ranging from one to six simultaneous loads.

From the prediction interval derivation, the estimates for the calibration and check system uncertainties must be in units of the balance response, mV/V. In order to convert the uncertainty estimates from Section 4.2 to mV/V, the primary sensitivities of the NTF-113C, listed in Table 18, can be used. The assumed estimates for the calibration and check system uncertainties in both engineering units (EU) and balance response units are tabulated in Table 30. With these uncertainty estimates and the calibration properties, from the manual stand calibration of the NTF-113C, the prediction intervals can be calculated for the check loads that were applied to

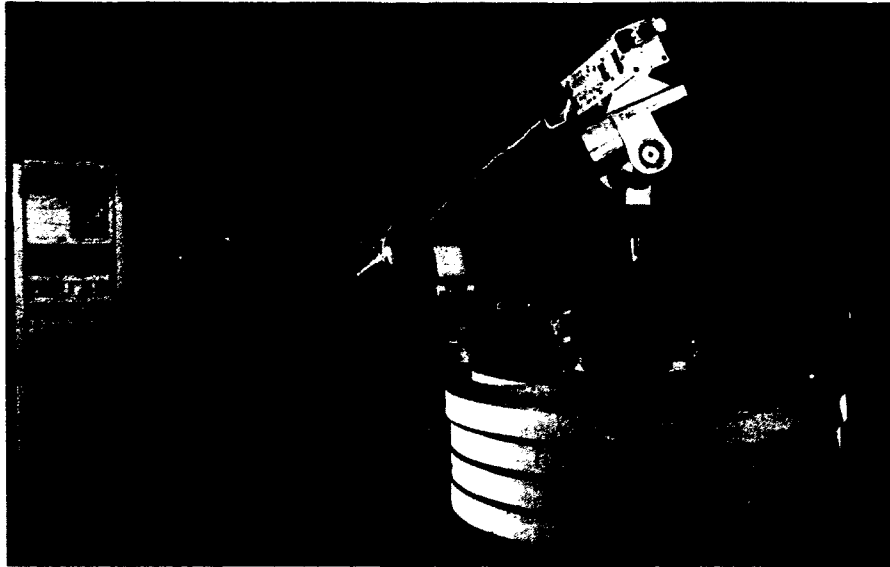


FIG. 31: ILS Check Load Demonstration at NASA LaRC NTF

TABLE 29: ILS Demonstration Applied Loads

| Point No. | F_x , lbs. | F_y , lbs. | F_z , lbs. | M_x , in-lbs. | M_y , in-lbs. | M_z , in-lbs. |
|-----------|-----------------|-----------------|-----------------|--------------------|--------------------|--------------------|
| 1 | 146.0 | -4.1 | -2498.8 | 34.5 | 4353.1 | 9.1 |
| 2 | 305.6 | 347.4 | -2459.9 | -3017.2 | 2879.9 | -781.5 |
| 3 | 146.1 | 5.5 | -2498.8 | -48.0 | 4352.4 | -12.3 |
| 4 | 146.1 | 5.3 | -2498.8 | -46.3 | 4352.5 | -11.9 |
| 5 | -330.3 | 993.2 | -2273.7 | -3565.9 | 2867.1 | -734.3 |
| 6 | -145.0 | -340.7 | -2475.5 | 2957.8 | -4312.0 | -766.7 |
| 7 | -144.9 | -339.8 | -2475.6 | 2950.2 | -4312.9 | -764.7 |
| 8 | -224.8 | 321.5 | -2472.1 | -2792.6 | -3611.3 | 723.6 |
| 9 | -146.0 | -334.9 | -2476.2 | 2907.7 | -4305.3 | -753.7 |
| 10 | -322.2 | -991.7 | -2275.5 | 3547.9 | 2797.1 | 716.6 |
| 11 | -70.3 | 627.3 | -2422.1 | -58.3 | -4840.6 | 1255.3 |
| 12 | -70.3 | 627.2 | -2422.2 | -57.6 | -4840.9 | 1255.2 |
| 13 | -327.3 | 985.1 | -2277.6 | -3487.5 | -2283.6 | 1488.9 |
| 14 | -72.0 | 617.9 | -2424.5 | 28.4 | -4830.8 | 1230.3 |
| 15 | -284.8 | -824.6 | -2346.1 | 1939.8 | -2807.0 | -1222.1 |
| 16 | 286.2 | 829.2 | -2344.3 | -1985.5 | 2787.7 | -1228.5 |
| 17 | 2.2 | -1.6 | -2503.0 | 13.0 | -20.9 | 0.0 |
| 18 | 174.0 | -305.5 | -2478.2 | 2652.5 | -1512.3 | -0.2 |
| 19 | 4.1 | -6.0 | -2503.0 | 51.6 | -36.8 | 0.0 |
| 20 | 3.9 | -6.7 | -2503.0 | 57.5 | -35.4 | 0.0 |
| 21 | 282.1 | -829.1 | -2344.8 | 1982.2 | 2824.7 | 1237.3 |

TABLE 30: Calibration and Check System Uncertainties

| | Units | F_x , lbs. | F_y , lbs. | F_z , lbs. | M_x , in-lbs. | M_y , in-lbs. | M_z , in-lbs. |
|--------------|-------|-----------------|-----------------|-----------------|--------------------|--------------------|--------------------|
| Manual Stand | EU | 0.615 | 1.476 | 2.058 | 12.35 | 6.981 | 4.668 |
| | mV/V | 1.678 | 0.724 | 0.648 | 0.847 | 0.757 | 0.807 |
| ILS | EU | 0.250 | 0.626 | 0.344 | 2.358 | 0.256 | 2.313 |
| | mV/V | 0.683 | 0.307 | 0.108 | 0.162 | 0.028 | 0.400 |

the balance using Equation 59. The computed intervals for the collected data will be made assuming a level of confidence of 95% with a Bonferroni correction from Equation 60 where p equals 6. This correction is implemented since all six load components are predicted simultaneously.

Equation 59 was used to estimate two sets of prediction intervals; one set included both the calibration and check system uncertainties and the other did not include both additional uncertainties. The residual errors between the applied, physics based, and balance estimated loads can be used to give an indication of the performance of the balance with the given regression model. With the residual errors, the prediction interval widths can be plotted about the zero axis. This plotting method is implemented, since the applied loads can have large ranges which may obscure the interval widths. The residuals for the all the load components of the balance are plotted with their respective intervals in Figures 32 through 37 in percent of full scale. The following plots include both sets of prediction intervals, where the black set represents without the additional uncertainties and the red includes them. Note that a confidence level of 95% is used for both estimated prediction interval sets.

In Figure 32, the majority of the residual error points are within the prediction interval that includes the calibration and check load system uncertainties, but the intervals without the additional uncertainty does not capture the majority of the points. This shows that when the prediction interval does not include the additional uncertainty due to the two load systems used, the resulting interval is too narrow to capture the majority of the points. In the data shown, only 9 out of 21 points are captured by the smaller interval, resulting in only a 42.9% capture rate which is much lower than the expected 95% defined by the set confidence level. The interval for points 5, 10, 13 and 15 have much larger intervals than the majority of the points, which may be due to a limitation of the applied F_x component with the manual stand.

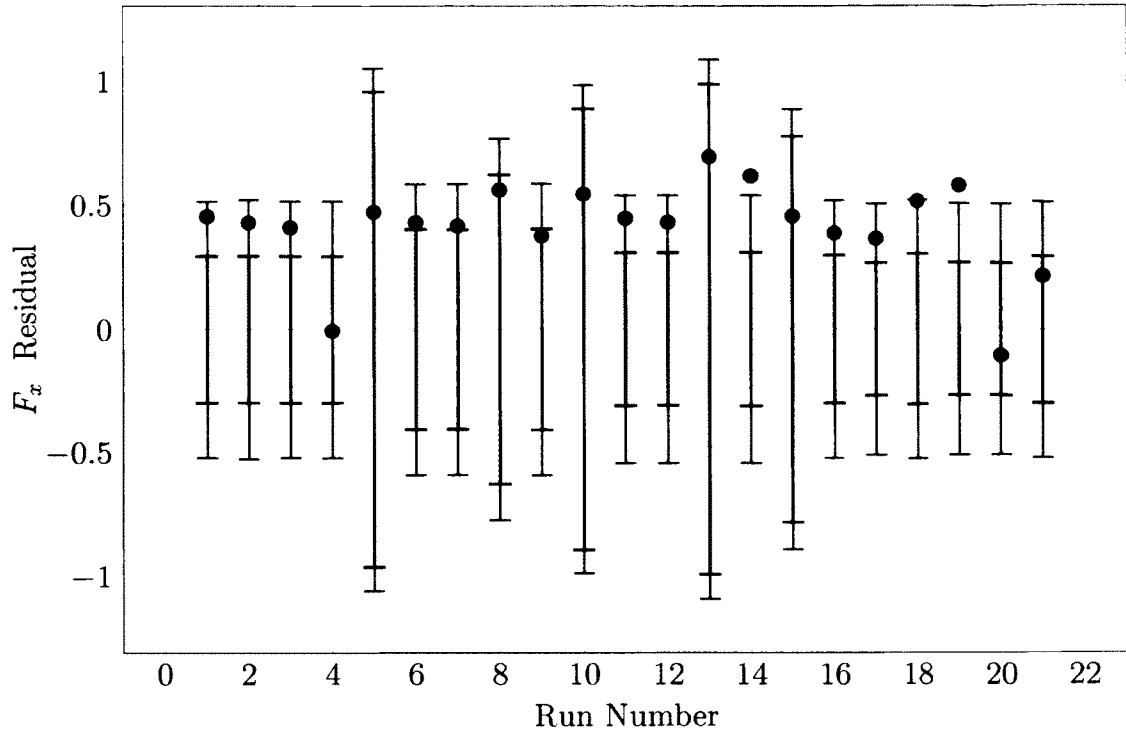
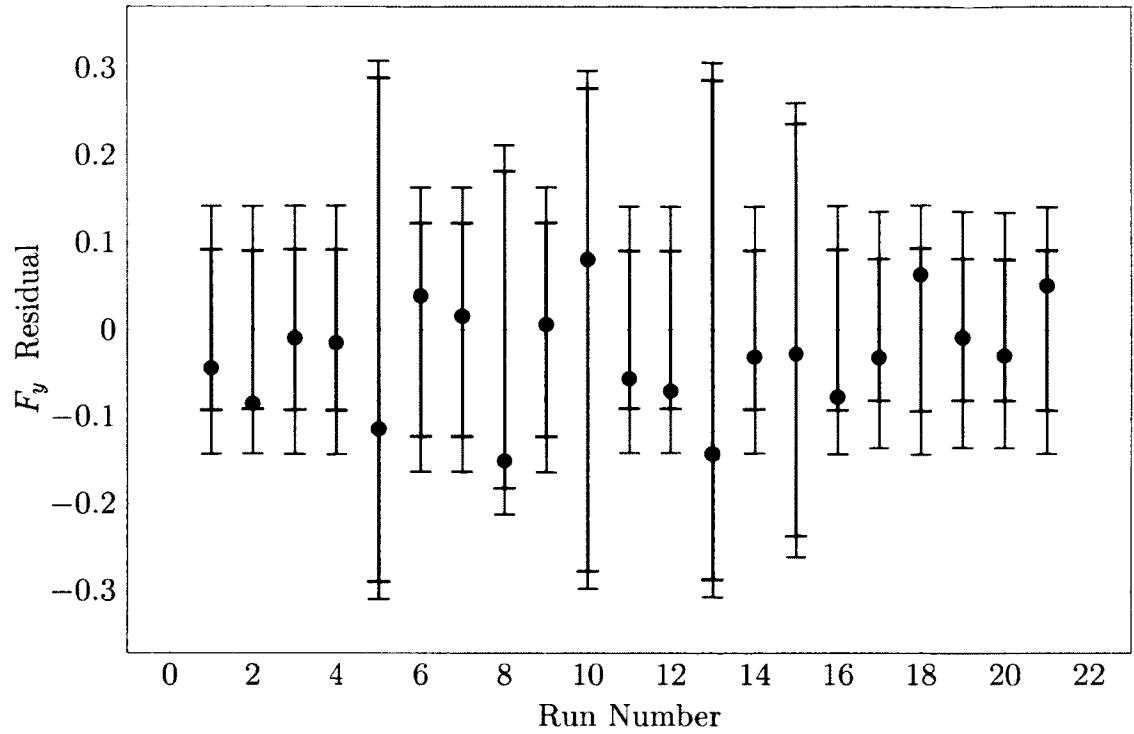
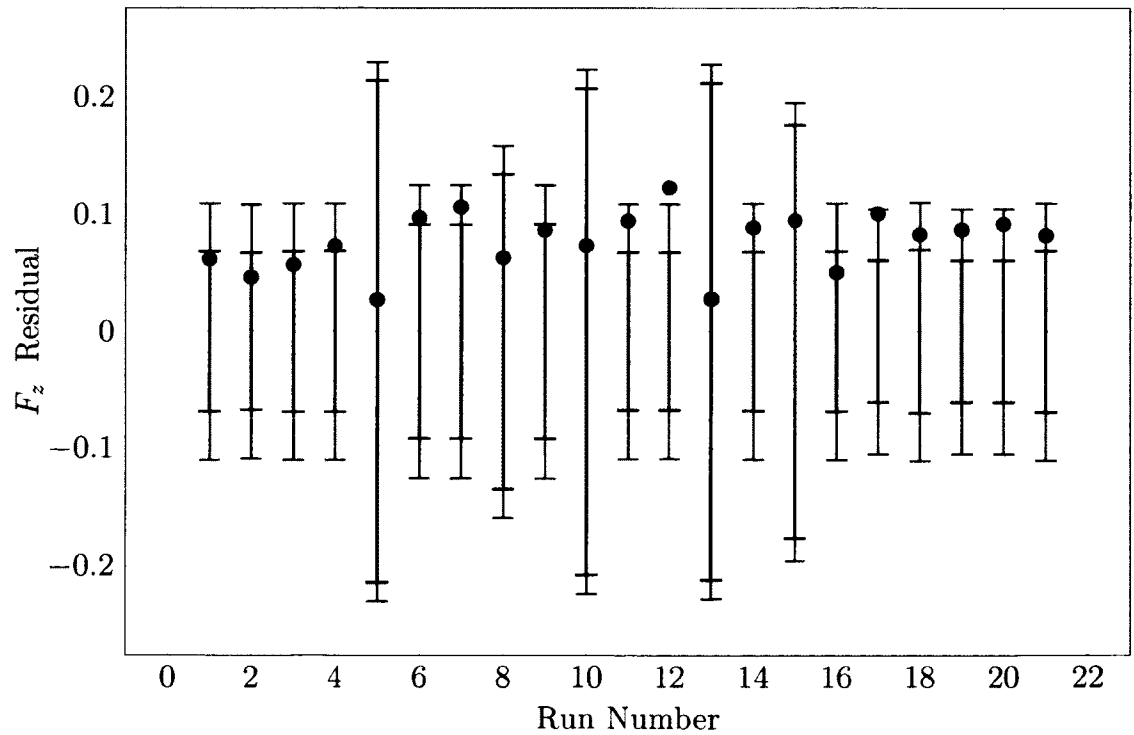


FIG. 32: F_x Residuals vs. Run

The manual stand calibration that was performed on the NTF-113C did not include negative F_x loads, which will lead to an increase in the variance for load combinations with high negative F_x loads, and in turn inflated intervals. The F_x residual errors are also seen to be biased high, where the applied load is larger than the estimated. This bias can be expected due to using two different systems for calibration and check loading of the balance, which may have slight differences in applied loads.

Full capture of every data point is illustrated by the F_y residuals in Figure 33 by both intervals. It is also shown that the data are not as biased as the F_x component. This lack of bias may suggest that the F_y component is applied similarly for both the calibration and check load system. It should be noted that the F_y component is not loaded to the same percentage of full scale as the F_x component, where F_y is only loaded to 24.1% whereas F_x is loaded to 82.5%. It would be beneficial to load the full range of loads in order to exercise the full range of the balance.

Similar to the F_x results, Figure 34 illustrates that for the F_z component the prediction interval with the additional uncertainties contains most of the points but not the interval without the additional uncertainties. Again, the F_z residuals are all

FIG. 33: F_y Residuals vs. RunFIG. 34: F_z Residuals vs. Run

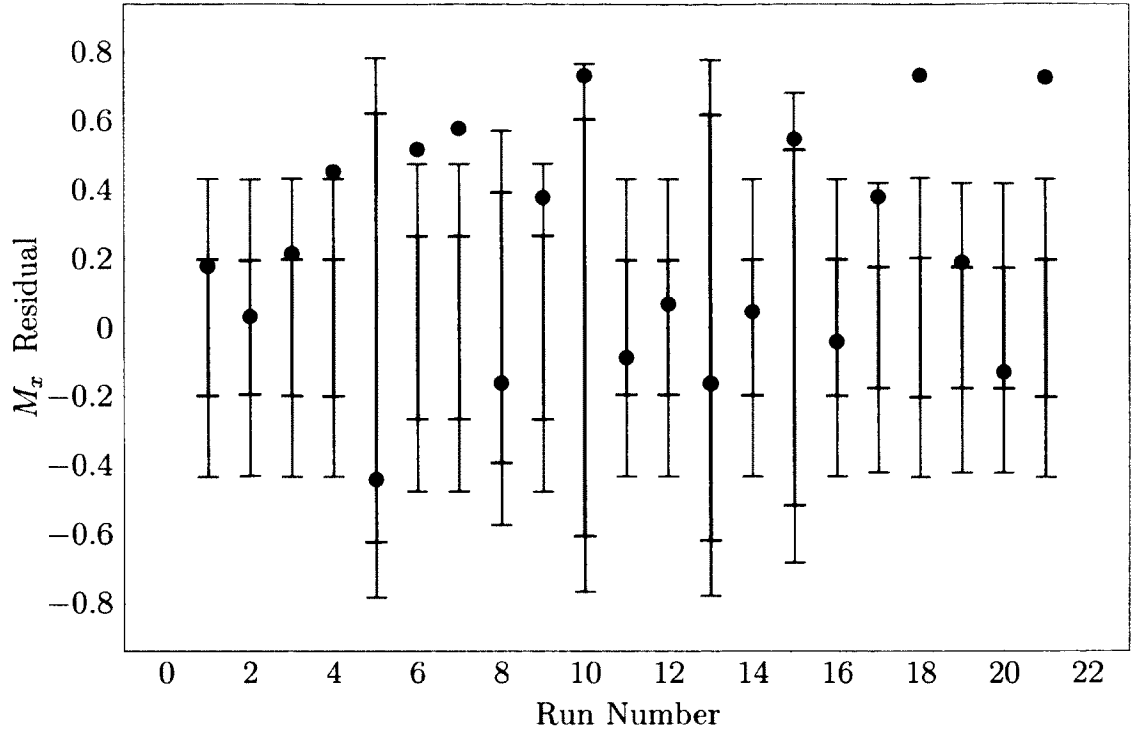


FIG. 35: M_x Residuals vs. Run

biased high, which signifies that the physics of the ILS may over predict the load that is applied, or the manual stand regression under estimates the load. The bias seen in the residuals may be due to only loading the F_z component around negative 2,500 lbs; loading in the positive F_z direction would be able to indicate if a bias truly exists. In F_z results, the prediction interval without the additional uncertainties captures more points than the F_x case, but only 10 out of 21 points which is less than 50%. For the wider intervals, only one point lies outside of the prediction interval bounds, which yields a capture rate of 95.2% as expected by the set confidence level. It should also be pointed out that points 5, 10, 13, and 15 have larger intervals for the same reason that was explained for the F_x results.

Illustrated in Figure 35 is the capture rate for the two interval sets for the M_x component. Again, it is shown that the prediction interval without the additional uncertainties fails to capture the proper number of points. The interval without the uncertainties only captures 13 out of the 21 points which is only 61.9%. When the additional uncertainties are included, 16 points are captured by the intervals, which is a capture rate of 76.2%. With this, the intervals still fail to meet the

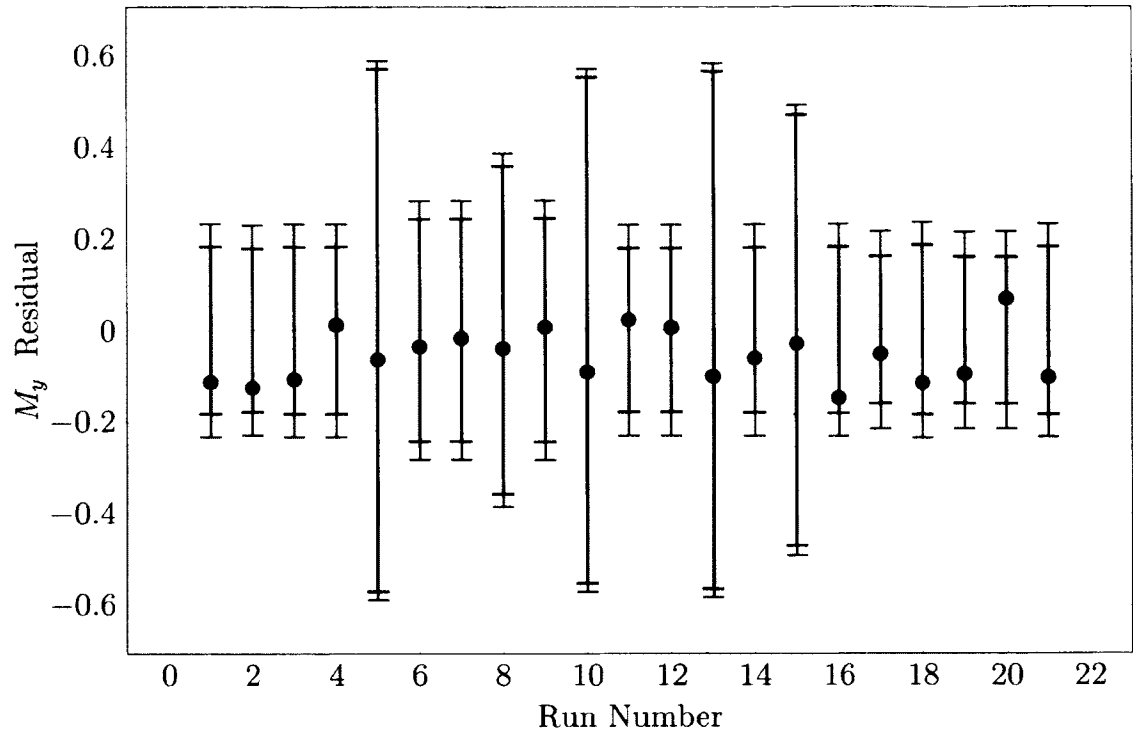


FIG. 36: M_y Residuals vs. Run

desired 95% capture rate for the M_x component. But as seen from the F_x and F_y components, for individual components the capture rates may vary. Since the six loads are simultaneously predicted, the results from all the components should be analyzed as a whole. From the low M_x capture rate, it can also be argued that the estimated uncertainty for this component is too small to represent the true systems. Several points that are outside of the intervals are not far off from the bounds, and that a small increase in the width may allow for it to be captured.

Figure 36 illustrates that the residuals of the M_y component exhibits similar results to the F_y component, such that the both intervals captures all the points. The M_y residuals have a slight negative bias, which can be associated with a difference in applied load location inducing slightly different moments. The high capture rate of the two intervals may suggest that they are too large to properly represent the data collected. The smaller interval is directly based on the regression results and calibration load schedule, which should best represent the calibration systems. This behavior may suggest that the calibration performed may have larger than expected errors that led to a larger interval width.

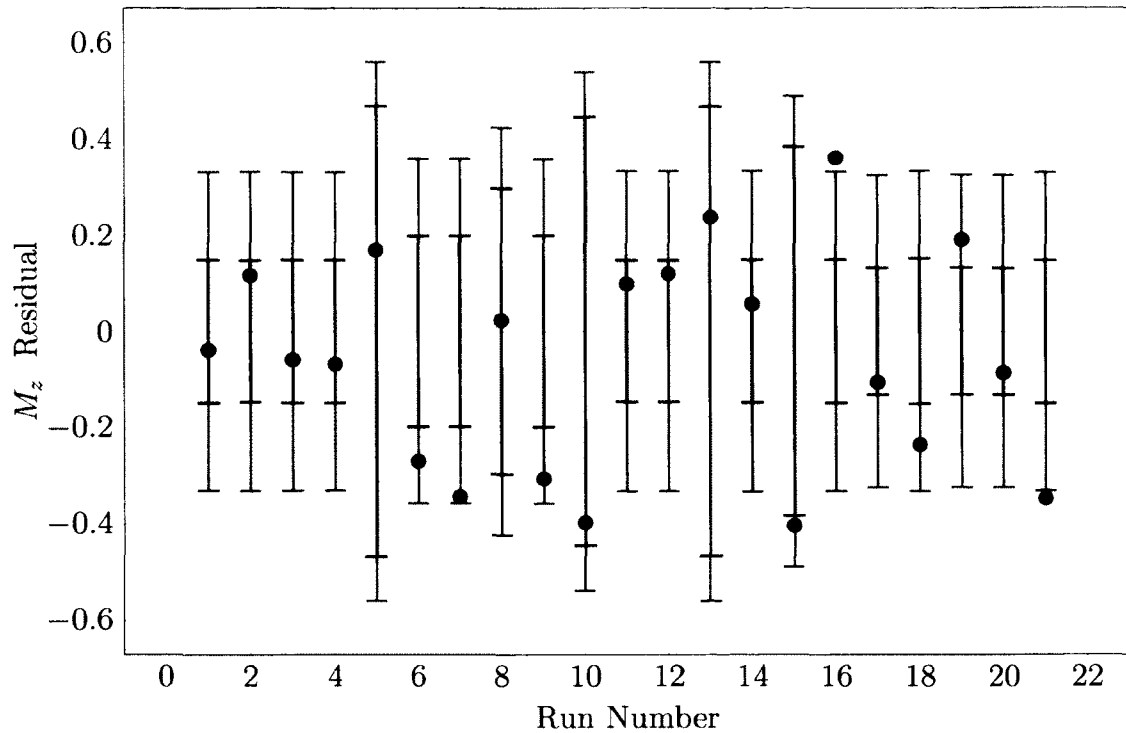


FIG. 37: M_z Residuals vs. Run

The M_z residuals in Figure 37 are seen to have good random distribution and are captured by the prediction interval with the additional uncertainty the majority of the time. This suggests that the intervals for this component do represent the data that was collected. The capture rate for the larger and smaller interval are 90.4% and 61.9%; again a perfect capture rate of 95% is not expected due to the small sample size of the data. It should be noted that the M_z component is only loaded to 19.0% of full scale, which shows that the prediction intervals work regardless of the magnitude of the applied loads.

The rejection rate for the individual load components and the total capture rates for both with and without the additional uncertainties, and the balance two-standard deviations, 2σ , are shown in Table 31. From these results it is evident that without the additional uncertainties or the use of 2σ will result in capture rates that are too low for the set confidence level. This shows that the common practice of using 2σ values to verify check load data may result in misinformed decisions regarding the results. This is also true for prediction interval without the additional uncertainties. With the inclusion of the additional uncertainties, the capture rate is closer to the

TABLE 31: Prediction Interval Capture Rates

| Component | With | Without | 2σ |
|------------|------|---------|-----------|
| F_x | 19 | 9 | 5 |
| F_y | 21 | 21 | 3 |
| F_z | 20 | 10 | 14 |
| M_x | 16 | 13 | 9 |
| M_y | 21 | 21 | 12 |
| M_z | 19 | 13 | 19 |
| Sum | 116 | 87 | 62 |
| Percentage | 92.1 | 69.0 | 49.2 |

TABLE 32: Manual Stand Prediction Interval Half Widths, Percent F.S.

| | | Fx | Fy | Fz | Mx | My | Mz |
|---------|-----|------|------|------|------|------|------|
| With | Max | 1.09 | 0.31 | 0.23 | 0.78 | 0.59 | 0.56 |
| | Avg | 0.63 | 0.18 | 0.13 | 0.50 | 0.31 | 0.38 |
| | Min | 0.51 | 0.14 | 0.10 | 0.42 | 0.22 | 0.32 |
| Without | Max | 0.99 | 0.29 | 0.21 | 0.62 | 0.57 | 0.47 |
| | Avg | 0.44 | 0.13 | 0.10 | 0.29 | 0.26 | 0.22 |
| | Min | 0.27 | 0.08 | 0.06 | 0.18 | 0.16 | 0.13 |

desired 95% capture rate for the given sample size. From these results, it is clear that the additional uncertainties must be included in order to have the proper capture rate set by the confidence level α . The lower than expected capture rate could be attributed to the under-estimation of the manual stand or ILS uncertainties that were used for the prediction intervals. Although, the number of check load points used for this study are relatively low, but are realistic for tunnel operations, with an increase in check loads the overall capture rate may approach 95%. This magnitude difference between the two intervals is shown in Table 32, where the maximum, average and minimum interval half widths are tabulated.

From Table 32, it is seen that the intervals with the additional uncertainty are around 20% to 70% larger in width than without. For the F_y , F_z and M_y components, the difference between the two intervals is much smaller, around 30% wider due to the smaller estimated uncertainties of the manual stand. The average half widths of the intervals are much larger than the quoted standard deviations of the balance, shown in Table 26. Although, these widths are not necessarily large and the averages

TABLE 33: SVS Prediction Interval Capture Rates

| Component | No. Captured |
|------------|--------------|
| F_x | 21 |
| F_y | 21 |
| F_z | 21 |
| M_x | 19 |
| M_y | 21 |
| M_z | 18 |
| Sum | 121 |
| Percentage | 96.0 |

are all below 0.24%. These half-width results with the 92.1% capture rate suggest that the uncertainties of a balance are underestimated when using the standard deviations and that the developed method should be implemented, but the input system uncertainties should be reevaluated.

The prediction interval can also be applied to the SVS calibration system available at NASA LaRC, since the NTF-113C has been calibrated on both systems. Lower load limits were used during this calibration due to the bearing load limit restriction of the SVS. The same methods that were used to calculate the prediction intervals for the manual stand are used for the SVS. The results from for this system were previously investigated, but several changes in the processing method were made [36]. The capture rate for each of the balance components are shown in Table 33 with the overall capture and percentage. From this table it is illustrated that the SVS captures 96% of the data points collected, which is higher than the manual stand results. Although, the number of captures per component differ from the manual stand results. The M_x and M_z are the only two components with the points falling outside the intervals. If more data were processed using this interval method a capture rate closer to 95% could be realized.

The maximum, average and minimum interval half-widths which were computed for the SVS are tabulated in Table 34. From these widths it is seen that the SVS has a more uniform distribution of interval half-widths, as seen by the small difference between the maximum and minimum values when compared to the manual results. This more uniform distribution is due to the calibration design used for the SVS that provides a more uniform variance distribution. When the SVS half widths are compared to the manual results, the SVS provides smaller interval widths. Since the

TABLE 34: SVS Prediction Interval Half Widths, Percent F.S.

| | F _x | F _y | F _z | M _x | M _y | M _z |
|-----|----------------|----------------|----------------|----------------|----------------|----------------|
| Max | 0.689 | 0.126 | 0.155 | 0.805 | 0.543 | 0.314 |
| Avg | 0.648 | 0.121 | 0.152 | 0.777 | 0.537 | 0.304 |
| Min | 0.623 | 0.116 | 0.146 | 0.753 | 0.520 | 0.295 |

capture rate is the same with smaller widths, the residuals of the SVS results are smaller than those of the manual stand. The results of the SVS provides smaller results overall primarily due to the calibration design, but also due to the lower load limits used that more represent the data which was collected.

From the prediction interval results of the manual and SVS calibration systems using the ILS as a check load system it is seen that the methods developed can be used to rigorously check force balances. Even with the difference in scale of the two systems the results are fairly consistent. With modifications to the check load system uncertainties to represent the uncertainty in the force applied by a wind tunnel, this method could be used to generate intervals about the measured forces during experimental testing.

CHAPTER 6

CONCLUSIONS

Uncertainties in the explanatory variables during a calibration and check of an instrument system are generally not considered when performing system level instrument check outs or data analysis. Ignorance of the systems's uncertainties may lead to misinformed decisions to be made in regards to the overall performance and accuracy of the instrument. Furthermore, the current use of two standard deviations does not rely on the information that is available regarding the calibration metrics and the calibration and check systems uncertainties. With the use of a prediction interval, the capture rate of confirmations or checks performed to the instrument may fall short of expected values. For multi-variate systems such as wind-tunnel balances where the desired estimate during use of the instrument is the explanatory variable, it is not clear how to implement a typical prediction interval, let alone include the additional uncertainties.

The derived prediction interval from this research addresses the issue of including additional uncertainties from the equipment used to perform the calibration and checks of an instrument. This prediction interval can be applied to the response variable of the system and includes the regression model, calibration and check system uncertainties in the form of variances. For instrument systems where the explanatory variable is desired, the method developed by Tripp and Tcheng is used to covert the interval widths over to the explanatory variable.

For multi-component force measurement devices, such as those used in wind tunnels, the uncertainty estimates of the calibration systems can be challenging. Manual stand calibration systems are highly specialized systems that present many uncertainty sources. These systems currently do not have an uncertainty estimate that can be used for the derived prediction interval methods. This research derived a final uncertainty estimate for the manual stand used at NASA LaRC using the propagation of error method. From the derivation of the system uncertainty, several observations were made for the NTF-113 and 20K stand combination:

- The deflections of the calibration body provides negligible effects to the overall uncertainty,

- Long arms are desired to reduce the overall uncertainty in the applied moments,
- The uncertainty in the angular position of the balance and the cable loads scales with the applied load,
- The methodology used to align the cable loads scales with the load ranges of the balance, such that the initial cable alignment is more accurate for lower load capacity balances.

A MCS was implemented on a unsimplified model of the manual stand, unlike the simplified model that was used for the propagation of error. A histogram of one of the force components showed that enough iterations were done to build a sample population of the output forces. The standard deviation results from the MCS provided good agreement with the propagation of error results, which were within 1%. These positive results shows that the assumptions that were used in the propagation of error derivations are valid, such as small angle approximation and no correlated uncertainties. With these results, either method could be used to estimate the uncertainties of calibration or check load systems. Propagation of error method does have added benefits of not requiring computational resources and can reveal factors that influence the overall uncertainty.

The developed prediction interval and methodology was implemented on check loads that were applied to the NTF-113C force balance using the ILS. This demonstration utilized the uncertainties that were estimated in this research in the interval calculations for the 20K manual stand at NASA LaRC. The prediction interval results demonstrated the need for the inclusion of the system uncertainties in the analysis of check loads. Intervals that lacked the additional uncertainties failed to capture the expected number of points. Intervals that included the additional uncertainties captured nearly the correct number of points in the acquired data. A capture rate of 92.1% and 96% was achieved, when 95% was expected due to the confidence level used in the prediction interval. Although, more data should be collected to further verify the methodology.

The method was also implemented with the calibration metrics from a SVS calibration of the NTF-113C and using the same measurement data as the manual stand. The results from the prediction intervals using the SVS calibration provided similar results to the manual stand and identical capture percentages. This showed that the

method developed does not only work for one system, but can be implemented on other systems.

With these favorable results, the derived prediction interval method could be modified to represent the application of load applied to a wind-tunnel model during testing. These intervals can then be used to quantify the uncertainty of the force measurements made. Further research could be made in this area to properly quantify these type of measurements and how the derived method should be implemented.

BIBLIOGRAPHY

- [1] AGARD. Wind Tunnel Flow Quality and Data Accuracy Requirements. Technical Report AGARD-AR-184, AGARD, 1982.
- [2] John D. Anderson. *Fundamentals of Aerodynamics*. McGraw-Hill, 5th edition, February 2010.
- [3] Melissa B. Rivers and Ashley Dittberner. Experimental Investigation of the NASA Common Research Model. In *28th AIAA Applied Aerodynamics Conference*, number AIAA 2010-4218, Chicago, Illinois, June 2010. AIAA.
- [4] John Vassberg, Mark Dehaan, Melissa Rivers, and Richard Wahls. Development of a Common Research Model for Applied CFD Validation Studies. In *26th AIAA Applied Aerodynamics Conference*, number 2008-6919, Honolulu, Hawaii, August 2008. AIAA.
- [5] William E. Milholen, Gregory S. Jones, David T. Chan, Scott Goodliff, Scott Anders, LaTunia G. Pack Melton, Melissa B. Carter, Brian G. Allan, and Francis Capone. Enhancements to the FAST-MAC Circulation Control Model and Recent High-Reynolds Number Testing in the National Transonic Facility. In *31st AIAA Applied Aerodynamics Conference*, San Diego, CA, 2013. AIAA.
- [6] Keith C. Lynn, Kenneth G. Toro, Drew Landman, David T. Chan, and Sundareswara Balakrishna. High-Reynolds Number Active Blowing Semi-Span Force Measurement System Development (Revisited). In *AIAA SciTech*, number AIAA 2014-0275, National Harbor, Maryland, January 2014. AIAA.
- [7] Richard DeLoach. Check-Standard Testing Across Multiple Transonic Wind Tunnels with the Modern Design of Experiments. In *28th Aerodynamic Measurement Technology, Ground Testing, and Flight Testing Conference*, number 2012-3174, New Orleans, Louisiana, June 2012. AIAA.
- [8] W. C. Randels and V. C. Plane. Force Measurements by Means of Resistance Wire Strain Gages. *Journal of the Aeronautical Sciences*, 10(1), 1947.
- [9] M. Ringel and D. Levin. Improved drag element for wind tunnel sting balances. *Journal of Aircraft*, 22(11), 1985.

- [10] Ray D. Rhew. Strain-Gage Balance Axial Section Design Optimization Using Design of Experiments. In *U.S. Air Force T&E Days*, Nashville, Tennessee, December 2005. AIAA.
- [11] AIAA. Recommended Practice: Calibration and Use of Internal Strain Gage Balances with Application to Wind Tunnel Testing. Technical Report R-091-2003, AIAA, 2003.
- [12] Alice X. Ferris. An Improved Method for Determining Force Balance Calibration Accuracy. In *39th International Instrumentation Symposium*, Albuquerque, New Mexico, May 1993. Instrument Society of America.
- [13] Raymond H. Myers and Douglas C. Montgomery. *Response Surface Methodology*. John Wiley & Sons, 2nd edition, 2002.
- [14] Iwan Philipsen and Raymond Bergmann. Some Contemplation on a Proposed Definition of Uncertainty for Balances. In *27th AIAA Aerodynamic Measurement Technology and Ground Testing*, Chicago, Illinois, July 2010. AIAA.
- [15] J. Tripp and P. Tchong. Determination of Measurement Uncertainties of Multi-Component Wind Tunnel Balances. In *18th AIAA Aerospace Ground Testing Conference*, Colorado Springs, CO, June. AIAA.
- [16] Mark E. Kammeyer and Mathew L. Rueger. Estimation of the Uncertainty in Internal Balance Calibration Through Comprehensive Error Propagation. In *26th AIAA Aerodynamics Measurement Technology and Ground Testing Conference*, Seattle, Washington, June 2008. AIAA.
- [17] George W. Bush. Executive Order 13419: National Aeronautics Research and Development. December 20, 2006.
- [18] David L. Smith. An Efficient Algorithm Using Matix Method to Sovle Wind-Tunnel Force-Balance Equations. Technical Report TN D6860, NASA Langley, August 1972.
- [19] Richard DeLoach and Norbert Ulbrich. A Comparison of Two Balance Calibration Model Building Methods. In *45th AIAA Aerospace Sciences Meeting and Exhibit*, number 2007-0147, Reno, NV, January 2007. AIAA.

- [20] Jim Simpson, Drew Landman, Rupert Giroux, Michelle Zeisset, Brian Hall, and Ray Rhew. Calibrating Large Capacity Aerodynamic Force Balances using Response Surface Methods. In *U.S. Air Force T&E Days*, number 2005-7601, Nashville, Tennessee, December 2005. AIAA.
- [21] Peter A. Parker. A Single-Vector Force Calibration Method Featuring the Modern Design of Experiments. In *39th AIAA Aerospace Sciences Meeting and Exhibit*, number 2001-170, Reno, NV, January 2001. AIAA.
- [22] Peter A. Parker and Tianshu Liu. Uncertainty Analysis of the Single-Vector Force Balance Calibration System. In *22nd AIAA Aerodynamic Measurement Technology and Ground Testing Conference*, number 2002-2792, St. Louis, Missouri, June 2002. AIAA.
- [23] Klaus Hufnagel and Matthias Quade. The 2nd Generation Balance Calibration Machine of Darmstadt University of Technology (TUD). In *45th AIAA Aerospace Sciences Meeting and Exhibit*, number 2007-148, Reno, Nevada, January 2007. AIAA.
- [24] Dennis Booth and David King. Automatic Balance Calibration System (ABCS) Upgrades. In *44th AIAA Aerospace Sciences Meeting and Exhibit*, number 2006-516, Reno, Nevada, January 2006. AIAA.
- [25] Masataka Kohzai, Makoto Ueno, Seigo Koga, and Norikazu Sudani. Wall and Support Interference Corrections of NASA Common Research Model Wind Tunnel Tests in JAXA. In *51st AIAA Aerospace Sciences Meeting including the New Horizons Forum and Aerospace Exposition*, number 2013-0963, Grapevine, Texas, January 2013. AIAA.
- [26] M.L.C.C. Reis, R.M. Castro, and O.A.F. Mello. Calibration uncertainty estimation of a strain-gage external balance. *Measurement*, 46(1):24 – 33, 2013.
- [27] Bureau International des Poids et Mesures, Commission électrotechnique internationale, and Organisation internationale de normalisation. Guide to the Expression of Uncertainty in Measurement. Technical report, 1995.
- [28] H. W. Coleman and W. G. Steele. *Experimentation, Validation, and Uncertainty Analysis for Engineers*. John Wiley and Sons, 3rd edition, 2009.

- [29] D.C. Montgomery, E.A. Peck, G.G. Vining, and J. Vining. *Introduction to Linear Regression Analysis*. Wiley New York, 3rd edition, 2001.
- [30] Maria L.C.C. Reis, Olympio A.F. Mello, and Sadahaki Uyeno. A Method for Estimation of the Calibration Uncertainty of an External Six-Component Wind Tunnel Balance. In *22nd AIAA Aerodynamic Technology and Ground Testing Conference*, St. Louis, MO, 2002.
- [31] Peter A. Parker, G. Geoffery Vining, Sara R. Wilson, John L. Szarka III, and Nels G. Johnson. The Prediction Properties of Classical and Inverse Regression for the Simple Linear Calibration Problem. *Journal of Quality Technology*, 42(4), October 2010.
- [32] Gerald J. Hahn and William Q. Meeker. *Statistical Interval: A Guide for Practitioners*. Wiley Interscience, 1991.
- [33] D.C. Montgomery. *Design and Analysis of Experiments*. John Wiley & Sons, New York, 7th edition, 2009.
- [34] Stephen B. Vardeman, Joanne R. Wendelberger, Tom Burr, Michael S. Hamada, Leslie M. Moore, J. Marcus Jobe, Max D. Morris, and Huaiqing Wu. Elementary Statistical Methods and Measurement Error. *The American Statistician*, 64(1), 2010.
- [35] Angela M. Dean and Daniel Voss. *Design and Analysis of Experiments*. Springer, 1999.
- [36] Drew Landman, Kenneth G. Toro, Sean A. Commo, and Keith C. Lynn. Prediction Interval Development for Wind-Tunnel Balance Check-Loading. *Journal of Aircraft*, 52(3), 2015.
- [37] Thomas R. Yechout, Steven L. Morris, David E. Bossert, and Wayne F. Hallgren. *Introduction to Aircraft Flight Mechanics*. AIAA, 2003.
- [38] Ahmed A. Shabana. *Computational Dynamics*. Wiley, third edition, 2010.
- [39] Paul Cella. Methodology for Exact Solution of Catenary. *Journal of Structural Engineering*, 125(12):1451–1453, December 1999.
- [40] James M. Gere. *Mechanics of Materials*. Thomson, sixth edition, 2006.

APPENDIX A

PREDICTION INTERVAL MATLAB CODE

A.1 PREDICTION INTERVAL FRONT END

The code written to import the proper data to implement the derived prediction interval methods is shown below.

```

%% *** USER SETTINGS *** %%
% SET THE BALANCE CATALOG FILENAME
BalCat = 'NTF113C_cat(Updated)';

%SET THE INPUT DATA FILENAME
InputFile = 'Manual_ILS_Data(2013July23).xlsx';

%Set the prediction interval output file name
OutputFile = 'ManualPIData.xlsx';

%%*** End OF USERS SETTINGS ***%%

%% Initialisation of POI Libs for xlwrite Function Used
% Set which folder contains the Java data
XLWritePath = 'poi_library/';

%Temporary add the Java paths to MATLAB
javaaddpath([XLWritePath 'poi-3.8-20120326.jar']);
javaaddpath([XLWritePath 'poi-ooxml-3.8-20120326.jar']);
javaaddpath([XLWritePath 'poi-ooxml-schemas-3.8-20120326.jar'
]);
javaaddpath([XLWritePath 'xmlbeans-2.3.0.jar']);
javaaddpath([XLWritePath 'dom4j-1.6.1.jar']);
javaaddpath([XLWritePath 'stax-api-1.0.1.jar']);

```

```

%% Read in the balance catalog
%Read balance Catalog
BalData = ReadBalCat( BalCat );

%% Read in the balance data
PData = dataset( 'XLSFile', InputFile );

PData.CLoads = [PData.X1_BalEstLoad, PData.X2_BalEstLoad,
                PData.X3_BalEstLoad, ...
                PData.X4_BalEstLoad, PData.
                X5_BalEstLoad, PData.
                X6_BalEstLoad ];

PData.AppLoad = [PData.X1_Applied, PData.X2_Applied, PData.
                X3_Applied, ...
                PData.X4_Applied, PData.X5_Applied, PData.
                X6_Applied ];

%Compute the prediction intervals
PData = Pred_Intvl_V3( PData, BalData, OutputFile );

%Prompt user that the processing completed
msgbox( 'Calculations Completed' )

```

A.2 PREDICTION INTERVAL BACK END

The code that was written to provide the prediction intervals of an estimated balance load and generate a report based on the calculations is shown below:

```

function PData = Pred_Intvl_V3(PData, BalData, OutputFile)
%Computes the prediction interval on an estimated factor
    given responses.
%
% Written by Kenneth Toro (NASA LaRC D209)

```

```

% Last Modified 2015-06-08 (YYYY-MM-DD)
%
%Introduction
% This function will compute a prediction interval on the
%   factors of a
% given calibration. This code was originally intended to be
%   used for
% force balances, but it not constrained to them specifically
%   . The code is
% written in a way to be as general as possible.
%
%Function Inputs
% The inputs to the function have been generalized to allow
%   data of any 2D
% array size. The code will automatically scale to the
%   inputs sizes,
% including the expansion of the factors.
%
%Note: need to generalize the excel output to n columns and
%   any input names
%
% Let "n" equal the number of factors. It is assumed that
%   there are also
% "n" number of responses, such that the linear portion of
%   the regression
% matrix is n by n.
%
% BalData.FullScales
% This input variable should be a 6 by n matrix, where the
%   rows are in the
% following order:
%   Full Scale High.....(Factor Units)
%   Full Scale Low.....(Factor Units)
%   Residual Degrees of Freedom.....(Unit-Less)

```

```

% Mean Square Error from the calibration..(Response Units
  Squared)
% Check System Uncertainty.....(Factor Units)
% Calibration System Uncertainty.....(Factor Units)
%
% BalData.CalMatEU
% This input variable is the regression model of the system
  under
% investigation. The regression model should be a m by n
  matrix, where n
% is the number of factors and m is the total number of
  coefficient terms.
% Currently the code assumes that the model is of second
  order nature, thus
% m should be:
% 
$$m = (n + 2)! / (2! * n!) - 1$$
, where ! is the factorial
  function
%
% BalData.xD
% This input variable is the design matrix of factor set
  points that were
% used for the calibration experiment, which was used to
  develop the
% supplied regression model. The design matrix should be k
  by n, where k
% is the number of individual factor set points, which should
  be large
% enough for the design matrix to have equal or greater rank
  than the
% number of estimated terms (m + 1).
%
% PData.CLoads
% This input variable is a list of factors that are desired
  to be check,

```

*% these values should be the inverse prediction based on
measured responses.*

% The

%

% PData.AppLoad

%

%

% OutputFile

%

%-Function Outputs

*% The function can output a formatted Excel spreadsheet,
which contains the*

% prediction interval information listed below:

% Prediction interval widths

% Prediction interval high and low limits

% Calculated t-statistic

% X and X_hat inputs

%% Import Data for Calculations

%Load balance information from file

FS = BalData.FullScales;

%Get the number of loads

[ncon, n] = size(PData.CLoads);

*%Set the order number, should be only 2. This script is not
setup for any*

%size order, yet...

M = 2;

%Calculate the number of model terms

*Mz = factorial(n + M)/(factorial(n)*factorial(M)) - 1;*


```

%Set parameters for t-statistic (Bonferroni adjustment)
alpha = 0.05;

% Calculate t stat for each response, extract MSE values
t = tinv(1-alpha/(2*n),FS(3,:));
MSe = FS(4,:); %microvolts ^2

%% Format Input Information for Prediction Interval
    Calculations
% Expand coded design matrix D to full 2nd order model matrix
    X (all
% terms) and convert to EUs
X = ExpandLoads( BalData.xD, Mz );

% Convert the B1 formatted calibration matrix to a formula
    form, adding the
% sensitivity back into the coefficients
Sens= BalData.CalMatEU(1,:)/1000; %EU
C1 =( BalData.CalMatEU((1:n)+1,:) ./ (ones(n,1)*Sens) )'; %EU
C2 =( BalData.CalMatEU(n+2:end,:) ./ (ones(Mz-n,1)*Sens) )'; %
    EU
Cal = [C1, C2]';

% Specify Bias error introduced by setting loads with ILS
% Results in force and moment units from MC simulation,
    convert to coded
% Multiply by sensitivity from coded regression model
Calbiassqr=(FS(5,:) ./ Sens).^2; %(microVolts/V)^2

% ILSbiassqr(1) is Bias error (variance) due to ILS for N, 2
    is A, 3 is P etc
Appbiassqr=(FS(6,:) ./ Sens).^2; %(microVolts/V)^2

% Expand load vector into model form.

```

```

ExpCon = ExpandLoads( PData.CLoads, Mz);

%Initialize empty cell matrices
ConRed    = cell.empty(n,0);
XXinv     = cell.empty(n,0);

%Loop through the balance components
for j = 1:n
    %Find the indices of the non-zero calibration
        coefficients
    Idx = Cal(:,j) ~= 0;

    %Reduces the following components to correlate with the
        non-zero
    %coefficients
    ConRed{j} = ExpCon(:,Idx);
    XXRe = X(:,Idx);
    XXinv{j} = inv(XXRe' * XXRe);
end %End j, components, Loop

%Initialize variables for efficiency
PIhalf = zeros(ncon,n);
dx      = zeros(ncon,n);

%% Calculate Prediction Interval
for i=1:ncon % index (row of confirmation matrix)
    for j=1:n % calculate each load, build prediction
        intervals)
        % j is the column that identifies the regress eqn.
            vector

        %Calculates the prediction interval on the jth y-
            component

```

```

SE = ( MSe(j)*(1 + ConRed{j}(i,:) * XXinv{j} * ConRed
      {j}(i,:)') + Appbiassqr(j) + Calbiassqr(j) )^0.5;
PIhalf(i,j) = t(j) * SE;

```

```

end %End j Loop

```

```

%Calculates the Jacobian based on the Tripp method

```

```

J = calcJacobian(PData.CLoads(i,:), C1, C2, n, Mz);

```

```

%Calculates the prediction interval on the x's

```

```

dx(i,:) = ( inv(J)*PIhalf(i,:)')';

```

```

end %End i Loop

```

```

%Calculates the prediction interval high and low

```

```

PIhiEU = PData.CLoads + dx;

```

```

PIlowEU = PData.CLoads - dx;

```

```

%Save the prediction interval to the output variable

```

```

PData.PIhiEU = PIhiEU;

```

```

PData.PIlowEU= PIlowEU;

```

```

keyboard

```

```

%% Write Output file

```

```

if not(isempty(OutputFile))

```

```

    % Header file of data and components

```

```

    HHeader = { 'Pt', 'Comp', 'Bal._Est._Load', 'Prediction', '
                95%_PI_low', 'Applied_Load', '95%_PI_high', 't' };

```

```

    VHeader = { 'NF', 'AF', 'PM', 'RM', 'YM', 'SF' };

```

```

    Out = HHeader;

```

```

    % Formats the relevant data and forms an output cell

```

```

    for i=1:ncon

```

```

        for j=1:n

```

```

            Add = { i, VHeader{j}, PData.CLoads(i,j), (PIhiEU(
                    i,j)+PIlowEU(i,j))/2, ...

```

```

        PIlowEU(i , j) , PData.AppLoad(i , j) , PIhiEU(i , j)
            ,t(j)};
    Out = [Out; Add];
end %End j, Component, Loop
Out = [Out; repmat({' '},1,8)]; %Add spacing between
    points
end %End i, Row, Loop

%Write data to excel file
xlwrite(OutputFile ,Out, 'PI_Report ');
end

end % Program end

%% Support functions %%
function [ OutputLoad ] = ExpandLoads( InputLoad , Mz)
%EXPANDLOADS Expands the input load full second order
% This script simply expands an input an array into a full
    second
% order array or the original. The output of this script
    is in the
% following order:
% [Original Array, 2 Factor Interactions , Squared Terms]
%
% Note that is it assumed that factors are in separate
    columns.
% Also note that any number of rows can be supplied.

%Get size the number of columns of the input array
[nRow, nCol] = size(InputLoad);

SIZE = Mz;
%Initialize iteration matrix
OutputLoad = zeros(nRow,SIZE);

```

```

OutputLoad(:,1:nCol) = InputLoad;

%Loop through each component combination
z = nCol+1;
for i = 1:nCol
    for j = i:nCol
        OutputLoad(:,z) = InputLoad(:,i).*InputLoad(:,j);
        z = z + 1;
    end %End j, Component, Loop
end %End i, Row, Loop

end %End function

function J = calcJacobian(Load, C1, C2, n, Mz)
%This function calculates the expanded load Jacobian based on
    the Tripp and
%Tchen method

%Calculate the number of 2FI and quadratic terms
SIZE = Mz - n;

%Initialize W
W = zeros(SIZE,n);

%Build the quadratic load Jacobian
z = 1;
for i = 1:n
    for j = i:n
        W(z,i) = Load(j);
        W(z,j) = W(z,j)+Load(i);
        z = z + 1;
    end
end
end

```

```
%compute the Jacobian
```

```
J = C1 + C2*W;
```

```
end %End Function
```

APPENDIX B

MANUAL STAND UNCERTAINTY MATLAB CODE - PROPAGATION OF ERROR

B.1 INTERFACE SCRIPT

Below is the MATLAB script that was written to read in the desired applied loads, pass the load to the uncertainty estimator, and save the output to file:

```
%Read in desired loads
[num, txt] = xlsread('ManualStandLoads.xlsx');
rows = size(num,1);

S_F = zeros(rows,3);
S_M = zeros(rows,3);

%Loop through the rows of the provide load sheet
for j = 1:rows
    %Set the applied loads
    for i = 1:size(num,2)
        Papp.(txt{i}) = num(j,i);
    end
    %Perform the uncertainty calculations
    [S_F(j,:), S_M(j,:)] = ManualStandUncertainty(Papp);
end
%Set the output data file header
Header = {'Fx', 'Fy', 'Fz', 'Mx', 'My', 'Mz' ...
    'sFx', 'sFy', 'sFz', 'sMx', 'sMy', 'sMz'};

%Output the data to file
cell2csv('UncertaintyResults.csv',[Header; num2cell([num, S_F
    , S_M])])
```

```

Header = { 'Fx', 'Fy', 'Fz', 'Mx', 'My', 'Mz' };
SMean = [mean(S_F), mean(S_M)];
SMeanFS= SMean./[400,4000,6500,9000,13000,6500]*100;

cell2csv('UncertaintySummary.csv', [ {'name'; 'Engineering_
    Units'; 'Percent_of_Full_Scale' }, ...
    [Header; num2cell([SMean;SMeanFS]) ] ] )

```

B.2 UNCERTAINTY ESTIMATOR

Below is the MATLAB script that was written to compute the uncertainty estimates for the force and moment components of a manual stand calibration system:

```

function [S_F, S_M] = ManualStandUncertainty(Papp)
%This function is written to provide an estimate for the
    uncertainty
    %of the NASA LaRC force balance manual stand calibration
    systems.

%The uncertainty estimates for the various noise contributors
    are
    %entered below and applied loads are entered into the
    function.

% Define system properties
    %Balance Angle Uncertainty
s.phi = (0.0244*pi)/180)/2; %Rad
s.theta = (0.0173*pi)/180)/2; %Rad

%Cable Angle Uncertainty
s.phi_c = (1/32)/(8*12)/2;
s.theta_c = (1/32)/(8*12)/2;
s.psi_c = (1/32)/(8*12)/2;

```


%Load Point Uncertainty

s.x = 0.0021/2; *%inches*

s.y = 0.0050/2; *%inches*

s.z = 0.0003/2; *%inches*

%Load Uncertainty

s.P = 0.0001/2; *%Percent of Full Scale*

%Electrical Uncertainty

s.DAQ = 0.0005; *%mV/V*

s.LineUp = 0.0005; *%mV/V*

s.BalSen = [365.9, 2035.2, 3167.5, 14602, 9208, 5772.7];

%Define Arm Lengths

Cal.MxArm = 40; *%inches*

Cal.MyArm = 52; *%inches*

Cal.MzArm = 40; *%inches*

%Define Cable Lengths

Cal.FyCable = 8*12; *%inches*

Cal.FxCable = 8*12; *%inches*

%Define Calibration Body

Cal.FixTip = 8.305; *%in*

Cal.FixWidth = 4; *%in*

Cal.CalBodyMz = 6; *%in*

%% Calculate Force and Moment Uncertainties

%Initialize Total Uncertainties

S.F = **zeros**(1,3);

S.M = **zeros**(1,3);

%Initialize Variables

ReduceFy = 0;

```

ReduceFz = 0;

if Papp.Fx_tilde = 0
    %Add Fx Cable Load
    %Calculate load point and magnitude
    P.Fx = Papp.Fx;
    P.y = 0;
    P.z = 0;
    P.x = Cal.FixTip;

    %Calculate the uncertainty from the hanger load
    [s_f, s_m] = FxCable(s, P);

    %Add the uncertainty to the total
    S.F = S.F + s_f + (s.BalSen(1:3)*s.LineUp).^2;
    S.M = S.M + s_m + (s.BalSen(4:6)*s.LineUp).^2;
end

if Papp.Fz_tilde = 0 || Papp.My_tilde = 0
    if Papp.Fy_tilde = 0 || Papp.Mz_tilde = 0
        %Calculate Fy loads and position for moment

        %Calculate load point and magnitude
        if Papp.Fy_tilde = 0
            P.Fy = Papp.Fy;
            P.x = Papp.Mz/P.Fy;
        else %when Fy = 0
            P.x = Cal.CalBodyMz;
            P.Fy = Papp.Mz/P.x;
        end

        P.y = 0;
        P.z = -Cal.FixWidth/2;
    end

```

```

    %Calculate the uncertainty from the hanger load
    [s_f, s_m] = FyCable(s, P);

    %Add the uncertainty to the total
    S_F = S_F + s_f + (s.BalSen(1:3)*s.LineUp).^2;
    S_M = S_M + s_m + (s.BalSen(4:6)*s.LineUp).^2;
end
if Papp.Mx_tilde = 0
    %Add Fz Hanger on Mx Arm

    %Calculate load point and magnitude
    P.Fz = Papp.Mx/Cal.MxArm;
    P.y = Cal.MxArm;
    P.z = Cal.FixWidth/2;
    P.x = 0;

    %Calculate the uncertainty from the hanger load
    [s_f, s_m] = FzHanger(s, P);

    %Add the uncertainty to the total
    S_F = S_F + s_f;
    S_M = S_M + s_m;

    %Reduce Any Fz Load
    ReduceFz = P.Fz;
end
if Papp.My_tilde = 0
    %Add Fz Hanger on My Arm

    %Calculate load point and magnitude
    P.Fz = Papp.My/Cal.MyArm;
    P.y = 0;
    P.z = -Cal.FixWidth/2;
    P.x = Cal.MyArm;

```

```

    %Calculate the uncertainty from the hanger load
    [s_f , s_m] = FzHanger(s , P);

    %Add the uncertainty to the total
    S_F = S_F + s_f;
    S_M = S_M + s_m;

    %Reduce Any Fz Load
    ReduceFz = ReduceFz + P.Fz;
end
if Papp.Fz ~ = 0
    %Add Fz Hanger at BMC
    %Calculate load point and magnitude
    P.Fz = Papp.Fz - ReduceFz;
    P.y = 0;
    P.z = Cal.FixWidth/2;
    P.x = 0;

    %Calculate the uncertainty from the hanger load
    [s_f , s_m] = FzHanger(s , P);

    %Add the uncertainty to the total
    S_F = S_F + s_f;
    S_M = S_M + s_m;
end
else
    if Papp.Mx ~ = 0
        %Add Fy Hanger on Mx Arm

        %Calculate load point and magnitude
        P.Fy = Papp.Mx/Cal.MxArm;
        P.y = Cal.FixWidth/2;
        P.z = Cal.MxArm;
    end
end

```

```

P.x = 0;

%Calculate the uncertainty from the hanger load
[s_f, s_m] = FyHanger(s, P);

%Add the uncertainty to the total
S_F = S_F + s_f;
S_M = S_M + s_m;

%Reduce Any Fy Load
ReduceFy = P.Fy;
end
if Papp.Mz ~ = 0
    %Add Fy Hanger on Mz Arm

    %Calculate load point and magnitude
    P.Fy = Papp.Mz/Cal.MzArm;
    P.y = Cal.FixWidth/2;
    P.z = 0;
    P.x = Cal.MzArm;

    %Calculate the uncertainty from the hanger load
    [s_f, s_m] = FyHanger(s, P);

    %Add the uncertainty to the total
    S_F = S_F + s_f;
    S_M = S_M + s_m;

    %Reduce Any Fy Load
    ReduceFy = ReduceFy + P.Fy;
end
if Papp.Fy ~ = 0
    %Add Fy Hanger at BMC

```

```

    %Calculate load point and magnitude
    P.Fy = Papp.Fy - ReduceFy;
    P.y = Cal.FixWidth/2;
    P.z = 0;
    P.x = 0;

    %Calculate the uncertainty from the hanger load
    [s_f , s_m] = FyHanger(s, P);

    %Add the uncertainty to the total
    S_F = S_F + s_f;
    S_M = S_M + s_m;
end
end

%Add Electrical Noise Uncertainty
S_F = S_F + (s.BalSen(1:3)*s.DAQ).^2;
S_M = S_M + (s.BalSen(4:6)*s.DAQ).^2;

%Take the square root of the computed uncertainties
%The values computed before are variances, i.e. s^2
S_F = sqrt(S_F);
S_M = sqrt(S_M);

function [s_F, s_M] = FzHanger(s, P)
%Define the uncertainty equations for a Fz hanger load

%This function can be used to estimate the uncertainty for
    both
%the force and moment components for a Fz load placed on the
%calibration body or a moment arm

s_F = [0,          0,          P.Fz^2]*      s.P^2 +
    ...

```

```

    [0,          P.Fz^2,    0]*          s.phi^2 +
      ...
    [P.Fz^2,    0,        0]*          s.theta
      ^2;

s_M = [P.y^2,      P.x^2,    0]*          s.P^2 +
      ...
      [(P.Fz*P.z)^2, 0,      (P.Fz*P.x)^2]* s.phi^2
      + ...
      [0,          (P.Fz*P.z)^2,(P.Fz*P.y)^2]* s.theta
      ^2 +...
      [0,          P.Fz^2,    0]*          s.x^2 +
      ...
      [P.Fz^2,    0,        0]*          s.y^2;

```

function [s_F, s_M] = FyHanger(s, P)

%Define the uncertainty equations for a Fy hanger load

*%This function can be used to estimate the uncertainty for
both*

*%the force and moment components for a Fy load placed on the
%calibration body or a moment arm*

```

s_F = [0,          P.Fy^2,    0]*          s.P^2
      + ...
      [0,          0,        P.Fy^2]*          s.phi
      ^2 + ...
      [P.Fy^2,    0,        0]*          s.
      theta^2;

s_M = [(P.Fy*P.z)^2, 0,      (P.Fy*P.x)^2]* s.P^2
      + ...
      [(P.Fy*P.y)^2, (P.Fy*P.x)^2, 0]*          s.phi
      ^2 +...

```

```

[0, (P.Fy*P.z)^2, (P.Fy*P.y)^2]* s.
  theta^2 +...
[0, 0, P.Fy^2]* s.x^2
  + ...
[P.Fy^2, 0, 0]* s.z
  ^2;

```

function [s.F, s.M] = FxCable(s, P)

%Define the uncertainty equations for a Fx cable load

*%This function can be used to estimate the uncertainty for
both*

*%the force and moment components for a Fx cable load placed
on the*

%calibration body or a moment arm

```

s.F = [P.Fx^2, 0, 0]* s.P^2
  + ...
  [0, 0, P.Fx^2]* s.
  theta_c^2 + ...
  [0, P.Fx^2, 0]* s.
  theta_c^2 + ...
  [0, 0, P.Fx^2]* s.
  theta^2;

```

```

s.M = [0, (P.Fx*P.z)^2, (P.Fx*P.y)^2]* s.P^2
  + ...
  [(P.Fx*P.y)^2, (P.Fx*P.x)^2, 0]* s.
  theta_c^2 + ...
  [(P.Fx*P.z)^2, 0, (P.Fx*P.x)^2]* s.
  psi_c^2 + ...
  [(P.Fx*P.y)^2, (P.Fx*P.z)^2, 0]* s.
  theta^2 +...

```



```

[0,          0,          P.Fx^2]*      s.y^2
+ ...
[0,          P.Fx^2,      0]*          s.z
^2;

```

function [s_F, s_M] = FyCable(s, P)

%Define the uncertainty equations for a Fy cable load

*%This function can be used to estimate the uncertainty for
both*

*%the force and moment components for a Fy cable load placed
on the*

%calibration body or a moment arm

```

s_F = [0,          P.Fy^2,      0]*      s.P^2
+ ...
[0,          0,          P.Fy^2]*      s.
    phi_c^2 + ...
[P.Fy^2,      0,          0]*          s.
    psi_c^2 + ...
[0,          0,          P.Fy^2]*      s.phi
^2;

```

```

s_M = [(P.Fy*P.z)^2, 0,          (P.Fy*P.x)^2]* s.P^2
+ ...
[(P.Fy*P.y)^2, (P.Fy*P.x)^2, 0]*      s.
    phi_c^2 + ...
[0,          (P.Fy*P.z)^2, (P.Fy*P.y)^2]* s.
    psi_c^2 + ...
[(P.Fy*P.y)^2, (P.Fy*P.x)^2, 0]*      s.phi
^2 + ...
[0,          0,          P.Fy^2]*      s.x^2
+ ...

```

[P.Fy², 0, 0]* s.z
^2;

APPENDIX C

MANUAL STAND UNCERTAINTY MATLAB CODE - MONTE CARLO SIMULATION

C.1 INTERFACE SCRIPT

Below is the MATLAB script that was written to read in the desired applied loads, pass the load to the Monte Carlo Simulation, and save the output to file:

```
%Read in desired loads
[num, txt] = xlsread('ManualStandLoads.xlsx');
rows = size(num,1);

F = zeros(rows,3);
M = zeros(rows,3);

%Set balance angle
Papp.Phi = 0;
Papp.Theta = 0;
Papp.Psi = 0;

%Set cable angle
Papp.PhiCable = 0;
Papp.ThetaCable = 0;
Papp.PsiCable = 0;

%Loop through the rows of the provide load sheet
for j = 1:rows
    %Set the applied loads
    for i = 1:size(num,2)
```

```

        Papp.(txt{i}) = num(j,i);
    end

    parfor k = 1:100000
        %Perform the uncertainty calculations
        [F(k,:,j), M(k,:,j)] = ManualStandUncertaintyMC(Papp)
        ;
    end

    F_StDev(j,:) = std( F(:,:,j) );
    M_StDev(j,:) = std( M(:,:,j) );
end

%Set the output data file header
Header = { 'Fx', 'Fy', 'Fz', 'Mx', 'My', 'Mz' ...
    'sFx', 'sFy', 'sFz', 'sMx', 'sMy', 'sMz' };

%Output the data to file
cell2csv('UncertaintyResultsMC.csv',[Header; num2cell([num,
    F_StDev, M_StDev])])

Header = { 'Fx', 'Fy', 'Fz', 'Mx', 'My', 'Mz' };
Mean = [mean(F_StDev), mean(M_StDev)];
MeanFS= Mean./[400,4000,6500,9000,13000,6500]*100;

cell2csv('UncertaintySummaryMC.csv', [ { 'name'; 'Engineering_
    Units'; 'Percent_of_Full_Scale' }, ...
    [Header; num2cell([Mean;MeanFS]) ] ] )

```

C.2 SYSTEM MODEL

Below is the MATLAB script that was written to perform the Monte Carlo Simulation for the force and moment components of a manual stand calibration system:

```

function [F, M] = ManualStandUncertaintyMC(Papp)
%This function is written to provide an estimate for the
    uncertainty

```

%of the NASA LaRC force balance manual stand calibration systems.

*%The uncertainty estimates for the various noise contributors are
%entered below and applied loads are entered into the function.*

%% Define system properties

%Balance Angle Uncertainty

s.phi = 0.0244/2; %Deg.

s.theta = 0.0173/2; %Deg.

%Cable Angle Uncertainty

*s.phi_c = asind((1/32)/(8*12))/2;*

*s.theta_c = asind((1/32)/(8*12))/2;*

*s.psi_c = asind((1/32)/(8*12))/2;*

%Load Point Uncertainty

s.x = 0.0021/2; %inches

s.y = 0.0050/2; %inches

s.z = 0.0003/2; %inches

%Load Uncertainty

s.P = 0.0001/2; %Percent of Full Scale

%Electrical Uncertainty

s.DAQ = 0.0005; %mV/V

s.LineUp = 0.0005; %mV/V

s.BalSen = [365.9, 2035.2, 3167.5, 14602, 9208, 5772.7];

%Define Arm Lengths

Cal.MxArm = 40; %inches

Cal.MyArm = 52; %inches

Cal.MzArm = 40; %inches

%Define Cable Lengths

*Cal.FyCable = 8*12; %inches*

*Cal.FxCable = 8*12; %inches*

```

%Define Calibration Body
Cal.FixTip    = 8.305; %in
Cal.FixWidth  = 4;    %in
Cal.CalBodyMz = 6;    %in

%% Calculate Force and Moment Uncertainties
%Initialize Total Uncertainties
F = zeros(3,1);
M = zeros(3,1);

%Initialize Variables
ReduceFy = 0;
ReduceFz = 0;

%Load Balance and Cable Angles
P.Phi = normrnd(Papp.Phi, s.phi);
P.Theta = normrnd(Papp.Theta, s.theta);
P.Psi = Papp.Psi;

%Set cable angle
P.PhiCable = Papp.PhiCable;
P.ThetaCable = Papp.ThetaCable;
P.PsiCable = Papp.PsiCable;

if Papp.Fx ~= 0
    %Add Fx Cable Load
    %Calculate load point and magnitude
    P.Fx = normrnd(Papp.Fx, s.P*Papp.Fx);
    P.y = 0;
    P.z = 0;
    P.x = Cal.FixTip;

    P = PerturbPos(P, s);

```

```

    %Calculate the uncertainty from the hanger load
    [f, m] = FxCable(s, P);

    %Add the uncertainty to the total
    F = F + f + (s.BalSen(1:3)*normrnd(0,s.LineUp) )';
    M = M + m + (s.BalSen(4:6)*normrnd(0,s.LineUp) )';
end

if Papp.Fz ~ = 0 || Papp.My ~ = 0
    if Papp.Fy ~ = 0 || Papp.Mz ~ = 0
        %Calculate Fy loads and position for moment

        %Calculate load point and magnitude
        if Papp.Fy ~ = 0
            P.Fy = normrnd(Papp.Fy,s.P*Papp.Fy);
            P.x = Papp.Mz/P.Fy;
        else %when Fy = 0
            P.x = Cal.CalBodyMz;
            P.Fy = Papp.Mz/P.x;
            P.Fy = normrnd(P.Fy,s.P*P.Fy);
        end

        P.y = -Cal.FixWidth/2;
        P.z = 0;

        P = PerturbPos(P, s);

        %Calculate the uncertainty from the hanger load
        [f, m] = FyCable(s, P);

        %Add the uncertainty to the total
        F = F + f + (s.BalSen(1:3)*normrnd(0,s.LineUp) )';
        M = M + m + (s.BalSen(4:6)*normrnd(0,s.LineUp) )';
    end
end

if Papp.Mx ~ = 0
    %Add Fz Hanger on Mx Arm

```

```

    %Calculate load point and magnitude
    P.Fz = Papp.Mx/Cal.MxArm;

    %Reduce Any Fz Load
    ReduceFz = P.Fz;

    P.Fz = normrnd(P.Fz, s.*P.Fz);
    P.y = Cal.MxArm;
    P.z = Cal.FixWidth/2;
    P.x = 0;

    P = PerturbPos(P, s);

    %Calculate the uncertainty from the hanger load
    [f, m] = FzHanger(s, P);

    %Add the uncertainty to the total
    F = F + f;
    M = M + m;

end
if Papp.My ~ = 0
    %Add Fz Hanger on My Arm

    %Calculate load point and magnitude
    P.Fz = Papp.My/Cal.MyArm;
    %Reduce Any Fz Load
    ReduceFz = ReduceFz + P.Fz;

    P.Fz = normrnd(P.Fz, s.*P.Fz);
    P.y = 0;
    P.z = -Cal.FixWidth/2;
    P.x = Cal.MyArm;

    P = PerturbPos(P, s);

```



```

    %Calculate the uncertainty from the hanger load
    [f, m] = FzHanger(s, P);

    %Add the uncertainty to the total
    F = F + f;
    M = M + m;

end
if Papp.Fz ~ = 0
    %Add Fz Hanger at BMC
    %Calculate load point and magnitude
    P.Fz = Papp.Fz - ReduceFz;
    P.Fz = normrnd(P.Fz, s.*P.Fz);
    P.y = 0;
    P.z = Cal.FixWidth/2;
    P.x = 0;

    P = PerturbPos(P, s);

    %Calculate the uncertainty from the hanger load
    [f, m] = FzHanger(s, P);

    %Add the uncertainty to the total
    F = F + f;
    M = M + m;
end
else
    if Papp.Mx ~ = 0
        %Add Fy Hanger on Mx Arm

        %Calculate load point and magnitude
        P.Fy = Papp.Mx/Cal.MxArm;
        %Reduce Any Fy Load
        ReduceFy = P.Fy;
    end
end

```

```

P.Fy = normrnd(P.Fy, s.*P.Fy);
P.y = Cal.FixWidth/2;
P.z = Cal.MxArm;
P.x = 0;

P = PerturbPos(P, s);

%Calculate the uncertainty from the hanger load
[f, m] = FyHanger(s, P);

%Add the uncertainty to the total
F = F + f;
M = M + m;

end
if Papp.Mz ~ = 0
    %Add Fy Hanger on Mz Arm

    %Calculate load point and magnitude
    P.Fy = Papp.Mz/Cal.MzArm;
    %Reduce Any Fy Load
    ReduceFy = ReduceFy + P.Fy;

    P.Fy = normrnd(P.Fy, s.*P.Fy);
    P.y = Cal.FixWidth/2;
    P.z = 0;
    P.x = Cal.MzArm;

    P = PerturbPos(P, s);

    %Calculate the uncertainty from the hanger load
    [f, m] = FyHanger(s, P);

    %Add the uncertainty to the total
    F = F + f;
    M = M + m;

```

```

end
if Papp.Fy ~= 0
    %Add Fy Hanger at BMC

    %Calculate load point and magnitude
    P.Fy = Papp.Fy - ReduceFy;
    P.Fy = normrnd(P.Fy, s.P*P.Fy);
    P.y = Cal.FixWidth/2;
    P.z = 0;
    P.x = 0;

    P = PerturbPos(P, s);

    %Calculate the uncertainty from the hanger load
    [f, m] = FyHanger(s, P);

    %Add the uncertainty to the total
    F = F + f;
    M = M + m;
end
end

%Add Electrical Noise Uncertainty
F = F' + (s.BalSen(1:3)*normrnd(0,s.DAQ) );
M = M' + (s.BalSen(4:6)*normrnd(0,s.DAQ) );

function [F, M] = FzHanger(s, P)
%Define the uncertainty equations for a Fz hanger load

%This function can be used to estimate the uncertainty for both
%the force and moment components for a Fz load placed on the
%calibration body or a moment arm

F = [0; 0; P.Fz];

```

```
F = AngleTransform( F, P.Phi, P.Theta, P.Psi);
```

```
R = [P.x; P.y; P.z];
```

```
M = cross(R,F);
```

```
function [F, M] = FyHanger(s, P)
```

```
%Define the uncertainty equations for a Fy hanger load
```

```
%This function can be used to estimate the uncertainty for both  
%the force and moment components for a Fy load placed on the  
%calibration body or a moment arm
```

```
P.Psi = P.Theta;
```

```
P.Theta = 0;
```

```
F = [0; P.Fy; 0];
```

```
F = AngleTransform( F, P.Phi, P.Theta, P.Psi);
```

```
R = [P.x; P.y; P.z];
```

```
M = cross(R,F);
```

```
function [F, M] = FxCable(s, P)
```

```
%Define the uncertainty equations for a Fx cable load
```

```
%This function can be used to estimate the uncertainty for both  
%the force and moment components for a Fx cable load placed on  
the  
%calibration body or a moment arm
```

```
F = [P.Fx; 0; 0];
```

```

P.ThetaCable = normrnd(P.ThetaCable , s.theta_c);
P.PsiCable = normrnd(P.PsiCable , s.psi_c);

F = AngleTransform( F, P.PhiCable , P.ThetaCable , P.PsiCable);

F = AngleTransform( F, P.Phi , P.Theta , P.Psi);

R = [P.x; P.y; P.z];

M = cross(R,F);

```

```

function [F, M] = FyCable(s, P)

```

```

%Define the uncertainty equations for a Fy cable load

```

```

%This function can be used to estimate the uncertainty for both
%the force and moment components for a Fy cable load placed on
the

```

```

%calibration body or a moment arm

```

```

F = [0; P.Fy; 0];

P.PhiCable = normrnd(P.PhiCable , s.phi_c);
P.PsiCable = normrnd(P.PsiCable , s.psi_c);

F = AngleTransform( F, P.PhiCable , P.ThetaCable , P.PsiCable);

F = AngleTransform( F, P.Phi , P.Theta , P.Psi);

R = [P.x; P.y; P.z];

M = cross(R,F);

```

```

function P = PerturbPos(P, s)

```

```
P.x = normrnd(P.x, s.x);
```

```
P.y = normrnd(P.y, s.y);
```

```
P.z = normrnd(P.z, s.z);
```

VITA

Kenneth G. Toro
Department of Aerospace Engineering
Old Dominion University
Norfolk, VA 23529

Kenneth began his research at NASA LaRC in 2012 under Dr. Drew Landman as an graduate research assistant working on calibration and analysis of force measurement systems. He joined the NASA Pathways program in 2014 as a cooperative student intern while continuing his research in force measurement system uncertainties. In addition to the research into the force measurement uncertainty, he has worked on several other projects at NASA LaRC in the analysis of data for entry, decent and landing. Prior to working at NASA, he has worked at Old Dominion University as a research assistant to support the University Wind Tunnel. He received a Bachelor's degree in Aerospace Engineering from Embry-Riddle University at Prescott, AZ and a Master's degrees in Mechanical and Aerospace Engineering from Old Dominion University at Norfolk, VA. He has co-authored several journal and conference papers on the topics of force measurement systems and experimental aerodynamics. His research interests are in measurement systems and experimental aerodynamics.